MIT

A TEST OF ECOLOGICAL OPTIMALITY FOR SEMIARID VEGETATION

by
GUIDO D. SALVUCCI
and
PETER S. EAGLESON

DEPARTMENT

OF

CIVIL

ENGINEERING

RALPH M. PARSONS LABORATORY
HYDROLOGY AND WATER RESOURCE SYSTEMS

Report Number 335

May, 1992

R92–17

A TEST OF ECOLOGICAL OPTIMALITY
FOR SEMIARID VEGETATION

by

Guido D. Salvucci

and

Peter S. Eagleson

RALPH M. PARSONS LABORATORY
HYDROLOGY AND WATER RESOURCE SYSTEMS

Report Number 335

May, 1992

A TEST OF ECOLOGICAL OPTIMALITY
FOR SEMIARID VEGETATION

by

GUIDO DANIEL SALVUCCI

Submitted to the Department of Civil Engineering
on May 8, 1992 in partial fulfillment of the
requirements for the Degree of Master of Science in
Civil Engineering

ABSTRACT

Three ecological optimality hypotheses (Eagleson, 1978 and 1982) which have utility in parameter reduction and estimation in a climate-soil-vegetation water balance model are reviewed and tested. The first hypothesis involves short term optimization of vegetative canopy density through equilibrium soil moisture maximization. The second hypothesis involves vegetation type selection again through soil moisture maximization, and the third involves soil genesis through plant induced modification of soil hydraulic properties to values which result in a maximum rate of biomass productivity.

The first hypothesis is found to be in excellent agreement with data observed at the Beaver Creek watershed in Central Arizona. The utility of this hypothesis in estimating soil properties is supported.

The second hypothesis is found to be physically unrealistic and alternatives to the hypothesis are studied.

Conditions at Beaver Creek are not appropriate for testing the third hypothesis.

While the locus of canopy densities predicted by the short term ecological hypothesis creates a condition of stress free transpiration in typical years, lower than mean annual rainfall may still lead to drought-induced stress. In order to quantify this phenomenon, the expected value of the time spent in stress, and the resulting reduced transpiration, are analytically derived. The results of this analysis are shown to be useful in gaining a quantitative understanding of the water environment of semiarid regions and the drought tolerance required of its local vegetation.

Thesis Supervisor: Dr. Peter S. Eagleson
Title: Edmund K. Turner Professor of Civil Engineering
        Professor of Earth, Atmospheric and Planetary Sciences

3

TABLE OF CONTENTS

4

16

NOTATION

A_o gravitational infiltration rate as modified by capillary

   rise, cm sec^{-1}

A_s shortwave albedo of moist surface, dimensionless

B evapotranspiration parameter, dimensionless

C evapotranspiration parameter, dimensionless

D Julian day

c soil pore disconnectedness index, dimensionless

E dimensionless evaporation effectiveness

E_{p_A} average annual potential evaporation, cm

E_{p_S} average testing season potential evaporation, cm

ET_{p_A} average annual potential evapotranspiration, cm

E_r surface retention loss, cm

$E_{r_{v_A}}$ annual surface retention loss from vegetation, cm

E_{s_j} interstorm bare soil evaporation, cm

ET_A annual evapotranspiration, cm

ET_A^* modified annual evapotranspiration, cm

ET_S testing season evapotranspiration, cm

$E_{v_A}^{**}$ annual modified transpiration of soil moisture, cm

E_{v_j} interstorm transpiration, cm

$E_{v_j}^*$ modified interstorm transpiration, cm

E_w winter evaporation, cm

$\bar{e}_p$ time average potential evaporation rate for bare soil, cm sec^{-1}

$\bar{e}_{P_s}$ testing season time average bare soil potential evaporation rate, cm sec^{-1}

$\bar{e}_{P_w}$ winter season time average potential evaporation rate, cm sec^{-1}

e_v transpiration rate, cm sec^{-1}

f_e bare soil exfiltration rate, cm sec^{-1}

f_e^* bare soil exfiltration capacity, cm sec^{-1}

f_i infiltration rate, cm sec^{-1}

f_i^* infiltration capacity, cm sec^{-1}

h storm depth, cm

h_o surface retention capacity, cm

I_j storm infiltration, cm

i precipitation rate, cm sec^{-1}

j storm counting index

$K(s)$ effective hydraulic conductivity, cm sec^{-1}

$K(1)$ saturated effective hydraulic conductivity, cm sec^{-1}

$k(1)$ saturated effective permeability, cm^2

k_v potential transpiration efficiency, dimensionless

k_{v_e} effective transpiration efficiency, dimensionless

k_{v_T} potential transpiration efficiency of overstory, dimensionless

k_{v_u} potential transpiration efficiency of understory, dimensionless

k_{v_*} lumped, or composite, potential transpiration efficiency, dimensionless

L_e latent heat of evaporation, calories

M vegetated fraction, or canopy density, dimensionless

M_o equilibrium vegetal canopy density, dimensionless

M_o^* climatic-climax canopy density, dimensionless

M_T overstory vegetal canopy density, dimensionless

M_u understory vegetal canopy density, dimensionless

M_* lumped, or composite, vegetal canopy density, dimensionless

m soil pore size distribution index, dimensionless

m_h mean storm depth, cm

m_{t_b} mean time between storms, sec

m_{t_r} mean storm duration, sec

m_{P_A} mean annual precipitation, cm

m_z rank order of observation of magnitude z

m_v mean number of storms per year

m_{v_S} mean number of storms in testing season

m_{v_W} mean number of storms in winter season

m_τ mean length of rainy season, sec

m_{τ_S} mean length of testing season, sec

m_{τ_W} mean length at winter season, sec

N average fractional cloud cover

N_r number of years of recorded data

n_e soil effective porosity, dimensionless

n_T total soil porosity, dimensionless

P_A annual precipitation, cm

P_S testing season precipitation, cm

P_W winter season precipitation, cm

$\bar{q}_b$ average net rate of outgoing long-wave radiation cal cm^2 sec^{-1}

$\bar{q}_i$ average seasonal rate of insulation at surface, cal cm^2

sec^{-1}

R_{g_A} annual groundwater runoff, cm

R_{s_A} annual surface runoff, cm

R_{s_j} storm surface runoff, cm

$R_{s_j}^{*}$ storm rainfall excess, cm

R_W winter soil moisture recharge, cm

RH_A average annual relative humidity, dimensionless

S_e exfiltration sorptivity, $\text{cm sec}^{-\frac{1}{2}}$

S_i infiltration sorptivity, $\text{cm sec}^{-\frac{1}{2}}$

s effective soil saturation, dimensionless

s_o equilibrium soil saturation, dimensionless

s_r residual soil saturation, dimensionless

s_T total soil saturation, dimensionless

T time in one year, sec

$\overline{T}_A$ average annual atmospheric temperature, °C

$\overline{T}_S$ average testing season atmospheric temperature, °C

t_b time between storms, sec

t_e time during which exfiltration takes place, sec

t_o time during which exfiltration takes place at the potential evaporation rate, $\overline{e}_p$, sec.

t_r duration of storm, sec

t_s time at which soil moisture storage is exhausted and transpiration ceases, sec.

t_s' time during which transpiration occurs, sec

t^{*} time at which surface retention is completely evaporated, sec

V_e equilibrium depth of soil moisture storage, cm

v rate of percolation, cm sec^{-1}

w rate of capillary rise, cm sec^{-1}

Y_S testing season basin yield, cm

Y_W winter season basin yield, cm

z elevation, cm

z_e exfiltration penetration depth, cm

z_r depth of root zone, cm

z_W depth to water table, cm

α reciprocal of mean time between storms, sec^{-1}

α_S reciprocal of mean testing season time between storms, sec^{-1}

β evapotranspiration efficiency, dimensionless

β_s bare soil evaporation efficiency, dimensionless

β_v vegetation transpiration reduction coefficient

γ_w specific weight of liquid water, dynes $\cdot$ cm^{-3}

δ reciprocal of mean storm duration, sec^{-1}

η reciprocal of mean storm depth, cm^{-1}

θ normalized evapotranspiration

κ parameter of gamma distribution of storm depths, dimensionless

λ parameter of gamma distribution of storm depths, cm^{-1}

μ dynamic viscosity of water, dynes $\cdot$ cm^{-2} $\cdot$ sec^{-1}

ϕ reciprocal of mean storm intensity, cm^{-1} sec

ϕ_i dimensionless infiltration diffusivity

ϕ_e dimensionless exfiltration diffusivity

χ ratio of water use to biomass production, gm c/gm H_2O

$\psi(1)$ saturated matrix potential, cm

ρ mass density of water, gm cm^{-3}

$\sigma^2_{P_A}$ variance of annual precipitation, cm^2

σ_ω surface tension of water, dynes $\cdot$ cm^{-1}

ω moisture content by weight, dimensionless

$E[\ ]$ expected value of $[\ ]$

$\Gamma[\ ]$ gamma function

$\gamma[\ ]$ incomplete gamma function

$\overline{[\ ]}$ expected value of $[\ ]$

CHAPTER 1

Introduction

Coupled climate, soil and vegetation water balances which incorporate stochastic climatic input variables and deterministic process physics have been used to show that for a given climate, certain values of soil parameters, vegetation density, and vegetation type give rise to maximum biomass production and/or to minimum stress conditions (Eagleson, 1978 and 1982; Tellers, 1980; Tellers and Eagleson, 1980; Eagleson and Tellers, 1982; Eagleson and Segarra, 1985; Arris, 1989; Arris and Eagleson, 1989). Based on the original findings (Eagleson, 1978), Eagleson (1982) hypothesized that in natural vegetation systems where growth is limited by water availability three equilibrium stages will be reached. On a short time scale vegetation density will adjust to that value which maximizes the equilibrium soil moisture. At maximum soil moisture the vegetation is least likely to be put into a state of stress in which it would be susceptible to disease and pests. On a longer time scale, the plants whose transpiration characteristics result in the highest equilibrium soil moisture (water limiting) and/or produce the most biomass annually (water not limiting) will become dominant. On a very long time scale, root growth and decay will modify the soil until the soil properties are those that support the largest canopy in the given climate.

The hypotheses have been tested (Eagleson and Tellers, 1982) on a limited number of sites, but without detailed knowledge of all the parameters involved.

These hypotheses, if verified, could have utility in a number of important ways. They can be used in conjunction with the water balance, upon which they are built, as additional equations, thus effectively reducing the number of unknown parameters to be estimated. Or, with a limited number of observed parameters, which can often be remotely sensed (e.g., canopy density), the hypotheses can be used to estimate parameters which also appear in other models of land surface processes (e.g., the soil hydraulic conductivity used in global circulation models). Additionally, they could be used to try to understand and predict the interactive feedback between climate change and the biospheric boundary conditions of the Earth.

In this document we review and test these hypotheses on a set of extensively gaged semiarid watersheds near Flagstaff, Arizona. For the first time we have independent measurements of all necessary input parameters, thus providing a more discriminating test of the hypotheses.

CHAPTER 2

Review of Statistical-Dynamic Water Balance

and Ecological Optimization Hypotheses

2.1 Water Balance

2.1.1 Framework. The foundation upon which the ecological optimization hypotheses are built is Eagleson's statistical-dynamic water balance model (Eagleson, 1978). It is a one-dimensional model of soil moisture dynamics forced by a stochastic climate. The model solves the equilibrium water balance in terms of a temporally and vertically averaged near-surface (on the order of the rooting depth, or one meter) soil moisture. This soil moisture determines the flux rates of moisture into and out of the near-surface soil column. For a complete review of the model see the original work (Eagleson, 1978) or Tellers, 1980; Tellers and Eagleson, 1980; El-Hemry, 1980 or El-Hemry and Eagleson, 1980. A brief review of the essential model features follows.

The soil moisture dynamics in the near surface soil column are governed by the concentration-dependent diffusion equation (i.e., Richard's equation). Eagleson (1978) modifies Phillips' (1960) approximate analytical solution to this equation to incorporate a distributed vegetal root sink and introduces the Brooks and Corey (1966) model of unsaturated soil hydraulic properties. He then averages the solutions over the ensemble of surface boundary and initial conditions which arise from a Poisson arrival of rainstorms in the form of rectangular pulses. These storms have

exponentially distributed intensity and exponentially distributed duration and between them the surface is subjected to a constant potential evaporation. In this way the expected value of the surface fluxes, i.e., storm infiltration ($E[I_j]$), interstorm exfiltration ($E[E_{s_j}]$) and interstorm transpiration ($E[E_{v_j}]$) are found.

The soil moisture dynamics at the bottom boundary of the near surface soil column are governed by the same physical laws. Here, however, Eagleson assumes that the randomly varying surface boundary condition is damped by the diffusive process occurring throughout the soil matrix and that the lower boundary of the soil column will therefore be at steady state. With this assumption, he finds percolative (v) and capillary rise (w) steady state fluxes at the bottom boundary.

In what follows, we will review how the expected values of the surface fluxes and of the fluxes out of the bottom of the soil control volume are derived, making modifications and corrections to Eagleson's (1978) work as appropriate. We will then transform these event-based surface fluxes and steady state bottom fluxes into annual water balance components. Finally, we will arrive at a mathematical statement for the average annual water balance.

2.1.2   Interstorm Bare-Soil Evaporation and Vegetal

   Transpiration

The Poisson arrival of storms implies an exponentially distributed time between storms (t_b). This exponentially distributed time is the evaporation "window" over which the expected value is taken. A typical example of this evaporation window and the process physics which occur within it is presented, for bare soil evaporation, in Fig. 2.1. Here the exfiltration capacity $(f_e^*, cm\ sec^{-1})$, is, from Eagleson (1978):

$$f_e^* = \frac{1}{2}S_e t^{-\frac{1}{2}} - Mk_v\bar{e}_p + w \qquad (2.1)$$

where

S_e =   exfiltration sorptivity (cm $sec^{-\frac{1}{2}}$)

M =   vegetated fraction, or canopy density
        (dimensionless)

k_v =   potential transpiration efficiency (dimensionless)

   = $\dfrac{\text{unstressed transpiration rate}}{\text{potential bare soil evaporation rate}}$

$\bar{e}_p$ =   time average potential evaporation rate for bare
        soil (cm sec^{-1})

w =   rate of capillary rise (cm sec^{-1})

As Figure 2.1 illustrates, the bare soil evaporation occurs during three distinct stages. The first stage is the evaporation of surface retention. This occurs at the bare soil potential rate $(\bar{e}_p)$ until the surface retention is exhausted (t^*). During the second stage, between t^* and $t^* + t_o$, moisture is drawn from within the soil. In this stage the maximum flux rate at

27

which the atmosphere can remove moisture (the time average potential bare soil evaporation rate, $\bar{e}_p$) is less than the exfiltration capacity (f_e^*) (dashed curve in Fig. 2.1), and thus limits the actual exfiltration rate (f_e) to the potential evaporation rate ($\bar{e}_p$). After $t^* + t_o$, exfiltration of moisture from the column proceeds at the rate f_e^*, which is now less than the potential evaporation rate, until the time $t* + t_e$, when exfiltration ceases.

Taking the expected value of the integral of the actual exfiltration rate (f_e) over all of the possible (exponentially distributed) time between storms gives, for the bare soil interstorm exfiltration

$$
\begin{aligned}
E[E_{s_j}] = \frac{\bar{e}_p}{\alpha} \cdot &\left\{ \left[\frac{\gamma[\kappa,\lambda h_o]}{\Gamma(\kappa)} - \left[1 + \frac{\frac{\alpha h_o}{\bar{e}_p}}{\lambda h_o}\right]^{-\kappa} \frac{\gamma\left[\kappa,\lambda h_o + \frac{\alpha h_o}{\bar{e}_p}\right]}{\Gamma(\kappa)} \right] e^{-BE} \right. \\
&+ \left\{1 - \frac{\gamma[\kappa,\lambda h_o]}{\Gamma(\kappa)}\right\} \cdot \left\{1 - e^{-BE - \frac{\alpha h_o}{\bar{e}_p}} \cdot \left[1 + Mk_v + (2B)^{\frac{1}{2}} \cdot E - \frac{w}{\bar{e}_p}\right] \right. \\
&\left. + e^{-CE - \frac{\alpha h_o}{\bar{e}_p}}\left[Mk_v + (2C)^{\frac{1}{2}}E - \frac{w}{\bar{e}_p}\right] + (2E)^{\frac{1}{2}}e^{\frac{-\alpha h_o}{\bar{e}_p}}\left[\gamma(\frac{3}{2},CE) - \gamma(\frac{3}{2},BE)\right] \right\} \\
&+ \left[1 + \frac{\frac{\alpha h_o}{\bar{e}_p}}{\lambda h_o}\right]^{-\kappa} \cdot \frac{\gamma[\kappa,\lambda h_o + \frac{\alpha h_o}{\bar{e}_p}]}{\Gamma(\kappa)} \cdot \left\{(2E)^{\frac{1}{2}} \cdot \left[\gamma(\frac{3}{2},CE) - \gamma(\frac{3}{2},BE)\right] \right. \\
&\left. \left. + e^{-CE}\left[Mk_v + (2C)^{\frac{1}{2}}E - \frac{w}{\bar{e}_p}\right] - e^{-BE} \cdot \left[Mk_v + (2B)^{\frac{1}{2}}E - \frac{w}{\bar{e}_p}\right] \right\} \right\}
\end{aligned}
$$

(2.2)
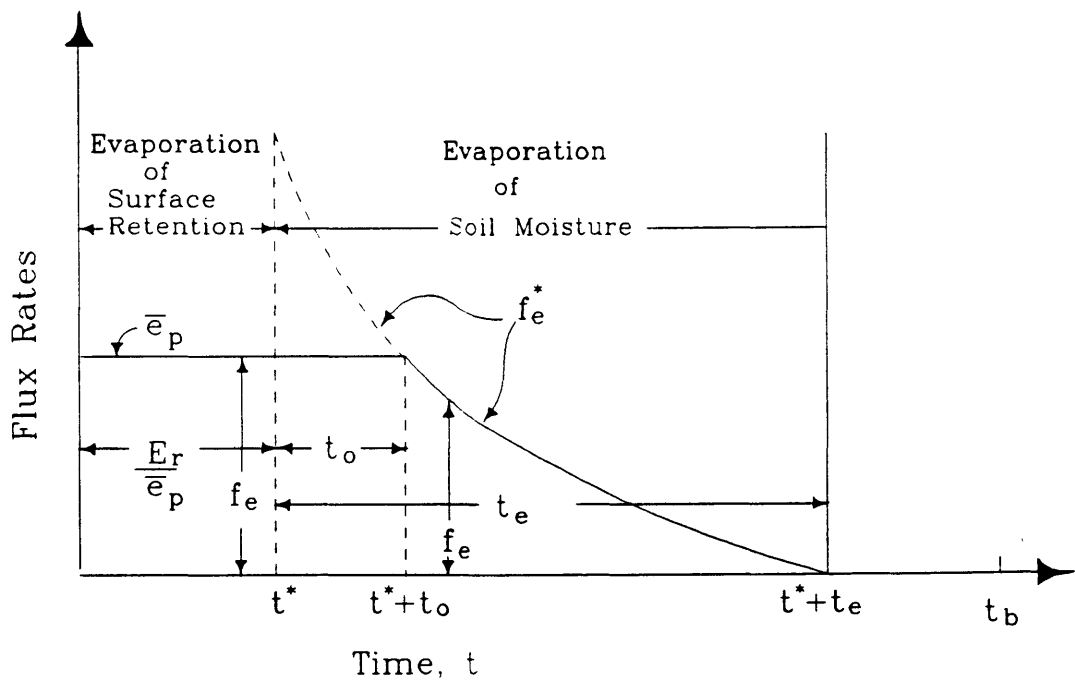
FIGURE 2.1: EVAPORATION FROM BARE SOIL

Here

$$B = \frac{1-M}{1+Mk_v - \frac{w}{\bar{e}_p}} + \frac{M^2 k_v + (1-M)\frac{w}{\bar{e}_p}}{2(1+Mk_v - \frac{w}{\bar{e}_p})^2} \qquad (2.3)$$

and

$$C = \frac{1}{2}(Mk_v - \frac{w}{\bar{e}_p})^{-2} . \qquad (2.4)$$

Also

α = reciprocal of mean time between storms (sec^{-1})

λ = parameter of gamma distribution of storm depth (cm^{-1})

κ = parameter of gamma distribution of storm depth (dimensionless)

h_o = surface retention capacity (cm)

$\bar{e}_p$ = bare soil potential evaporation rate ($cm\ sec^{-1}$)

k_v = potential transpiration efficiency (dimensionless)

M = vegetated surface fraction (dimensionless)

w = capillary rise rate ($cm\ sec^{-1}$)

E = evaporation effectiveness (dimensionless)

$\gamma[\ ]$ = incomplete gamma function

$\Gamma()$ = gamma function

E, the dimensionless evaporation effectiveness, is related to the soil and climate parameters through

30

$$E = \frac{2\alpha n_e K(1) \psi(1)}{\pi m \overline{e}_p{}^2} \phi_e s^{d+2} \qquad (2.5)$$

Here,

d   =   soil diffusivity index (dimensionless)

n_e = soil effective porosity

$K(1)$ = saturated hydraulic conductivity (cm sec^{-1})

$\psi(1)$ = saturated soil matrix potential (cm)

m   = soil pore size distribution index

(dimensionless) = $1/(d - 2)$

s   = effective soil moisture saturation (dimensionless)

ϕ_e = dimensionless exfiltration diffusivity

(dimensionless)

The interstorm transpiration is modelled as a constant flux rate (e_v) at some proportion (k_v) of the bare soil potential evaporation rate over the interstorm period. The expected value of interstorm transpiration is thus:

$$E[E_{v_j}] = e_v \cdot \alpha^{-1} = k_v \overline{e}_p \, \alpha^{-1} \qquad (2.6)$$

2.1.3   Storm Infiltration and Surface Runoff

The expected value of the surface runoff ($E[R_{s_j}]$) generated from a storm is found in a manner similar to the above derivation for interstorm evaporation. Here, however, the expected values are taken over the joint probability distribution of storm intensity (i) and duration (t_r).

31

Figure 2.2 illustrates the process physics responsible for runoff generation during a typical storm. The potential infiltration rate, f_i^*, is given by Eagleson (1978) as

$$f_i^* = \frac{1}{2} S_i t^{-\frac{1}{2}} + A_o \qquad (2.7)$$

where,

S_i = infiltration sorptivity (cm sec^{-1})

A_o = gravitational infiltration rate as modified by capillary rise (cm sec$^{-1)}$)

Initially, the storm fills the surface retention capacity, h_o. After this, as long as the potential infiltration rate, f_i^*, is greater than the storm intensity, i, no runoff is generated. Beyond time $t_o + h_o/i$, however, the storm's intensity exceeds the ability of the soil to infiltrate it and runoff is produced at a rate of i - f_i^*. This continues until the storm ends at time t_r.

Taking the expected value of the time integral of the runoff production rate over the joint probability distributions of intensity and duration and correcting for surface retention filling gives:

$$E[R_{s_j}] = \phi^{-1} \delta^{-1} \cdot e^{-G-2\sigma} \Gamma(\sigma+1) \sigma^{-\sigma} - E[E_r] \qquad (2.8)$$
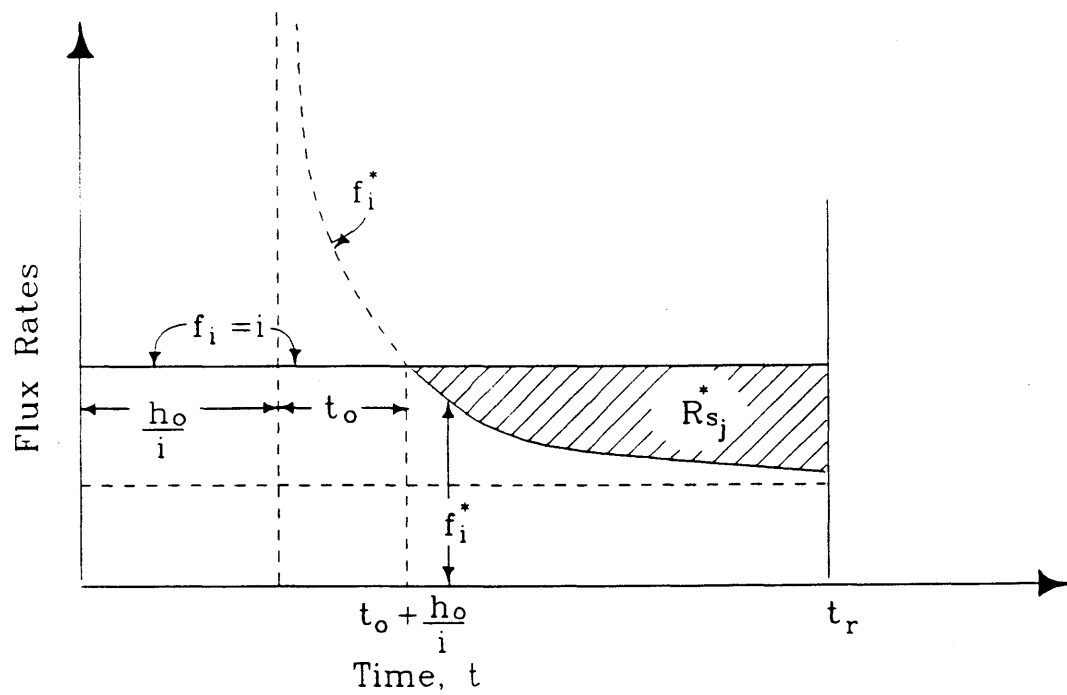
FIGURE 2.2: SURFACE RUNOFF GENERATION

DURING TYPICAL STORM

Here

$$G = \phi K(1) \left[\frac{1+s^c}{2} - \frac{w}{K(1)} \right] \qquad (2.9)$$

and

$$\sigma = \left[\frac{5 n_e \eta^2 K(1) \, \psi(1) \, (1-s)^2 \phi_i \, (d,s)}{6 \pi \delta m} \right]^{\frac{1}{3}} \qquad (2.10)$$

and

c = soil pore disconnectedness index (dimensionless)

        = $2d - 1$

η = reciprocal of mean storm depth (cm^{-1})

ϕ = reciprocal of mean storm intensity (cm^{-1})

δ = reciprocal of mean storm duration (sec^{-1})

ϕ_i = dimensionless infiltration diffusivity

$E[E_r]$ = expected value of surface retention loss

The other variables have been defined previously.

The storm infiltration, I_{s_j}, is simply the storm depth minus the runoff and surface retention requirement. Averaged this becomes

$$E[I_{s_j}] = E[h_j] - E[R_{s_j}^*] \qquad (2.11)$$

34

where $E[R_{s_J}^*]$ is equal to the expected value of storm runoff ($E[R_{s_j}]$) plus the expected value of surface retention loss ($E[E_r]$).

2.1.4   Percolation and Capillary Rise

As was previously discussed, a percolation component and, where a water table exists, a capillary rise component are also included at the lower boundary of the soil control volume. Both are steady state fluxes.

The percolation component is:

$$v(s) = K(1)s^c \qquad (2.12)$$

and occurs over the rainy season (m_r).

The capillary rise is:

$$w = K(1)\left[1 + \frac{\frac{3}{2}}{mc-1}\right]\left[\frac{\psi(1)}{z_w}\right]^{mc} \qquad (2.13)$$

and occurs throughout the year (T).

In the above,

$$z_w = \text{depth to water table;}$$

the other variables have been previously defined.

2.1.5   The Average Annual Water Balance

The Poisson arrival of storm depths (which are assumed to be gamma distributed) implies a certain distribution of annual (or seasonal) precipitation and a specific mean annual precipitation,

$$\overline{P}_A = m_v \cdot m_h \qquad (2.14)$$

where

$$m_v = \text{mean number of storms per year (season)}$$

$$m_h = \text{mean storm depth (cm)}$$

By setting the average annual precipitation equal to the sum of the expected values of annual (seasonal) evapotranspiration, percolation, capillary rise and runoff, the water balance equation becomes:

$$E[P_A] = E[ET_A] + E[R_{s_A}] + E[R_{g_A}] \qquad (2.15)$$

where

P_A = annual precipitation (cm)

ET_A = annual evapotranspiration (cm)

R_{s_A} = annual surface runoff (cm)

R_{g_A} = annual net groundwater runoff (percolation-capillary rise)

The annual expected values of the surface fluxes are each the sum of the mean number of the respective individual events. For example:

$$E[R_{s_A}] = m_v \cdot E[R_{s_j}] \qquad (2.16)$$

here

m_v = mean number of storms per year

$E[R_{s_j}]$ = mean storm runoff (cm)

The expected value of annual evapotranspiration ($E[ET_A]$) is similarly the sum of the mean number, m_v, of individual events, this time interstorm evaporation "windows". In this case, however, the mean flux is given by the weighted sum of two subcomponents: the bare-soil evaporation and the vegetal transpiration. These

36

are linearly weighted by their areal fraction, M and (1-M), as:

$$E[ET_A] = \left[(1-M) \cdot E[E_{s_j}] + M \cdot E[E_{v_j}]\right] \cdot m_v \qquad (2.17)$$

The expected value of the annual net groundwater runoff is simply the net difference between the product of each of its steady state components (v and w) and the season length over which they apply:

$$E[R_{g_A}] = m_\tau v - Tw \qquad (2.18)$$

At first glance there would appear to be many ways for the left-hand side (L.H.S.) of Eq. (2.15) to equal the right hand side (R.H.S.). This is where the state variable, the soil moisture (s), comes in. Each component on the R.H.S. of Eq. (2.15) is a function of this soil moisture. For one value of the soil moisture, the net inputs and outputs to the soil column are balanced. This will be referred to as the "equilibrium" soil moisture (s_0). In this way the breakdown of the average annual precipitation into the individual water balance components is determined.

Figure 2.3 demonstrates this dependence of the individual water balance components on soil moisture and shows the equilibrium soil moisture. Note that the equilibrium soil moisture, s_0, is the soil saturation for which the curve representing the sum of the (normalized) mean annual bare soil evaporation, transpiration, groundwater and surface water (the right-hand side of Eq. (2.15) normalized by $E[P_a]$) takes on the value one (the left-hand side of Eq. (2.15) normalized by $E[P_a]$. The parameter values used in this figure are consistent with a clay soil in a humid climate.
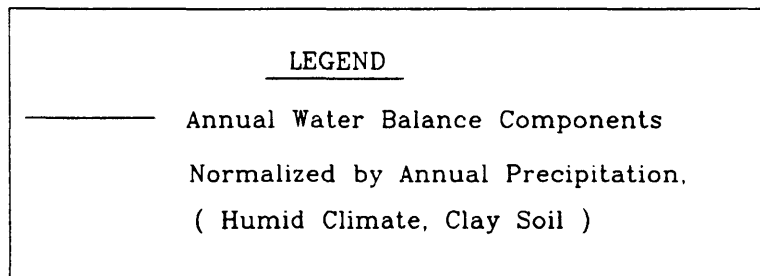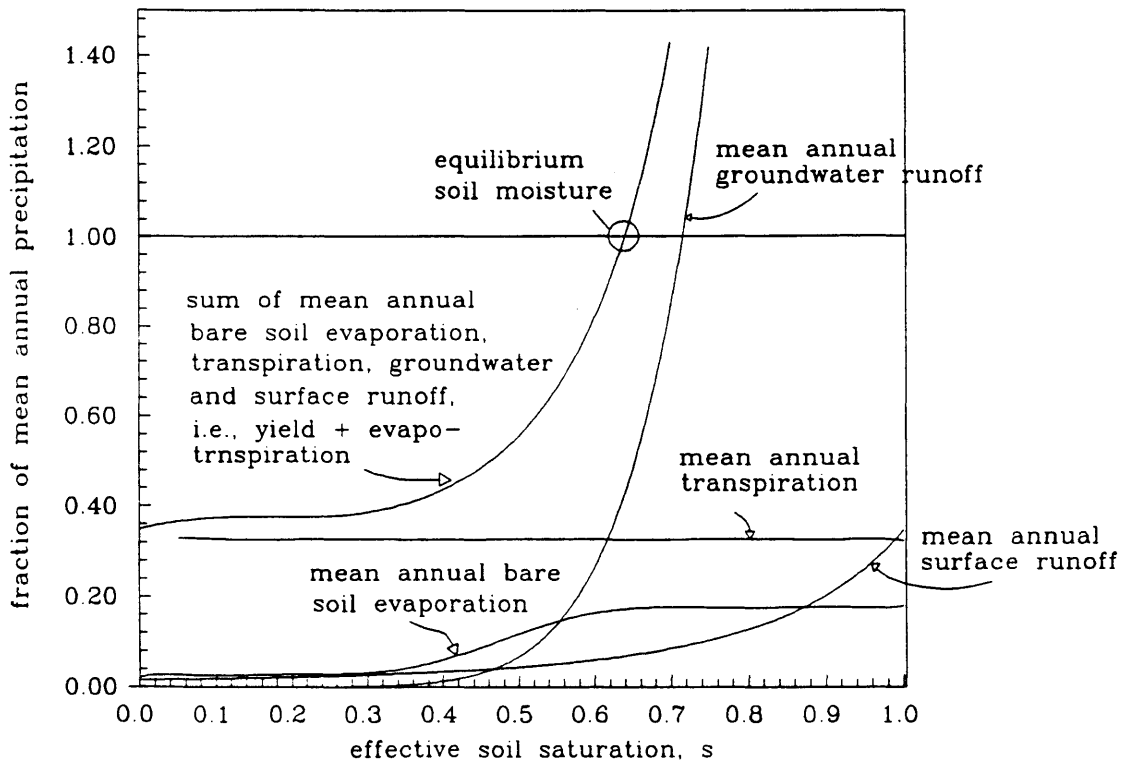
FIGURE 2.3: COMPONENTS OF WATER BALANCE

In full, the water balance is determined by the following 14 physically meaningful parameters:

Climate parameters:

$\bar{e}_p$ potential bare soil evaporation rate (time averaged)

(cm sec^{-1})

$\bar{T}_A$ annual average temperature (degrees celsius)

Vegetation and land surface parameters:

M   vegetated surface fraction (canopy density) (dimensionless)

k_v potential transpiration efficiency (i.e., plant coefficient, ratio of unstressed transpiration rate to potential bare soil evaporation rate) (dimensionless)

h_o surface retention capacity (cm)

Soil parameters:

k(1)   effective intrinsic permeability (cm^2)

c   pore disconnectedness index (dimensionless)

n_e effective medium porosity (dimensionless)

ψ(1)   saturated soil matrix potential (suction) (cm)

Precipitation distribution parameters

m_{t_b} mean time between storms (sec)

m_{t_r} mean storm duration (sec)

κ shape parameter of gamma distribution (dimensionless)

m_{P_A} average annual precipitation (cm)

m_τ mean length of rainy season (sec)

39

All other input parameters can be derived from the above independent parameters. For example, for the mean number of storms, m_v, we have

$$m_v = \frac{m_\tau}{m_{t_b} + m_{t_r}}$$

(2.19)

2.1.6 The Distribution of Annual Yield

By making certain first order approximations, we can rewrite Eq. (2.15) in terms of annual values (rather than mean annual values). The probability distribution of the right hand side of Eq. (2.15) can then be associated with the derived probability distribution of the left hand side, the annual precipitation. The probability distribution of the annual catchment yield (R_{g_A} + R_{s_A}) is thereby estimated.

Because the yield is easily (and often) measured over many years, the derived distribution can be compared with the observed population distribution. This can serve as a test of the water balance model and the parameter values used in it. For example, if we use an ecological optimality hypothesis to estimate a soil parameter value, and the derived distribution of yield (using this estimate) matches the observed distribution, we have a high degree of confidence in the soil parameter estimate.

It is important to note that it is the ability of the model to determine, with a single set of parameter values, the breakdown of precipitation into yield and evaporation over a wide spread of annual precipitation amounts, that demonstrates the robustness of the model. If the breakdown of precipitation between yield

40

and evaporation was the same ratio, no matter what the precipitation (i.e., if the system was linear), then the solution would be trivial. It is the nonlinear dependence of the evaporation and yield on the _same_ soil moisture which makes the derivation of the distribution of yield from annual precipitation non-trivial and gives the model its character.

2.2 Ecological Optimization Hypotheses and Their Use in Parameter Reduction and Estimation

Eagleson (1982) formulates three ecological optimality hypotheses regarding the expected state of vegetation in a natural (i.e., undisturbed) system which is presumed to be in an equilibrium state.

Over a short time scale he argues that the vegetation canopy density (M) will equilibrate with the climate and soil to the value at which the equilibrium soil moisture (s_o) will be at a maximum. That there is a maximum soil moisture at intermediate canopy densities can be seen in Figure 2.4, reproduced from Eagleson (1978), where this behavior was first noted. Mathematically, the location of this canopy density can be found by elementary calculus:

$$\frac{\partial s_o}{\partial M}\bigg|_{k_v, climate, soil} = 0 \qquad (2.20)$$
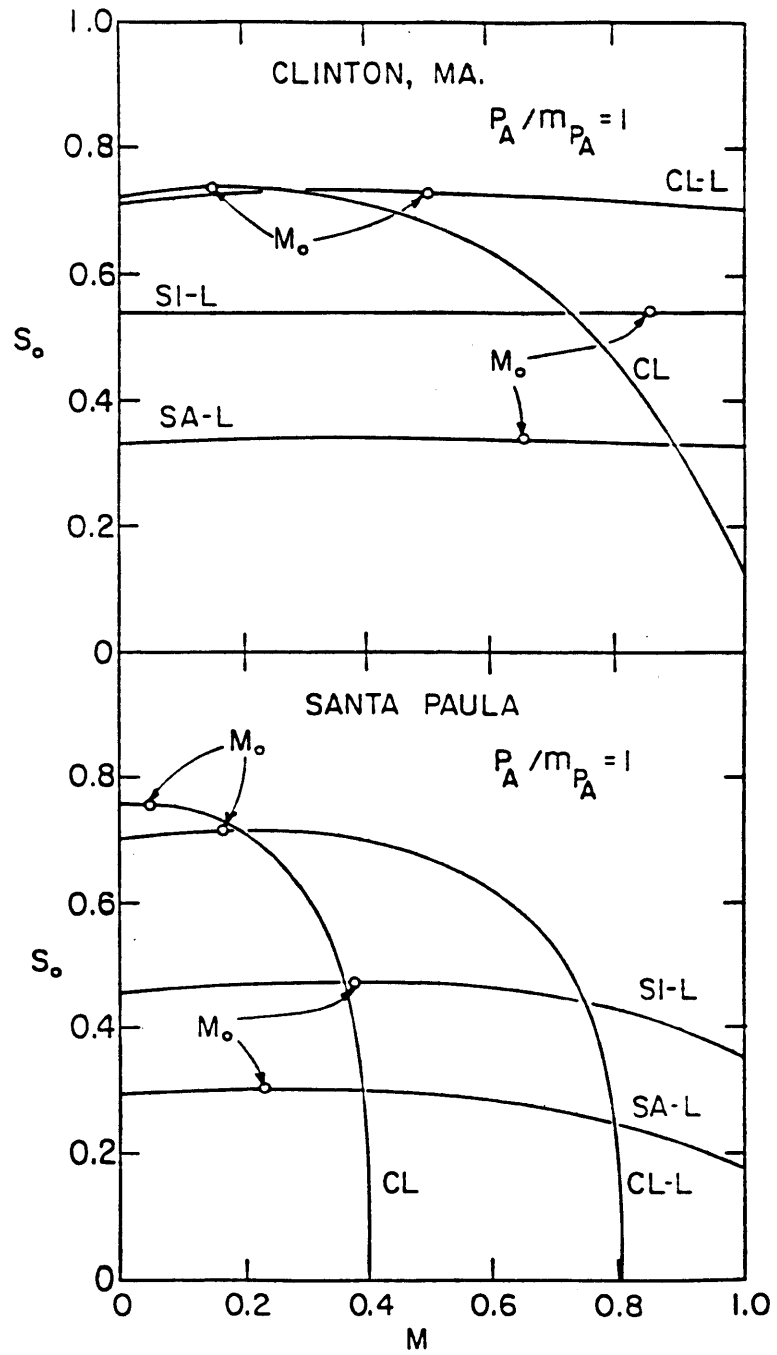
FIGURE 2.4: OPTIMUM CANOPY DENSITIES AT CLINTON, MA AND SANTA PAULA, CA

Eagleson (1982) has shown that provided M and k_v are independent, this is mathematically equivalent to minimizing the evapotranspiration and can thus be written (for analytic convenience):

$$\frac{\partial E[ET_A]}{\partial M}\Big|_{k_v, climate, soil} = 0 \qquad (2.21)$$

The canopy density for which the above relationships hold will be called the "optimum" canopy density (M_o).

Over a longer time scale (on the order of generations of individual plant life), Eagleson argues that the plant species most likely to survive and flourish in an undisturbed system will be those whose potential transpiration efficiency (k_v) result in the maximum equilibrium soil moisture. As above, this can be expressed mathematically as

$$\frac{\partial s_o}{\partial k_v}\Big|_{M, climate, soil} = 0 \qquad (2.22)$$

Over a still longer time scale, Eagleson argues that through addition of organic matter to the soil, the vegetation will alter the soil physical properties toward equilibrium values at which the optimum canopy density (M_o) of Eq. (2.20) is itself a maximum. The soil physical properties which are assumed to change are:

k(1): the soil permeability (cm^2)

and

c: the soil pore disconnectedness index (dimensionless).

Mathematically:

$$\frac{\partial M_o}{\partial k(1)}\Big|_c = 0 \qquad (2.23)$$

43

and

$$\frac{\partial M_o}{\partial c}\Big|_{k(1)} = 0 \qquad\qquad (2.24)$$

Simultaneous use of these four Eqs. (2.21-2.24) and the water balance Eq. (2.15) can reduce the original set of one equation and fourteen parameters to the original equation and ten parameters.

2.3   Errata in Published Literature

2.3.1   Second Optimization Hypothesis

In the process of reviewing and programming the routines to solve the water balance equation and the ecological optimization equations, it was discovered that there are no roots to Eq. (2.22); i.e., as a result of model construction,

$$\frac{\partial s_o}{\partial k_v}\Big|_{M, climate, soil} \neq 0 \qquad\qquad (2.25)$$

The figures and text which refer to the existence of this root in Eagleson (1982) and Eagleson and Tellers (1982) are in error insofar as their use of Eq. 2.25 is concerned; the roots to Eq. 2.22 upon which these figures are based arose from an error in computer programming.

The figures affected along with the relevant text are, for Eagleson (1982):

Figure 7   (the curves marked "optimum vegetation")

Figures 11, 12, 13

Figure 14   (the curve marked "vegetal equilibrium")

and for Eagleson and Tellers (1982):

44

Figure 1

Figure 7 (the curves marked "complete vegetal equilibrium")

Figure 17

Figure 19   (the curve marked "k_{v_0}")

The reason why there is no root (i.e., no intermediate value of k_v at which the soil moisture is a maximum) is that for any given canopy density, lowering k_v means that the annual precipitation must be balanced by more percolation, surface runoff and bare soil fraction evaporation, all of which increase with increasing soil moisture. The maximum soil moisture, in fact, will always result from a closed canopy (M=1) with the lowest possible k_v. In this scenario the bare soil fraction of evaporation is zero (since the canopy is closed) and the transpiration is vanishingly small (since $k_v \rightarrow 0$).

The percolation and surface runoff thus balance the whole annual precipitation, which implies a large equilibrium soil moisture. In general, lowering k_v will always increase the equilibrium soil moisture.

2.3.2   Rescaling of Evapotranspiration Efficiency

       Data in Past Work

In Eagleson and Tellers (1982), figure 4 on page 345 (reproduced here as figure 2.5) shows a test of the short-term equilibrium canopy density hypothesis (First Optimization Hypothesis) for eleven catchments. The graph shows the relationship between the optimum canopy density (M_0) and the

corresponding evapotranspiration efficiency β (the actual evapotranspiration divided by the potential evapotranspiration), for three values of k_v. The hypothesized relationships (solid lines) are the result of solving the short term optimality equation (in evaporation form) (2.21), for M_o as a function of the key normalizing variable of ET_A, the dimensionless evaporation effectiveness parameter E. The inverse of this relation, $E(M_o)$, is then substituted back into the evapotranspiration equation, leaving ET_A a function of M_o. The solid lines of Fig. 2.5 are this relationship, $ET_A(M_o)$, modified by normalizing ET_A by the potential evapotranspiration (ET_{P_A}), which produces $\beta(M_o)$.

The observed β, M_o pairs are shown as the boxes of figure 2.5 for comparison with the hypothesized relationship $(B(M_o))$. The observed values in the figure, however, are the result of normalizing the actual evapotranspiration by the average annual potential evaporation (E_{P_A}), instead of the average annual potential evapotranspiration (ET_{P_A}). The average annual potential evapotranspiration is the weighted sum of the bare soil potential evaporation and the vegetated fraction potential transpiration, i.e.,

$$ET_{P_A} = [(1 - M)\bar{e}_p + Mk_v \bar{e}_p]m_v\alpha^{-1} \qquad (2.26)$$

which differs significantly from the average annual potential evaporation (E_{P_A})

$$E_{P_A} = \bar{e}_p \cdot m_v \cdot \alpha^{-1} \qquad (2.27)$$

for all values of k_v except unity.

For comparisons between the observations and hypothesis,

46

the hypothesized relationship (solid lines, figure 2.5) should
be replaced by the function $ET_A(M_o)$ normalized by E_{P_A}. This
new function will be called the normalized evapotranspiration
theta,

$$\theta(M_o) = \frac{E[ET_A]}{E_{P_A}} = \frac{E[ET_A]}{\overline{e}_p \cdot m_v \cdot \alpha^{-1}} \qquad (2.28)$$

as opposed to the evapotranspiration efficiency ($\beta(M_o)$):

$$\beta(M_o) = \frac{E[ET_A]}{ET_{P_A}} = \frac{E[ET_A]}{\{(1 - M_o)\overline{e}_p + M_o k_v \overline{e}_p\} \cdot m_v \cdot \alpha^{-1}} \qquad (2.29)$$

This replacement has been made and is presented as Fig. 4.7
in Section 4.3.2.
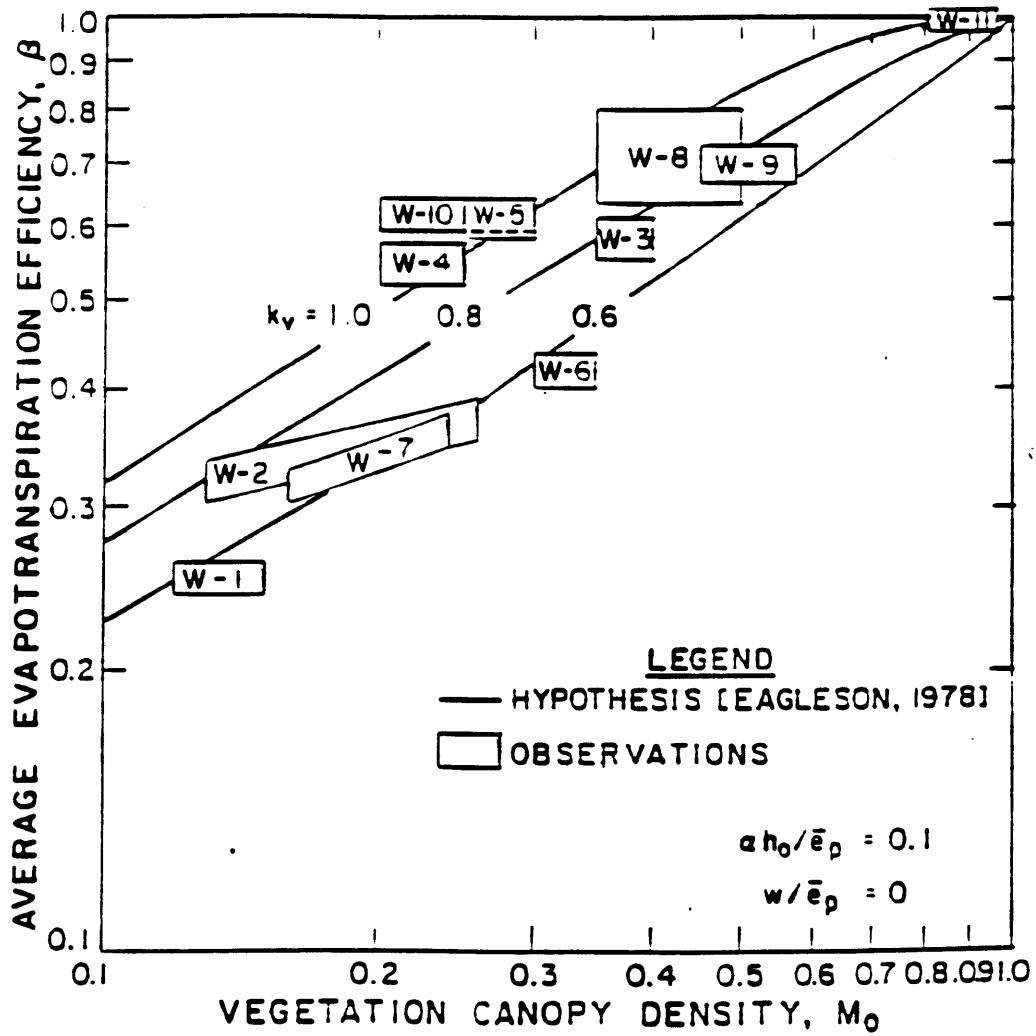
FIGURE 2.5: UNCORRECTED SHORT TERM
OPTIMALITY TEST FROM EXISTING LITERATURE

CHAPTER 3

An Expected Value Approach to Reducing Transpiration During

Drought-Induced Stress

3.1 Motivation

An approximate method for determining the partitioning of annual precipitation, P_A, (as opposed to mean annual precipitation, $\overline{P}_A$) into evapotranspiration and yield has been derived by Eagleson (1978). In that work Eagleson shows that to first order this partitioning can be determined by replacing the mean annual precipitation on the left hand side of the water balance equation (2.15) with the annual precipitation. This methodology allows us to explore the hydrologic environment (in particular the moisture conditions) to which the plant system is subjected in years of atypical rainfall.

Of particular interest are the drought conditions brought on by years of low annual precipitation. A measure of the likelihood and intensity of these extreme events is the variance of annual precipitation, $\sigma^2_{P_A}$. Eagleson (1978) shows that for the assumed precipitation model the variance is:

$$\sigma^2_{P_A} = \frac{\overline{P}_A^2}{m_v} (1 + \frac{1}{\kappa})$$

(3.1)

In general, semi-arid and arid climates have few storms (m_v) and small kappas, leading to high annual variances.

49

When exploring the water balance in these atypically dry years, however, the methodology presented by Eagleson (1978) can be problematic. In particular, there are certain values of annual precipitation, below a critical value, which cannot be balanced by the right-hand side of 2.15. Two methods for modifying the water balance equation which make solution possible under these conditions will be discussed. One has already been studied by past researchers (Metzger, 1980; Metzger and Eagleson, 1980), and one will be proposed in this document. First, however, it is necessary to illustrate how this condition occurs.

The situation occurs as a result of the dry limit (i.e., $s \rightarrow 0$) behavior of the evapotranspiration component of the water balance. From Chapter 2 we have, for the expected value of annual evapotranspiration:

$$E[ET_A] = \left[(1-M)E[E_{s_j}] + M \cdot E[E_{v_j}] \right] m_v \qquad (3.2)$$

As the soil moisture approaches zero in trying to balance a small annual precipitation with small annual evapotranspiration and annual yield (both of which decrease with decreasing soil moisture, see Fig. 2.3), the bare soil component, $E[E_{s_j}]$, which is a function of soil moisture, effectively approaches zero but the vegetal component $E[E_{v_j}]$, which is not modelled as a function of soil moisture, remains constant.

Consequently, for any annual precipitation for which the annual transpiration is greater, a soil moisture cannot be found for which the R. H. S. of the water balance equation (2.15)

50

balances P_A. Mathematically this condition is:

$$Mk_v \bar{e}_p m_v \alpha^{-1} > P_A$$

Two possible water balance model modifications which would allow solutions under this condition are:

1) the inclusion of an annual change in soil moisture storage. This _annual_ storage will be proportional to the

difference between the long-term average equilibrium soil moisture
(found by solving the water balance equation (2.15) for the mean
annual precipitation (P_A) and the equilibrium soil moisture which
solves the storage modified water balance equation for the given
annual precipitation; and 2) inclusion of an upper limit on
interstorm transpiration (E_{v_j}). This upper limit will be a
function of the equilibrium soil moisture. The expected value
of annual evapotranspiration, Eq. (3.2), will thus no longer
have a moisture independent dry limit.

The first possible modification has been explored thoroughly
by Metzger (1980) and Metzger and Eagleson (1980). The second
possibility will be explained in what follows.

3.2 Theory and Final Equations for Transpiration Reduction Coefficient (β_v)

3.2.1 Assumptions

The assumption that transpiration is constant in time and
not a function of soil moisture was made in the derivation of
the expected value of annual evapotranspiration (Eagleson, 1978d).
It was justified on the basis that "the stressed condition is
unstable in the long run due to increased susceptibility to
drought and disease"
(pg. 734, paragraph 5).

While this transpiration assumption is most likely true
in the mean sense, i.e., at equilibrium canopy density in years
of close to mean annual precipitation, it must be modified for
years of low precipitation.

52

The reduced transpiration will be incorporated into the current formulation of the expected value of evapotranspiration by making it a function of the equilibrium soil moisture storage (V_e). This storage will be the equilibrium soil moisture multiplied by the effective porosity and root depth:

$$V_e = n_e\, s_o\, z_r \qquad (3.3)$$

The expected value of transpiration will be made dependent upon this storage in that this storage will be the upper limit of interstorm evapotranspiration.

Following is a derivation of the expected value of interstorm evapotranspiration over the exponentially distributed time between storms (the evaporation "window") with the original assumption of <u>constant</u> transpiration over any length of evaporation "window" replaced by a model with constant transpiration only <u>until</u> the finite soil moisture storage (V_e) is exhausted.

The derivation follows identically the methodology of Eagleson (1978) upon which it is based.

The assumptions pertaining to the derivation are:

1) "Zeroth order" approximation for soil moisture (i.e., replace actual time varying soil moisture with space time average and reset this soil moisture (s) to the equilibrium soil moisture (s_o) at the beginning of each evaporation event.

53

2) There is some depth of soil which contains the active and depletable soil moisture and this depth is equal to the root depth (z_r).

3) This depth (z_r) is greater than or equal to the exfiltration penetration depth.

4) The vegetation transpires at a constant rate $e_v = k_v \cdot \bar{e}_p$ until the soil moisture storage (V_e) is exhausted. Trees transpire to soil moisture potentials of approximately fifteen bars negative pressure (Larcher, 1983, p. 237) and their transpiration rate is only variable, on average, between negative five and negative fifteen bars (data from Bunce et al., 1977; Brix, 1962; Havranek and Benecke, 1978; Hinckley et al., 1975; Hinckley et al., 1978; Larcher, 1983; averaging from Arris, 1989; and Arris and Eagleson, 1989). Because the soil moisture at negative five bars is so small, (see Table 3.1), it will take a long time, t_5, to reach this state. As long as $t_5 > m_{t_b}$, this "on/off" step function model of transpiration should create only negligibly small errors. We will examine the value of t_5/m_{t_b} in a subsequent section.

Table 3.1

<u>Soil Moisture Transpiration Limits in Four Typical Soils</u>

[1]   Values from Bras 1990, p. 352.
[†]   Calculated with Brooks and Corey model, see Appendix
       B.2.1 for review of model.

	CLAY	SILTY-LOAM	SANDY-LOAM	SAND
$\psi(1)$[1]	90 cm	45 cm	25 cm	15 cm
m[1]	0.44	1.2	3.3	5.4
s @-15 bars[†]	0.1	<.001	$< 10^{-10}$	10^{-17}
s @-5 bars[†]	0.16	<.003	$< 10^{-8}$	$< 10^{-14}$

5) The time between storms is exponentially distributed,

i.e., the probability density function (p.d.f.) is

$$f_t(t_b) = \alpha e^{-\alpha t_b} \qquad (3.4)$$

where α is the inverse of the mean time between storms (m_{t_b})

6) The bare soil exfiltration capacity (f_e^*) remains as it

appears in the original derivation (Eagleson 1978d):

$$
f_e^* = \begin{cases} \bar{e}_p & t \leq t_o + t^* \qquad\qquad (3.5) \\[2ex] \frac{1}{2}S_e t^{-\frac{1}{2}} - Mk_v\bar{e}_p + w & t^* + t_o < t < t_e + e^* \end{cases}
$$

where S_e is the exfiltration desorptivity.

$$
S_e = \sqrt{\frac{2\bar{e}_p^2 E}{\alpha}} \qquad\qquad (3.6)
$$

and all other terms have been defined in the review in Section 2.1.2.

7) Transpiration and exfiltration begin when the surface retention deposited by the last storm (of depth h) is completely evaporated. This time (t^*) is given by

$$
t^* = \begin{cases} \dfrac{h}{\bar{e}_p}, & h < h_o \qquad\qquad (3.7) \\[2ex] \dfrac{h_o}{\bar{e}_p}, & h \geq h_o \end{cases}
$$

where h_o is the surface retention capacity.

To accomplish the goal of replacing the constant interstorm transpiration with one whose upper bound is the finite soil moisture storage, we must first find the time at which the stored moisture is exhausted, and then rework the expected value problem under these new conditions.

3.2.2. Derivation of Time Until Stress (t_s)

This "time until stress", t_s, is found by setting the expression for the depth of evapotranspired water from the soil column equal to the soil moisture storage (V_e). This depth may be expressed as the time integral of the weighted rates of bare soil evaporation (f_e) and vegetal transpiration (e_v). These rates were reviewed in Chapter 2 and are illustrated here in Figs. 3.1 and 3.2.

As can be seen in these figures, only surface retention is evaporated until t^*, and thus t^* is the lower limit of the integral equation for exhausted moisture storage.

$$V_e = \int_{t^*}^{t_s} [(1-M) f_e + M \cdot e_v] d\tau \tag{3.8}$$

Now, substituting Eqs. 3.3, 3.5 and 3.6 into 3.8, and setting $e_v = k_v \cdot \bar{e}_p$ from assumption 4, one obtains:

$$n_e s_o z_r = \int_{t^*}^{t^*+t_o} (1-M)\bar{e}_p d\tau + \int_{t_o}^{t_e} (1-M)\left[\frac{1}{2}\sqrt{\frac{2\bar{e}_p^2 E}{\alpha}} \cdot t^{-\frac{1}{2}} - Mk_v\bar{e}_p + w\right] d\tau + \int_{t^*}^{t_s} Mk_v\bar{e}_p d\tau \tag{3.9}$$
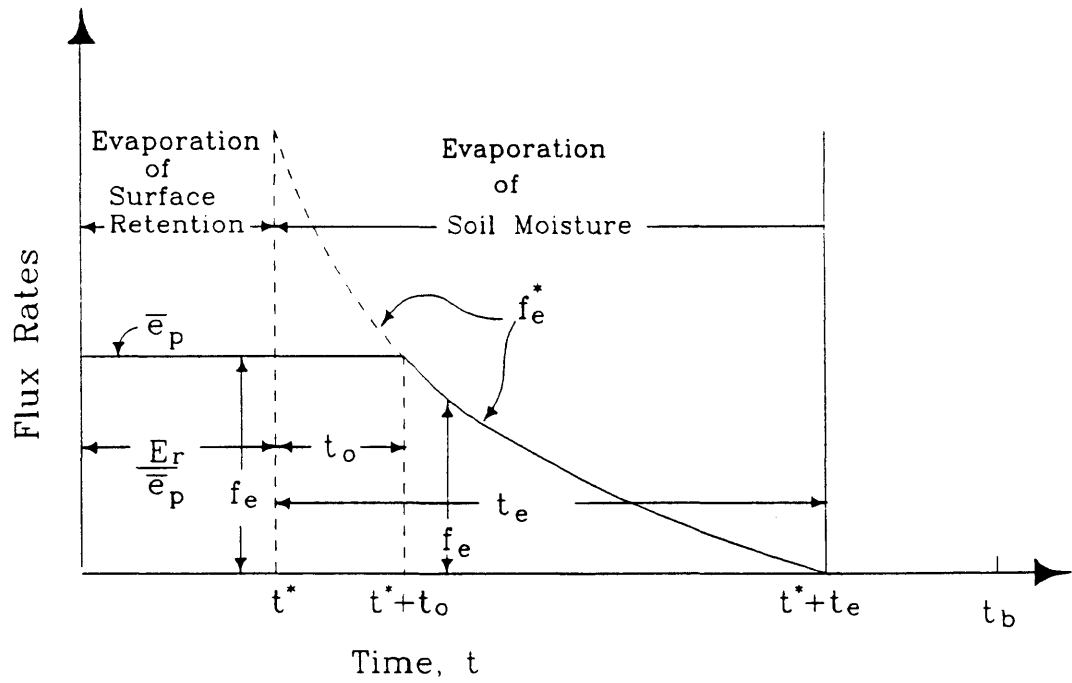
FIGURE 3.1: RATE OF BARE SOIL EVAPORATION
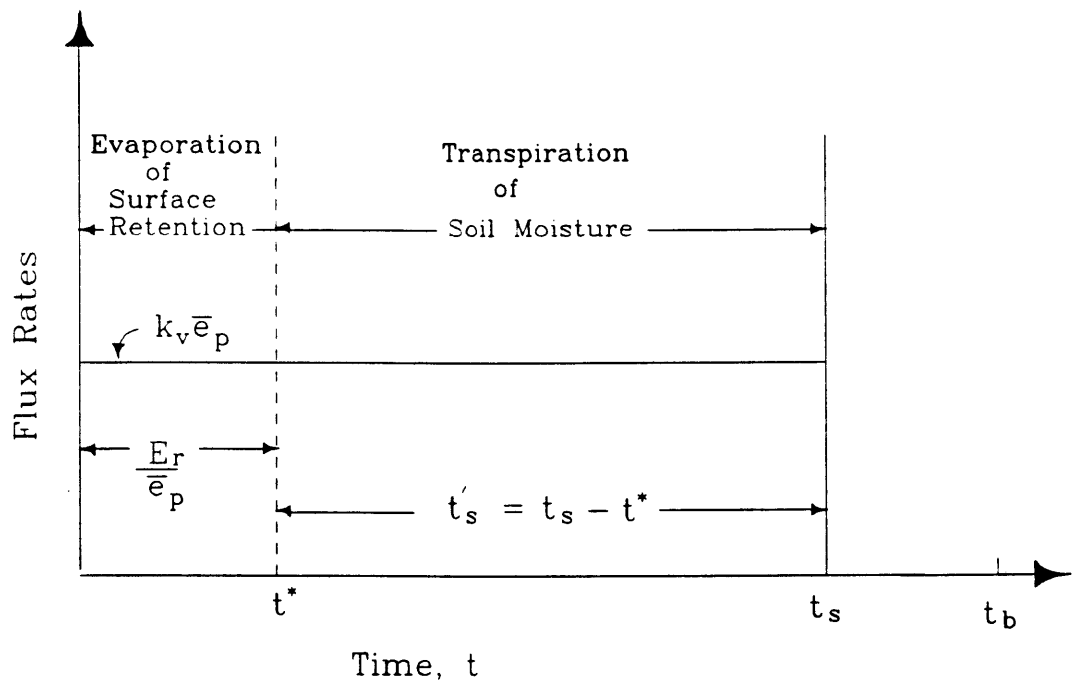
FIGURE 3.2: RATE OF VEGETAL TRANSPIRATION

Integrating and solving for t_s we have:

$$t_s = \left\{ \frac{n_e s_o z_r - (1-M)\left[\bar{e}_p t_o + \sqrt{\frac{2\bar{e}_p^2 E}{\alpha}}\left(t_e^{\frac{1}{2}} - t_o^{\frac{1}{2}}\right) - (Mk_v\bar{e}_p - w)(t_e - t_o)\right] + Mk_v\bar{e}_p t^*}{Mk_v\bar{e}_p} \right\}$$

(3.10)

Following Eagleson (1978d), this equation can be simplified by substituting the following dimensionless expressions into Eq. (3.10):

$$t_o = \frac{B \cdot E}{\alpha}$$

(3.11)

$$t_e = \frac{C \cdot E}{\alpha}$$

(3.12)

where

$$B = \frac{1-M}{1+Mk_v - \frac{w}{\bar{e}_p}} + \frac{M^2 k_v + (1-M)\frac{w}{\bar{e}_p}}{2\left(1+Mk_v - \frac{w}{\bar{e}_p}\right)^2}$$

(3.13)

and

$$C = \frac{1}{2}\left(Mk_v - \frac{w}{\bar{e}_p}\right)^{-2}$$

(3.14)

60

yielding:

$$t_s = t^* + \frac{1}{\alpha}\left[\frac{n_e S_o z_r \alpha}{Mk_v \bar{e}_p} + CE\frac{w}{\bar{e}_p}\left(\frac{1}{k_v} - \frac{1}{Mk_v}\right) + BE\frac{w}{\bar{e}_p}\left(\frac{1}{Mk_v} - \frac{1}{k_v}\right) + CE(1-M)\right.$$

$$\left. + BE\left(M - 1 - \frac{1}{Mk_v} + \frac{1}{k_v}\right) + (2B)^{\frac{1}{2}}\cdot E\cdot\left(\frac{1}{Mk_v} - \frac{1}{k_v}\right) + (2C)^{\frac{1}{2}}\cdot E\left(\frac{1}{k_v} - \frac{1}{Mk_v}\right)\right]$$

(3.15)

For future reference, we will also define the time during which
the vegetation is transpiring (t'_s). This will be the time in
between the completion of evaporation of surface retention (t^*)
and the time until stress (t_s), i.e.

$$t'_s = t_s - t^* = \frac{1}{\alpha}\left[\frac{n_e S_o z_r \alpha}{Mk_v \bar{e}_p} + CE\frac{w}{\bar{e}_p}\left(\frac{1}{k_v} - \frac{1}{Mk_v}\right) + BE\frac{w}{\bar{e}_p}\left(\frac{1}{Mk_v} - \frac{1}{k_v}\right) + CE(1-M)\right.$$

$$\left. + BE\left(M - 1 - \frac{1}{Mk_v} + \frac{1}{k_v}\right) + (2B)^{\frac{1}{2}}\cdot E\cdot\left(\frac{1}{Mk_v} - \frac{1}{k_v}\right) + (2C)^{\frac{1}{2}} E\left(\frac{1}{k_v} - \frac{1}{Mk_v}\right)\right]$$

(3.16)

Table 3.2

Estimates of t_5/m_{t_b} at Beaver Creek, AZ

([†]Soil properties from Bras 1990, p. 352)

M = 0.4

Soil\k_v	0.2	0.4	0.6	0.8	1.0
Clay[†]	2.3×10^2	1.1×10^2	6.1×10^1	2.6×10^1	$s_5 > s_o$
Silty-Loam[†]	2.8×10^2	1.3×10^2	7.7×10^1	3.8×10^1	1.2×10^0
Sandy-Loam[†]	2.6×10^2	1.2×10^2	7.1×10^1	3.3×10^1	1.2×10^0
Sand[†]	2.5×10^2	1.1×10^2	6.7×10^1	3.0×10^1	1.7×10^0
Springer-ville	2.0×10^2	9.6×10^1	5.7×10^1	2.9×10^1	1.4×10^{-1}

The values of t_5/m_{t_b} listed in Table 3.2 are sufficiently large, for all but the clay and Springerville soil-high k_v entries to ensure that the approximation error in assumption #4 is small. When this ratio is small, it is recommended that the substitutions $t_s = t_5$ and $s_0 = s_0 - s_5$ be made in the equations (3.22 - 3.25) derived in the following sections. This recommended substitution was not made in the current analysis.

Substituting

$$t_s = t_5 \qquad , \quad [t_5 \equiv t(\psi = -5\,bars)]$$

$$s_0 = s_0 - s_5 \qquad , \quad [s_5 \equiv s(\psi = -5\,bars)]$$

3.2.3   The Modified Expected Value of Evapotranspiration

($(E[ET_A^*])$)

3.2.3.1   Modified Expected Value of Interstorm Bare Soil Evaporation

The preceding analysis does not affect the expected value of bare soil evaporation ($[E_{s_j}]$) as long as the time until stress (t_s) is greater than the time at which exfiltration stops ($t^* + t_e$). This condition will always be satisfied as long as assumption 3 holds, i.e., as long as the root depth, z_r, is greater than or equal to the penetration depth of exfiltration. This can be guaranteed by explicitly setting z_r equal to the exfiltration penetration depth (z_e) given by Eagleson (1978c):

$$z_e = 4 \cdot (D_e \frac{1}{\alpha})^{\frac{1}{2}} + \frac{1}{\alpha} \cdot \frac{K(1)s_0^c}{n_e} \qquad (3.17)$$

$$D_e = \frac{\pi \; \bar{e}_p^2 \; E}{2 \, n_e^2 \, s_0^2 \, \alpha} \qquad (3.18)$$

Under these conditions, the expected value of bare soil interstorm evaporation will remain as in Eq. 2.2.

3.2.3.2 Modified Expected Value of Interstorm Transpiration $(E[E_{v_j}^*]$

Taking the expected value of the integral of the new interstorm transpiration rate (e_v) (Figure 3.2) over all the initial surface retention conditions (resulting from the gamma distributed storm depths) and over all the possible exponentially distributed times between storms gives:

$$E[E_{v_j}^*] = \int \int E_{v_j}^*(h, t_b) \, dh \, dt_b \qquad (3.19)$$

Assuming that the previous (i.e., j-1) storm depth (which is responsible for the current surface retention) and the current time between storms are independent, we have:

$$f(h, t_b) = f_H(h) \, f_T(t_b) = \frac{\alpha \lambda (\lambda h)^{\kappa-1} e^{-\lambda h - \alpha t_b}}{\Gamma(\kappa)} \qquad (3.20)$$

Now, separating the integral in (3.19) into the two regimes of e_v behavior (i.e., $e_v = k_v e_p$ for $t \le t_s$, and $e_v = 0$ for $t > t_s$) and into the two regimes of the surface retention effect (i.e., $h < h_0$ in which the last storm did not fill the surface retention capacity, and $h \ge h_0$ in which it did, we find:

64

$$E[E_{v_j}^*] = \int_0^{h_0} f(h)\,dh \cdot \left[\int_0^{\tau_s' + \frac{h}{\bar{e}_p}} k_v \bar{e}_p t_b\, f(t_b)\,dt_b + \int_{\tau_s' + \frac{h}{\bar{e}_p}}^{\infty} k_v \bar{e}_p [\tau_s' + \frac{h}{\bar{e}_p}] \cdot f(t_b)\,dt_b \right]$$

$$+ \int_{h_0}^{\infty} f(h)\,dh \cdot \left[\int_0^{\tau_s' + \frac{h_0}{\bar{e}_p}} k_v \bar{e}_p t_b \cdot f(t_b)\,dt_b + \int_{\tau_s' + \frac{h_0}{\bar{e}_p}}^{\infty} k_v \bar{e}_p [\tau_s' + \frac{h_0}{\bar{e}_p}]\, f(t_b)\,dt_b \right]$$

(3.21)

Integrating Eq. 3.21 we find:

$$E[E_{v_j}^*] = \frac{k_v \bar{e}_p}{\alpha} \left[\frac{\gamma(\kappa, \lambda h_0)}{\Gamma(\kappa)} - e^{-\alpha t_s'} \left(1 + \frac{\alpha}{\bar{e}_p}\right)^{-\kappa} \cdot \frac{\gamma(\kappa, (\lambda + \frac{\alpha}{\bar{e}_p}) h_0)}{\Gamma(\kappa)} \right.$$

$$\left. + \left(1 - e^{-\alpha\left(t_s' + \frac{h_0}{\bar{e}_p}\right)}\right) \cdot \left(1 - \frac{\gamma[\kappa, \lambda h_0]}{\Gamma(\kappa)}\right) \right]$$

(3.22)

3.2.3.3 Final Equations

If we define β_v, the transpiration reduction coefficient, as the modified interstorm transpiration ($E[E_{v_j}^*]$) divided by the potential interstorm transpiration ($E[E_{v_j}]$) we have

$$\beta_v = \frac{E[E_{v_j}^*]}{E[E_{v_j}]}$$

(3.23)

substituting the expression for $E[E_{v_j}]$ from the review in

Chapter 2 (Eq. 2.6) and simplifying we have

$$\beta_v = 1 - e^{-\alpha t'_s} \left[\left(1 + \frac{\alpha}{\lambda \bar{e}_p}\right)^{-\kappa} \frac{\gamma\left(\kappa, \left(\lambda + \frac{\alpha}{\bar{e}_p}\right) h_o\right)}{\Gamma(\kappa)} + e^{-\frac{\alpha h_o}{\bar{e}_p}} \left(1 - \frac{\gamma(\kappa, \lambda h_o)}{\Gamma(\kappa)}\right) \right]$$

(3.24)

where t'_s is given by Eq. 3.16. Note that as t'_s approaches infinity (as would occur at large soil moisture and root depths), β_v approaches unity, or "unstressed" transpiration. Also note that for the simplified case of no surface retention ($h_o = 0$) Eq. (3.24) reduces to

$$\beta_v = 1 - e^{-\alpha t'_s}$$

(3.25)

Following Eagleson (1982), we can also define a bare soil evaporation efficiency, β_s, which is the expected value of bare soil interstorm evaporation divided by the potential bare soil interstorm evaporation:

$$\beta_s = \frac{E[E_{s_j}]}{\bar{e}_p \alpha^{-1}}$$

(3.26)

Now, substituting Eq. 2.2 for $E[E_{s_j}]$ into Eq. (3.26), we obtain:

$$\beta_s = \frac{\gamma[\kappa,\lambda h_0]}{\Gamma(\kappa)} - \left[1 + \frac{\frac{\alpha h_0}{\bar{e}_p}}{\lambda h_0}\right]^{-\kappa} \frac{\gamma[\kappa,\lambda h_0 + \frac{\alpha h_0}{\bar{e}_p}]}{\Gamma(\kappa)} e^{-BE} + \left\{1 - \frac{\gamma[\kappa,\lambda h_0]}{\Gamma(\kappa)}\right\}\left\{1 - e^{-BE - \frac{\alpha h_0}{\bar{e}_p}}\right.$$

$$\cdot \left[1 + Mk_v + (2B)^{\frac{1}{2}} E - \frac{w}{\bar{e}_p}\right] + e^{-CE - \frac{\alpha h_0}{\bar{e}_p}}\left[MK_v + (2C)^{\frac{1}{2}} E - \frac{w}{\bar{e}_p}\right]$$

$$\left. + (2E)^{\frac{1}{2}} e^{-\frac{\alpha h_0}{\bar{e}_p}} [I(\frac{3}{2},CE) - I(\frac{3}{2},BE)]\right\}$$

$$+ \left[1 + \frac{\frac{\alpha h_0}{\bar{e}_p}}{\lambda h_0}\right]^{-\kappa} \frac{\gamma[\kappa,\lambda h_0 + \frac{\alpha h_0}{\bar{e}_p}]}{\Gamma(\kappa)}\left\{(2E)^{\frac{1}{2}}[\gamma(\frac{3}{2},CE) - \gamma(\frac{3}{2},BE)]\right.$$

$$\left. + e^{-CE}\left[Mk_v + (2C)^{\frac{1}{2}} E - \frac{w}{\bar{e}_p}\right] - e^{-BE}\left[Mk_v + (2B)^{\frac{1}{2}} - \frac{w}{\bar{e}_p}\right]\right\}$$

(3.27)

Finally, using 3.23, 3.24, 3.26 and 3.27 in 3.2, we have for the modified expected value of annual evapotranspiration $(E[ET_A^*])$:

$$E[ET_A^*] = [\frac{m_v \bar{e}_p}{\alpha}] \cdot [(1-M)\beta_s + M\beta_v k_v] \qquad (3.28)$$

3.3 Application and Discussion

3.3.1 Equilibrium Soil Moisture and Transpiration Reduction

Replacing the original formulation of $E[ET_A]$ of Eq. (2.17) with the modified evapotranspiration, $E[ET_A^*]$ (Eq. (3.28)) allows us to solve the annual water balance in years where $Mk_v\bar{e}_p m_v\alpha^{-1} > P_A$.

67

In order to see how the system behaves with this new formulation we present the following contour plots of the equilibrium soil moisture (Fig.3.3) and $\beta_v k_v$ (Fig. 3.4) in M-k_v space for a typical Beaver Creek watershed.

The region on the soil moisture contour plot (Fig. 3.3) where the soil moisture contours decrease rapidly (e.g., .34, .14, .04) which will be referred to as the soil moisture "cliff", exists for those sets of values of M and k_v for which the annual potential transpiration ($M k_v \bar{e}_p m_v \alpha^{-1}$) is nearly equal to the annual precipitation. It is in this region that the transpiration is reduced from its potential rate, $k_v \bar{e}_p$, to the reduced rate, $\beta_v k_v \bar{e}_p$. This behavior can also be seen in the $\beta_v k_v$ contour plot (Fig. 3.4). In this figure, $\beta_v k_v = k_v$ (i.e., $\beta_v = 1$) to the left of the cliff. There the transpiration is potential (unstressed). As the canopy density is increased at a given k_v and approaches that value for which $M k_v \bar{e}_p m_v \alpha^{-1}$ approaches P_A, β_v drops rapidly, as can be seen in the abrupt corner of the $\beta_v k_v$ contours.

Also note that the solutions to the short term ecological optimality hypothesis ($\partial s_o / dM \mid_{k_v} = 0$) can be seen in Fig. 3.3 as the locus of M-k_v pairs for which the soil moisture does not change with M, holding k_v constant.
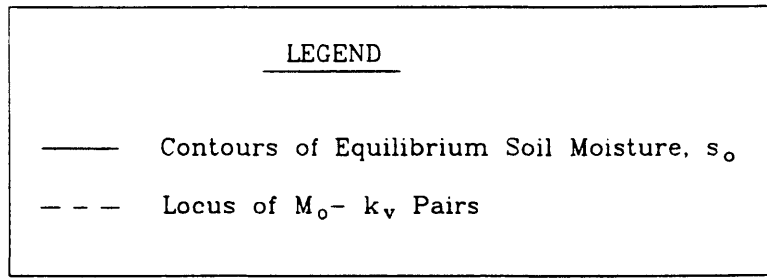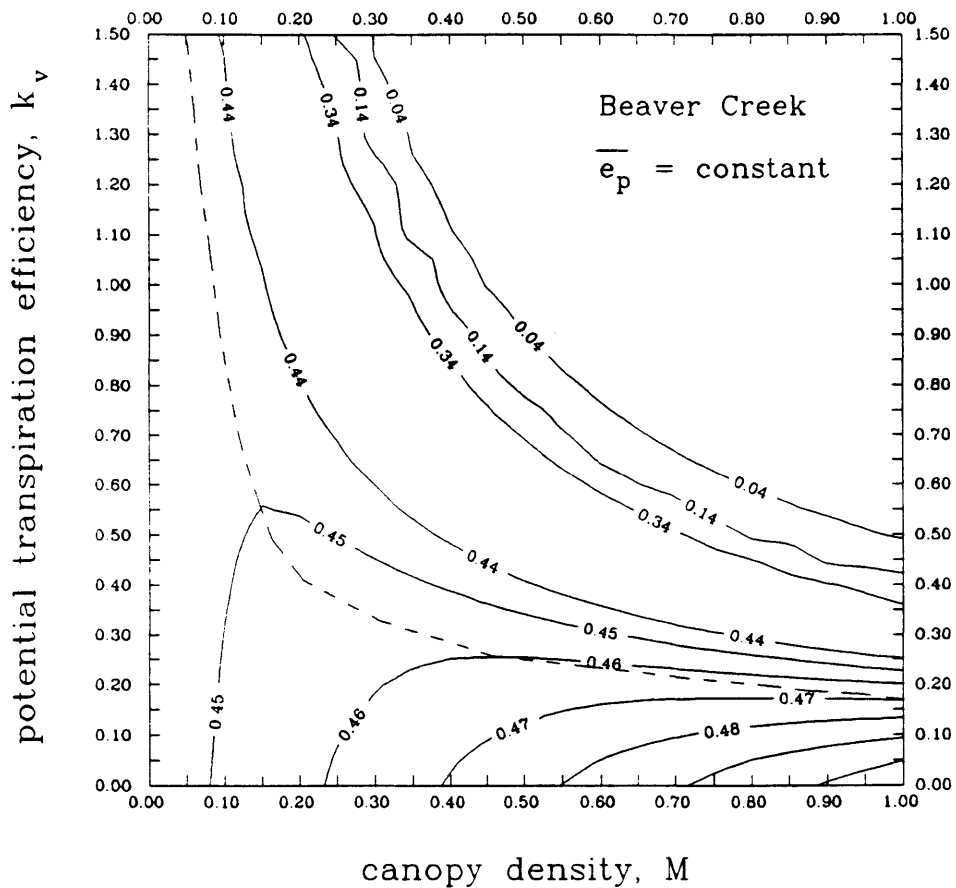
FIGURE 3.3: CONTOURS OF EQUILIBRIUM
SOIL MOISTURE IN CANOPY DENSITY –
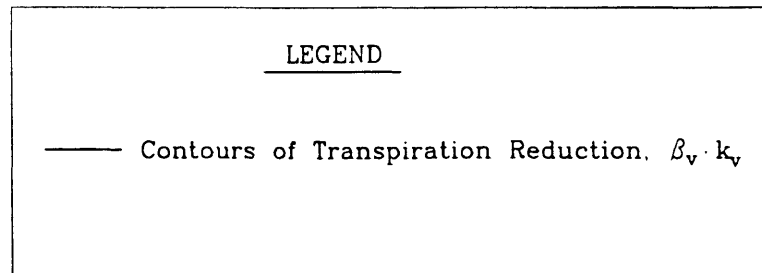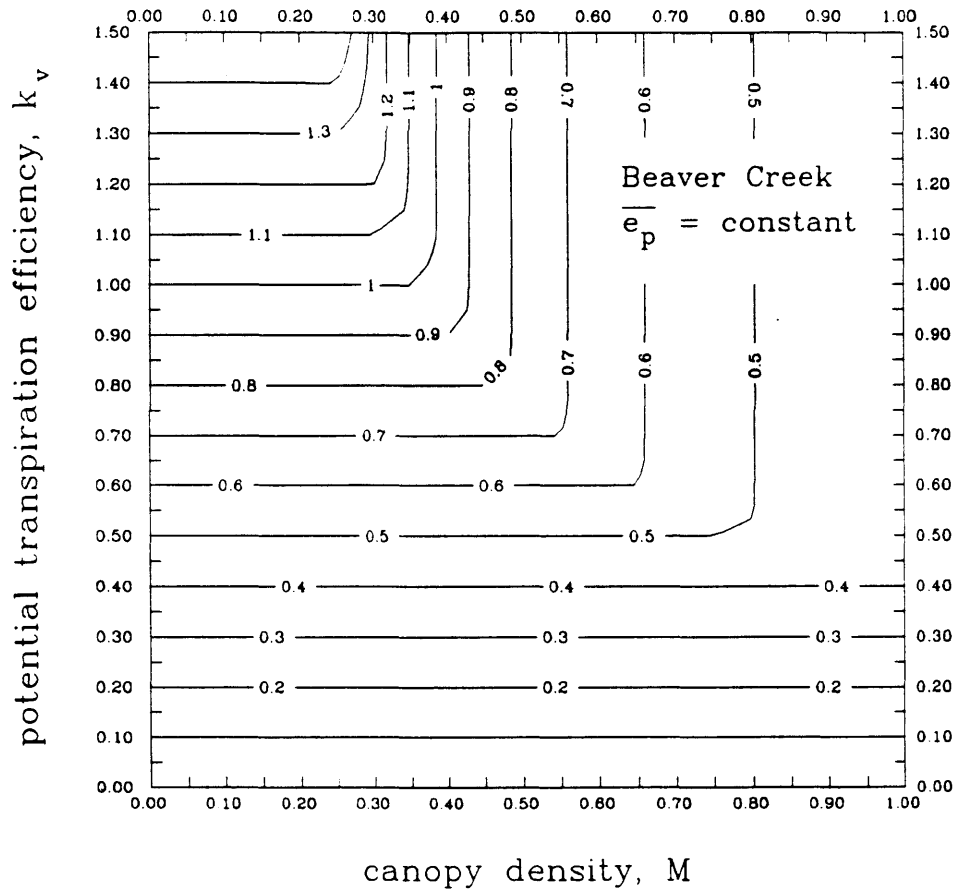POTENTIAL TRANSPIRATION EFFICIENCY
SPACE

FIGURE 3.4: CONTOURS OF TRANSPIRATION
REDUCTION IN CANOPY DENSITY –
POTENTIAL TRANSPIRATION EFFICIENCY
SPACE

Note that this locus (the dashed line of Fig. 3.3) of optimal (and hypothetically equilibrium) canopy densities are well to the left of the soil moisture cliff. This is completely consistent with Eagleson's assumption that at equilibrium the canopy will transpire at the unstressed (potential) rate.

It is also interesting to see how these plots change for a year of less precipitation (i.e., a drought year). At Beaver Creek the probability of getting less than half of the mean annual precipitation is fifteen percent (see Appendix A, Fig. A.1). This condition could therefore be expected to be realized multiple times in the life span of a typical tree. Note in Figs. 3.5 and 3.6 how the "cliff" has steepened and shifted to the left, nearing what was the locus of the hypothesized optimum canopy density (dashed line, Fig. 3.3). In semiarid climates, we conclude, vegetation must be suited to periodic conditions of stress even at their optimum canopy densities. These conditions are not encountered in humid climates where the mean annual precipitation greatly exceeds the potential evapotranspiration and the variance of mean precipitation is low.

This soil moisture cliff represents a condition under which mean evaporation exhausts the mean precipitation in the mean time between storms. When the precipitation is progressively less than this value the stored soil moisture is exhausted over a smaller and smaller fraction of the evaporation window $(t_s/t_b \rightarrow 0)$.
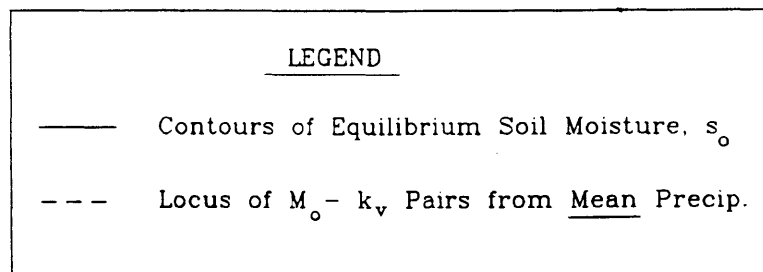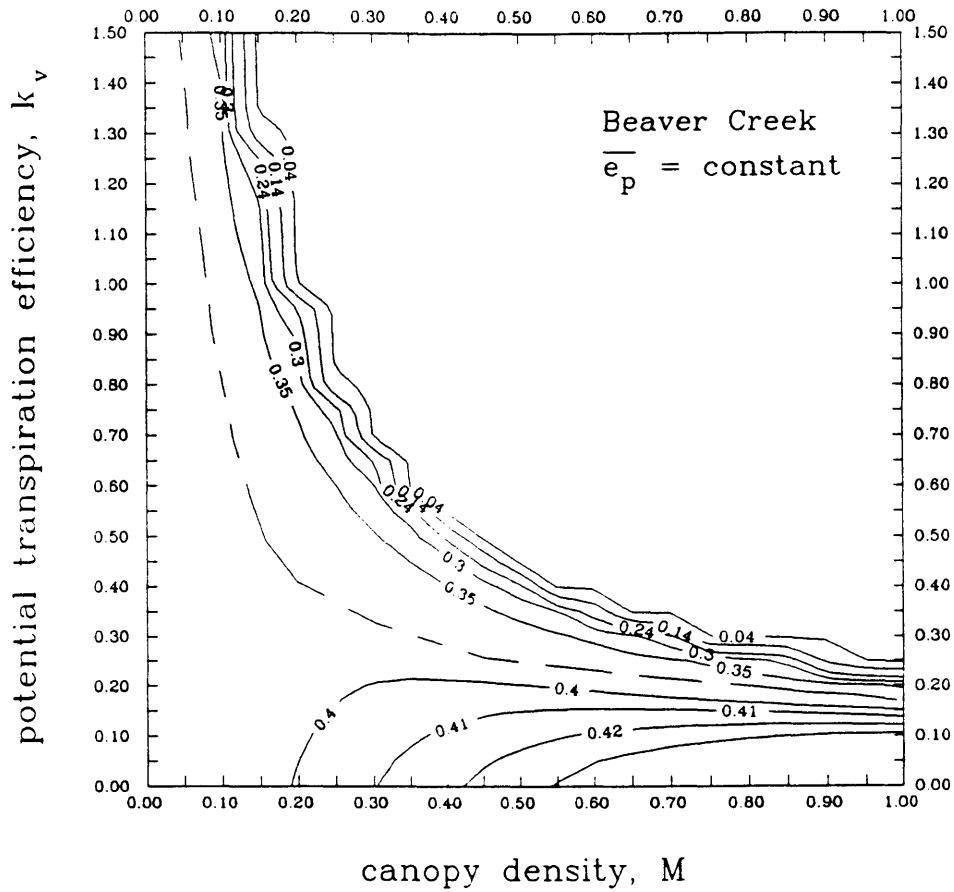
71

FIGURE 3.5: CONTOURS OF EQUILIBRIUM
SOIL MOISTURE IN CANOPY DENSITY —
POTENTIAL TRANSPIRATION EFFICIENCY
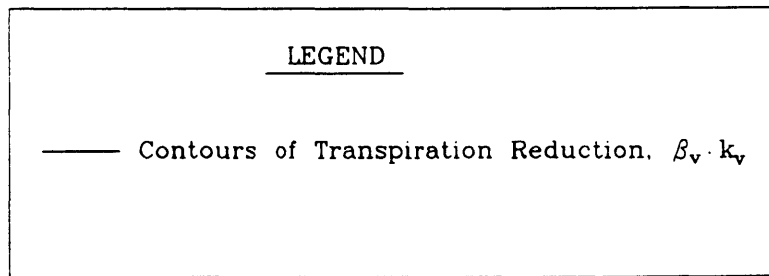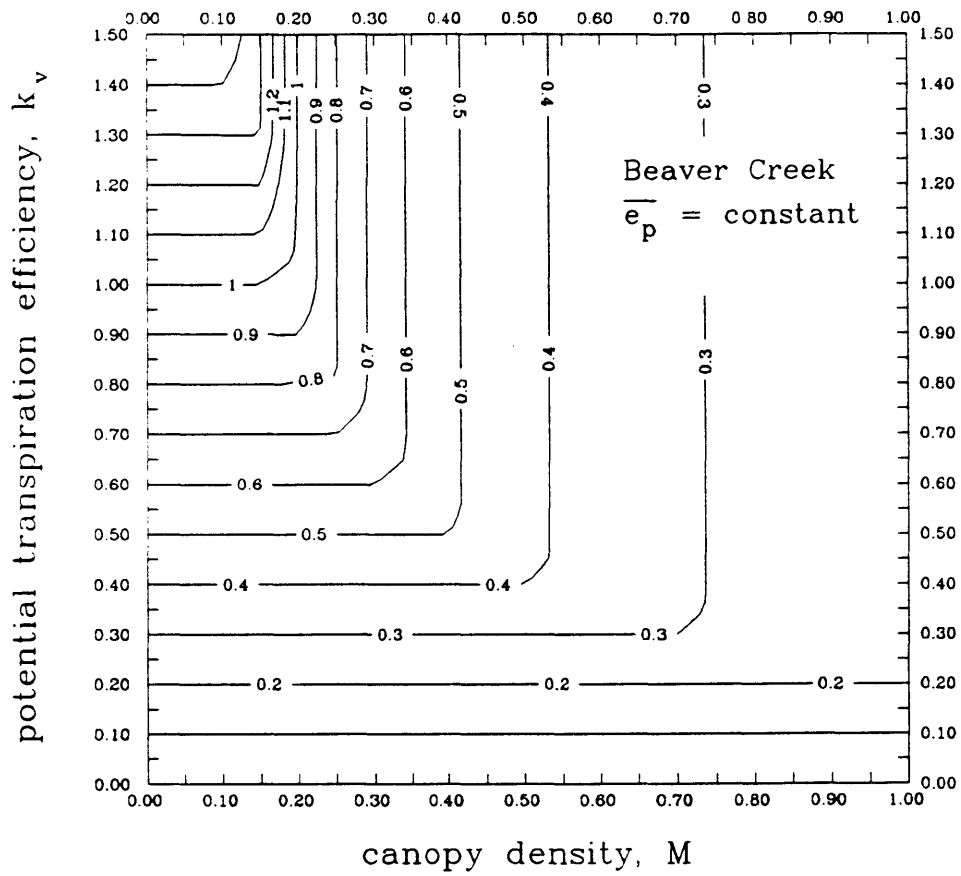SPACE UNDER CONDITIONS OF ONE HALF
MEAN SEASONAL PRECIPITATION

FIGURE 3.6: CONTOURS OF TRANSPIRATION
REDUCTION IN CANOPY DENSITY –
POTENTIAL TRANSPIRATION EFFICIENCY
SPACE UNDER CONDITIONS OF ONE HALF
MEAN SEASONAL PRECIPITATION

Also note that for any given canopy density in Figs. 3.3
and 3.5, the equilibrium soil moisture monotonically increases
with decreasing k_v. This illustrates the invalidity of the medium
term ecological optimality hypothesis ($\partial s_o/\partial k_v = 0$) as was pointed
out in Section 2.3.1.

3.3.2   Transpiration

Another revealing contour plot is that of the annual
transpiration of soil moisture $(E_{v_A}^{**})$, i.e., the total
evapotranspiration from the vegetated fraction ($M\beta vk_v e_p m_v/\alpha$) minus
the annual evaporation of surface retention on the vegetation
$(E_{r_{v_A}})$. Eagleson (1978) derives the expected value of this
vegetated fraction surface retention evaporation as:

$$E[E_{r_{v_A}}] = \frac{k_v \bar{e}_p m_v}{\alpha} \cdot \left\{ 1 - e^{-\alpha h_0/\bar{e}_p} \cdot \frac{\Gamma(\kappa, \lambda k_v h_o)}{\Gamma(\kappa)} \right.$$

$$\left. - \left[1 + \frac{\alpha h_0/\bar{e}_p}{\lambda k_v h_0} \right]^{-\kappa} \cdot \frac{\gamma\left[\kappa, \left(\lambda k_v h_0 + \frac{\alpha h_0}{\bar{e}_p}\right)\right]}{\Gamma(\kappa)} \right\}$$

(3.29)

$(E_{v_A}^{**})$ is plotted in M - k_v space in Fig. 3.7. Here, the
general behavior of increasing transpiration with increases in
M and k_v is apparent. At the locus of M - k_v pairs which resulted
in the soil moisture cliff, the rate of return of additional
transpiration with increases in either M or k_v diminishes sharply.
Whereas transpiration is a useful surrogate of biomass production

74

(since carbon assimilation through the stomata always involves water loss to the atmosphere), this plot can be thought of as indicative of biomass growth potential. Note that whereas a decline of k_v (at a given M) results in higher equilibrium soil moisture (Fig. 3.3) and less stressed transpiration (movement away from the cliff in Fig. 3.4), it also leads to less biomass growth potential (Fig.3.7).

Perhaps the dominant species will be that with a k_v which most favorably balances this tradeoff between stressed transpiration and biomass accumulation.

3.4. A Possible Species Competition Model

A quantitative model which would allow competition between species of different k_v in which the change in canopy (over aseason) of each species is positively related to transpiration (i.e., growth) and negatively related to the fraction of time spent in stress ($E[(t_b-t_s)/t_b]$) has been considered. In this model each species, acting through changes in its group canopy density, affects the equilibrium soil moisture (s_o) of the whole system. Since the time spent in stress and the transpiration are dependent on s_o, each species affects the growth and death of the other species. This model would suffer, however, from the increase in the number of parameters required to quantitatively predict the dominant (i.e., highest equilibrium canopy density) species. Specifically, for each species allowed to "compete" in the model, a coefficient relating transpiration to increases in canopy density and one relating the stress

fraction to decreases in canopy density would have to be specified. These coefficients would probably be very difficult, if not impossible, to measure in nature. Without coefficient estimates from actual measurements, one could use the model to arrive at any "answer" by merely adjusting the coefficients. The model would thus lack the utility as a tool in accomplishing the functions (e.g., parameter estimation and reduction) discussed in the introduction (Chapter 1).
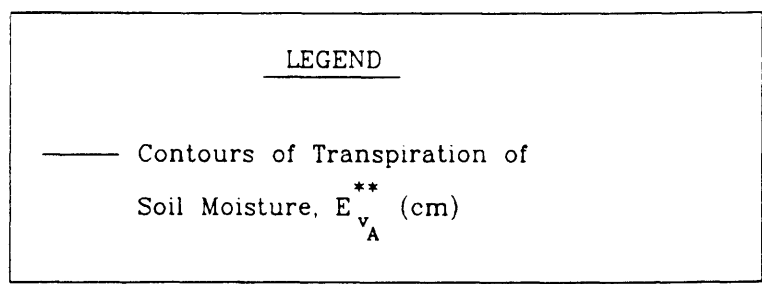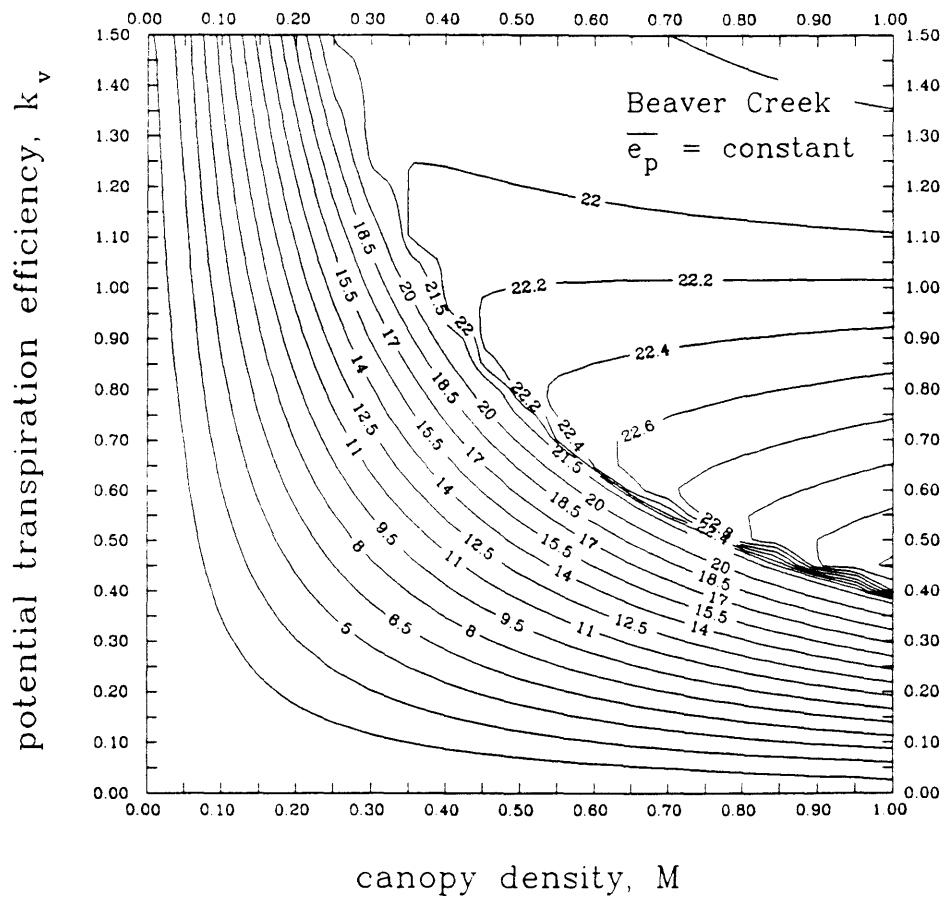
FIGURE 3.7: CONTOURS OF TRANSPIRATION
OF SOIL MOISTURE IN CANOPY
DENSITY – POTENTIAL TRANSPIRATION
EFFICIENCY SPACE

CHAPTER 4

Tests of Ecological Optimality

4.1. Beaver Creek Site Description

The tests of ecological optimality have been applied to
the Beaver Creek Experimental Watershed in the Coconino Forest
in Central Arizona (see Figure 4.1). The area was divided
into eighteen extensively gaged watersheds by the U.S. Forest
Service in the late 1950s in order to test the effect of tree
removal on basin yield. Due to the nature of the Forest
Service study, each watershed has a different history of
monitoring and treatment (e.g., tree cabling, pesticide
spraying, etc.). Because this study is applicable to natural-
ly vegetated watersheds, only the untreated watershed data
years have been used. The untreated records range from five
to twenty-five years per watershed. For a review of the
Forest Service findings on the tree removal-water yield issue,
see Clary et al., 1974 and Brown et al., 1974.

The climate and vegetation of the watersheds vary rapidly
with elevation (Figures 4.2 and 4.3). Below the lowest gaged
watershed is arid semi-desert. This gives way to semiarid
pinyon-juniper woodland above (at about five thousand feet)
and finally to ponderosa pine forest at elevations of
6,500 feet.

The soils are shallow and generally clayey (Williams, et
al., 1967; also see Appendix B.2.2). The precipitation is
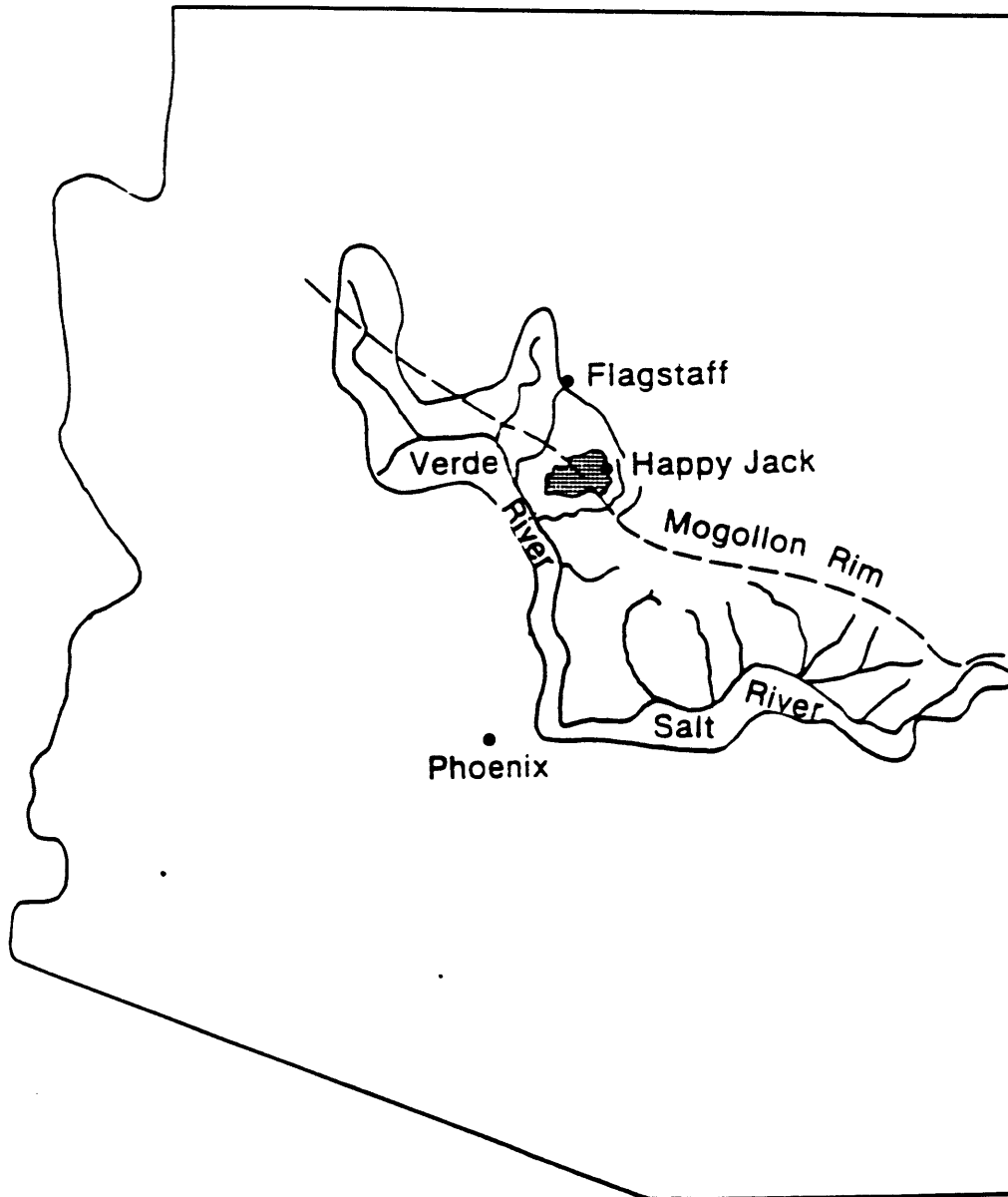
State of Arizona

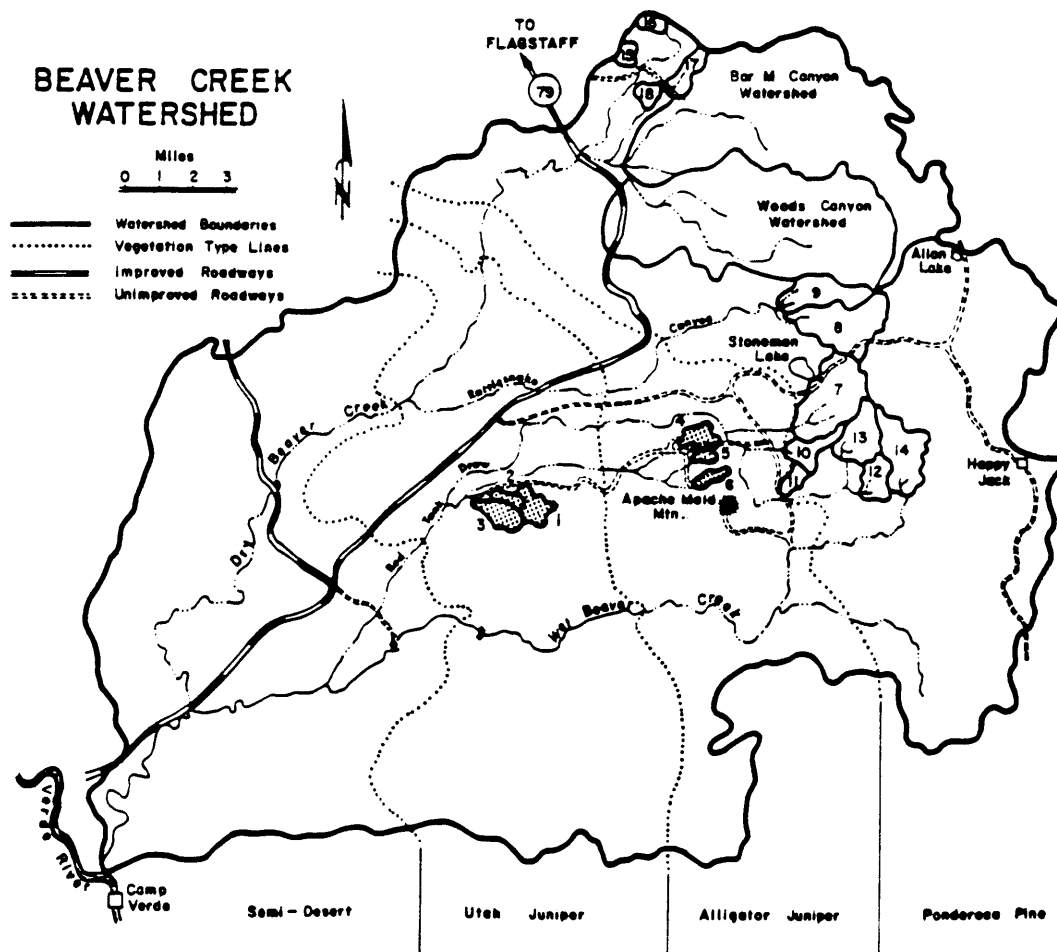FIGURE 4.1: BEAVER CREEK LOCATION MAP
(BAKER, 1982)

FIGURE 4.2: BEAVER CREEK WATERSHED
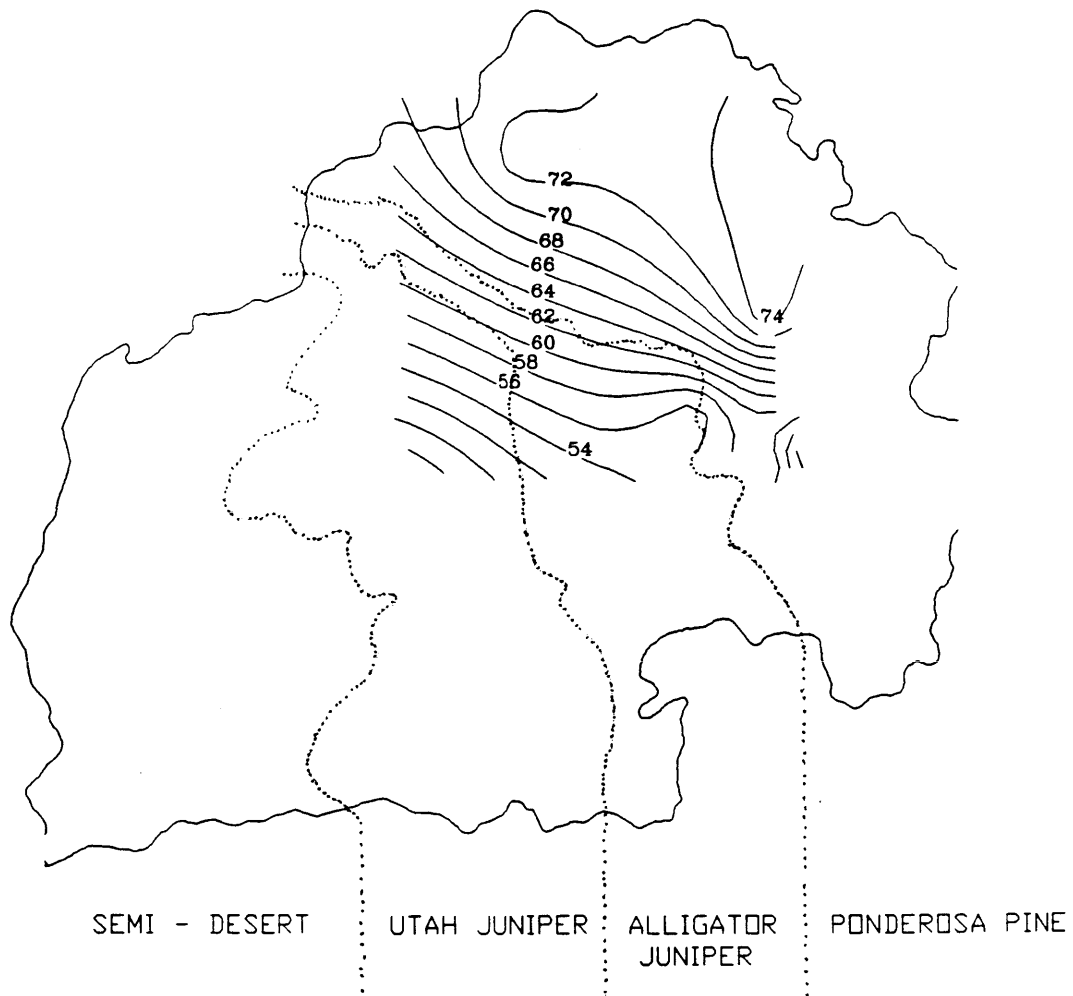(CLARY ET AL., 1974)

FIGURE 4.3: MEAN ANNUAL ISOHYETS AT
BEAVER CREEK ARIZONA (CM.)

highly seasonal, consisting primarily of convective thundershowers in the summer (July, August and September) and frontal storms in the winter (October through April) (Baker, 1982). May and June have little precipitation. Most of the runoff is produced in the winter and spring from snowmelt and less than two percent of the precipitation is lost to deep percolation because the shallow soil is underlain by a relatively impervious lava bedrock (Baker, 1982). This lack of deep percolation means that the observed streamflow is truly capturing the total basin yield. That these pinyon-juniper woodlands will make an excellent test of Eagleson's hypotheses is supported by Neil West's remarks (North American Terrestrial Vegetation, p. 224, 1988), in which he states that, due to severe water limitations, junipers will often spread their roots two to three times their crown diameter. This kind of laterally distributed root sink is one of the assumptions of the water balance model on which the ecological optimality hypotheses are based.

4.2 Considerations Regarding Testing Season

4.2.1 Choice of Testing Season

In past tests of the ecological optimality hypotheses (Eagleson and Tellers, 1982), the season during which the hypotheses were assumed to apply was the growing season, which was assumed to coincide with the rainy season for the catchments tested. In Beaver Creek, however, the rainy season includes the cold winter months (when low winter temperatures

significantly reduce transpiration) and excludes the warm spring. This seasonality, which can be seen in the moving twenty-eight day "window average" of temperature, precipitation, percent snow, and streamflow for watersheds two and eighteen (Figs. 4.4 and 4.52), necessitates a more careful choice of testing season.

Additionally, snow is not explicitly accounted for in the dynamics of the water balance model, and thus represents another constraint upon the choice of season.

Williams et al. (1967), report the first and last days of the growing season for Montezuma Castle, AZ, which is at an elevation significantly lower than the lowest tested watershed (3100 ft. vs. 5100 ft.), and Flagstaff, AZ, which is higher than the highest tested watershed (7800 vs. 7300 ft.). Linear interpolation between these elevations results in the growing seasons listed in Table 4.1.

It was decided, however, that this method of linear interpolation ignores the local micro-climate of the individual watersheds and that this microclimate (e.g., exposure) might contribute to the variations in canopy density. To capture this effect, we instead used 28-day average percentage of precipitation that was either snow or mixed rain and snow as the index of the onset and end of the testing season, arbitrarily choosing fifty percent as the limiting value. This choice results in a longer testing season than the first method (see Table 4.2) but has the benefit of excluding snow from the moisture dynamics of the water balance in a
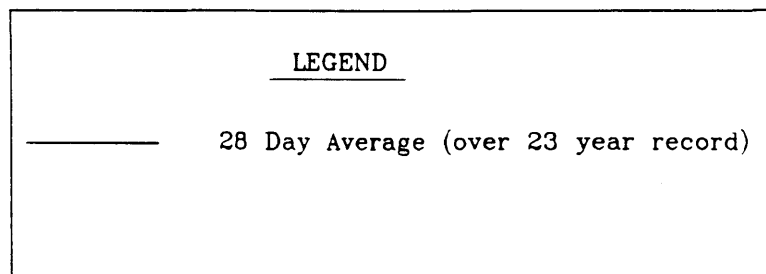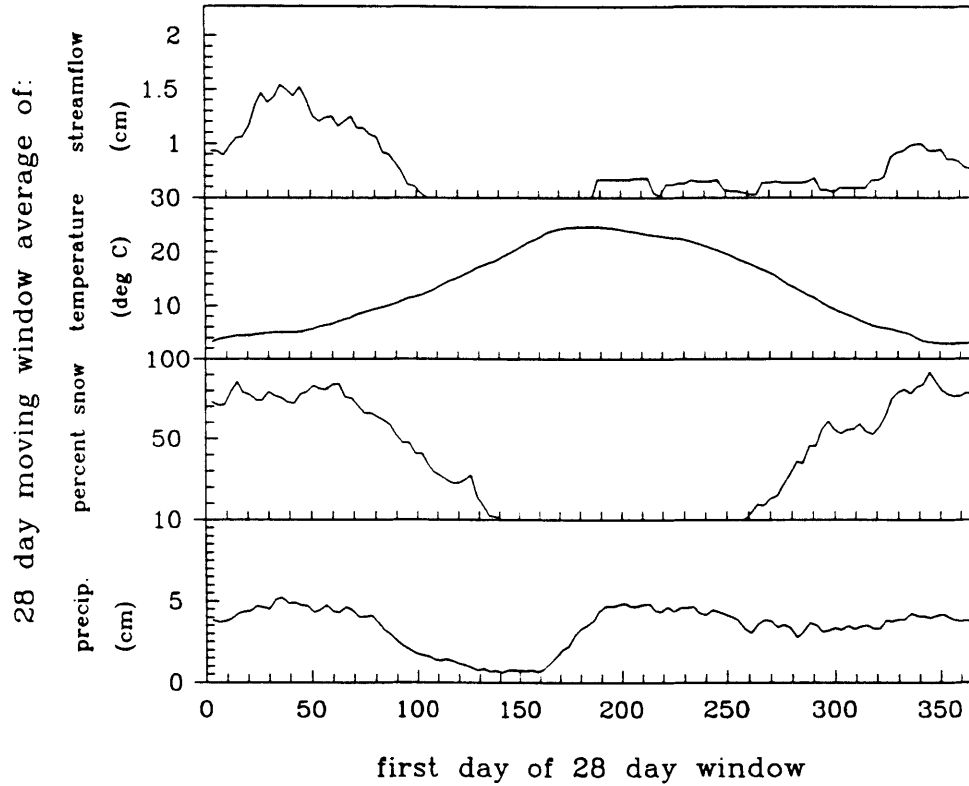
FIGURE 4.4: TWENTY—EIGHT DAY MOVING WINDOW AVERAGE OF HYDROLOGIC AND CLIMATIC VARIABLES AT BEAVER CREEK WATERSHED #2
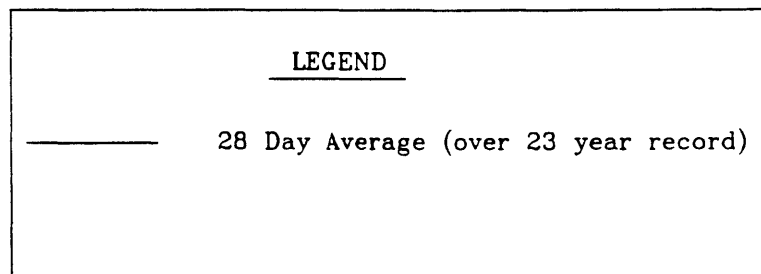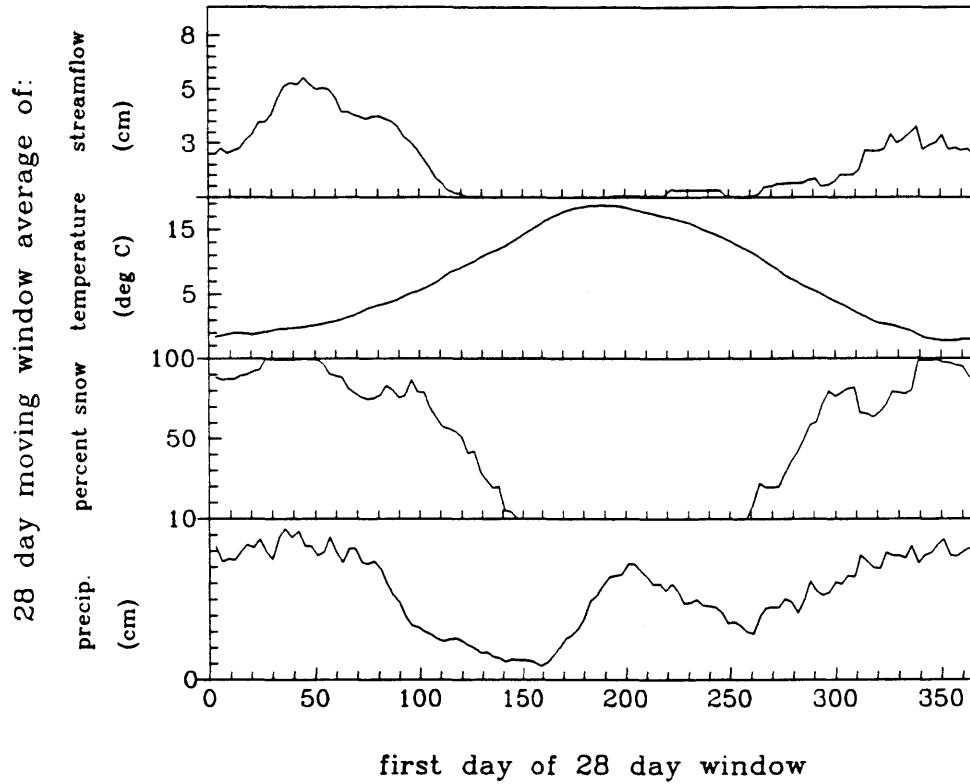
FIGURE 4.5: TWENTY–EIGHT DAY MOVING WINDOW AVERAGE OF HYDROLOGIC AND CLIMATIC VARIABLES AT BEAVER CREEK WATERSHED #18

TABLE 4.1

Growing Season at Beaver Creek

WATERSHED	ELEVATION MID-AREA (FT.)	FIRST DAY	LASTDAY	LENGTH
1	5,500[1]	130	284	154
2	5,240[1]	126	287	161
3	5,200[1]	125	287	162
4	6,250[1]	141	278	137
5	6,420[1]	144	276	132
6	6,450[1]	144	276	132
7	6,620[2]	147	275	128
8	7,300[2]	157	268	111
9	7,198[2]	155	269	114
10	6,520[2]	145	275	130
11	6,410[2]	144	276	132
12	7,054[2]	153	271	118
13	7,201[2]	155	269	114
14	7,198[2]	155	269	114
15	6,900[2]	151	272	121
16	7,100[2]	154	270	116
17	6,939[2]	152	272	120
18	6,739[2]	149	273	124

[1] estimated from topographic maps

[2] Baker, 1986

TABLE 4.2

Less than Fifty Percent Snow Season

	FIRST	LAST	LENGTH
1	10 Apr	31 Oct	205
2	13 Apr	31 Oct	202
3	10 Apr	03 Dec	238
4	25 Apr	22 Oct	181
5	25 Apr	22 Oct	181
6	19 Apr	19 Oct	184
7	28 Apr	16 Oct	172
8	01 May	16 Oct	169
9	25 Apr	19 Oct	178
10	01 May	16 Oct	169
11	04 May	16 Oct	166
12	22 Apr	16 Oct	178
13	13 May	19 Oct	160
14	01 May	19 Oct	172
15	13 May	25 Oct	166
16	28 Apr	22 Oct	178
17	28 Apr	22 Oct	178
18	13 May	25 Oct	166

systematic way. The resulting lapse rate of the growing season length with elevation ($\approx$ 20 days/1000 ft) is consistent with that reported by Lowe (1985, p. 86) for Arizona (15-30 days/1000 ft). The longer testing season also has the benefit of reducing the uncertainty in the soil moisture recharge during the non-testing season. Estimating this recharge, which we will refer to as "winter soil moisture recharge", is the subject of the next section.

4.2.2   Estimation of Winter Soil Moisture Recharge

Separating the testing season from the rest of the year introduces the possibility of a carryover in soil moisture storage from the winter non-testing season, when precipitation generally exceeds evapotranspiration, to the summer testing season, when the opposite is true. In order to estimate this soil moisture recharge (which could play an important role in getting the vegetation through the summer months), a set of simple approximations were made. They are:

During the winter:

1)   There is no evaporation from the vegetated fraction
       M, and

2)   The bare soil fraction (1-M), evaporates at the
       winter potential rate.

With these assumptions, the winter evaporation (E_w) becomes:

88

$$E_W = (1 - M)\,\overline{e}_{P_W}\,m_{V_W}\,\alpha_W^{-1} \qquad\qquad (4.1)$$

where

m_{V_W} = mean number of winter storms (sec)

α_W = inverse of mean time between winter storms (sec^{-1})

$\overline{e}_{P_W}$ = winter potential evaporation rate (cm sec^{-1})

To within about two percent, the product of the mean number of storms and the mean time between storms ($m_V \cdot \alpha^{-1}$) may be approximated by the mean season length (m_T) (i.e., the total duration of storms, $m_V \delta^{-1}$, is negligible in comparison with the total duration of interstorms, $m_V \cdot \alpha^{-1}$). With this approximation, 4.1 simplifies to

$$E_W = (1 - M)\,\overline{e}_{P_W} m_{T_W} \qquad\qquad (4.2)$$

And the winter soil moisture recharge (R_W) is:

$$R_W = P_W - E_W - Y_W = P_W - (1-M)\,\overline{e}_{P_W} m_{T_W} - Y_W \qquad (4.3)$$

where

P_W = non-testing season ("winter") precipitation, and

Y_W = non-testing season ("winter") streamflow.

The winter average potential evaporation rate, $\overline{e}_{P_W}$ is estimated in Appendix B.1.

The maximum errors that could be associated with the above formulation are bounded by the limits of the assumptions (1 and 2). That is, the most soil moisture recharge (R_W)

would occur if there were no winter evaporation whatsoever, in which case

$$R_{w,max} = P_w - Y_w \qquad (4.4)$$

The least soil moisture recharge would occur if the whole landsurface (bare and vegetated), evaporated at the winter potential rate, in which case the winter evaporation becomes:

$$\overline{E}_w = \overline{e}_{P_w} \cdot m_{T_w} \qquad (4.5)$$

and the recharge becomes:

$$R_{w,min} = P_w - \overline{e}_{P_w} \cdot m_{T_w} - Y_w \qquad (4.6)$$

This range in our estimate of winter soil moisture recharge ($R_{w,min}$ to $R_{w,max}$) will be quantified and serve to bracket our best estimate of R_w as given by Eq. (4.3). The range will appear in the error bars of testing season normalized evapotranspiration in the tests that follow.

4.3   Tests of Short Term Equilibrium Canopy Density Hypothesis

4.3.1   Assumptions

In this instance, it is assumed that trees, grass and shrubs draw from the same soil moisture reserve. Whereas the soil is only one meter deep on these watersheds, and grasses in semiarid regions often have rooting depths measured in meters (Larcher, 1983), this assumption is probably valid. The assumption is also consistent with past use of the water

90

balance model (El-Hemry, 1980; El-Hemry and Eagleson, 1980) and past tests of ecological optimality (e.g., Eagleson and Tellers, 1982; Tellers, 1980 and Tellers and Eagleson, 1980), where different vegetation types in the same watersheds are lumped into a single composite canopy cover.

The possibility of keeping the vegetative components separate will be explored in Section 4.7.

The tree canopy density (M_T) on the woodland watersheds (e.g., the pinyon-juniper watersheds numbered one through six on Figure 4.2) have been previously calculated from aerial photographs (Baker, personal communication) and their values are reported by Clary et al. (1974). The average tree canopy density of the twelve forested watersheds (e.g., the ponderosa pine watersheds numbered seven through eighteen) was reported by Baker (1986). See Table 4.3 for these values.

Jasinski and Eagleson (1990), using remotely sensed radiation data and stochastic estimation theory, estimated the tree canopy density of watershed #4 to be 0.23.

The understory density, which is comprised mostly of shrubs, forbs and perennial grasses (Clary, et al., 1974), was estimated from measurements of herbage production by assuming a linear relation between herbage production (in pounds/acre) and canopy density. The average (pre-watershed treatment) herbage yield was 194 lbs/acre for watersheds one, two and three and 518 lbs/acre for watersheds four, five and six (Clary et al., 1974). For the Ponderosa Pine watersheds (seven through eighteen) it was 198 lbs/acre (Brown et al.,

1974). The maximum herbage yield where there were no competing trees was 1150 lbs/acre (Clary et al., 1974). Based on corresponding photographs in that publication, we will assume that this corresponds to a closed understory canopy (i.e., $M_u = 1$). Our linearity assumption thus gives the following understory canopies:

$$M_u = \frac{194}{1150} = 0.17 \qquad \text{(WS \#1, 2, 3)}$$

$$M_u = \frac{518}{1150} = 0.45 \qquad \text{(WS \#4, 5, 6)}$$

and

$$M_u = \frac{194}{1150} = 0.17 \qquad \text{(WS \#7 - 18)}$$

In order to estimate the lumped (composite) canopy density (M_*) it is assumed that "understory" occupies only that surface which is unshaded by the overstory. This is perhaps the simplest model of their above ground interaction. That is, under the trees the suppression of understory transpiration is complete while out from under the trees the understory transpires freely without shielding by the trees. (For a more complex model of this interaction see Eagleson and Segarra, 1985).

The analytical expression of this assumption is

$$M_* = M_T + (1 - M_T)M_U \qquad (4.7)$$

The final lumped canopy densities resulting from this method are listed individually for the six woodland watersheds and as an average for the forested watersheds in Table 4.3.

TABLE 4.3

Observed Canopy Densities at Beaver Creek Watershed

	M_T	M_u	M_*
1	.28 ± .02	.17	.40 ± .02
2	.30 ± .02	.17	.42 ± .02
3	.28 ± .02	.17	.40 ± .02
4	.12 ± .01	.45	.52 ± .01
5	.14 ± .01	.45	.53 ± .01
6	.13 ± .02	.45	.52 ± .02
7 - 18	.83 ± .03	.17	.85 ± .03

Similarly, the potential transpiration efficiency of the overstory (k_{v_T}) and understory (k_{v_u}), are lumped into a composite k_{v_*}. To retain the same total transpiration we write

$$M_* k_{v_*} \bar{e}_P = M_T k_{v_T} \bar{e}_P + [M_u (1 - M_T) k_{v_u} \bar{e}_P] \qquad (4.8)$$

or

$$k_{v_*} = \frac{(M_T) k_{v_T} + (M_u (1 - M_T)) k_{v_u}}{M_T + M_u (1 - M_T)} \qquad (4.9)$$

k_{v_T} and k_{v_u} are estimated with a method developed by Arris (1989). This estimation is done in Appendix B.3 and the results are listed in Table 4.4. In all of the testing that

follows, the capillary rise (w) will be identically set to zero (i.e., Eq. (2.13) will not be used). This implies that there is no accumulation of percolated water on the impermeable bedrock at the bottom of the soil control volume at Beaver Creek.

Table 4.4

Estimated Potential Transpiration Efficiencies at Beaver Creek

Watershed	k_{v_T}	k_{v_u}	k_{v_*}
1 - 6	.6	.6	.6
7 - 18	NA	NA	NA

4.3.2 Tests

As discussed in Section 2.3.2, it is possible to test the short term hypothesis (hypothesis 1) by solving Eq. (2.21) $\partial E[E_{T_A}]/\partial M|_{k_v,climate,soil} = 0$ for E, the dimensionless evaporation effectiveness, as a function of the optimum density, M_o (i.e., the canopy for which Eq. (2.21) holds). The resulting function, $E(M_0)$, can then be substituted into the equation for θ, the normalized evapotranspiration. θ will now be a

function of M_o, k_v, and three other dimensionless parameter groups, $\alpha h_o/\bar{e}_p$, κ and λh_o.

Tellers (1980) performed a sensitivity analysis of $\theta(M_o)$ (for $k_v = 1$) on these parameters and his results are presented in Figs. 4.6 and 4.7. These three dimensionless parameters do not vary greatly over the Beaver Creek and $\theta(M_o)$ is not strongly dependent upon them. The function $\theta(M_o)$ will thus be evaluated at the average value of these parameters so that the results may be presented on a single graph.

To compare the hypothesized relationship, $\theta(M_o)$ with our observations at Beaver Creek, we need to estimate θ. The testing season evapotranspiration (ET_S) was estimated as the average observed testing season precipitation (P_S) minus the average observed testing season runoff (Y_S) plus the average estimated winter soil moisture recharge (R_w). The testing season potential evaporation is:

$$E_{P_S} = \bar{e}_{P_S} m_{v_S} \alpha_S^{-1} \qquad (4.10)$$

where

$\quad m_{v_S}$ = mean number of testing season storms

$\quad \bar{e}_{P_S}$ = testing season potential evaporation rate (cm sec^{-1})

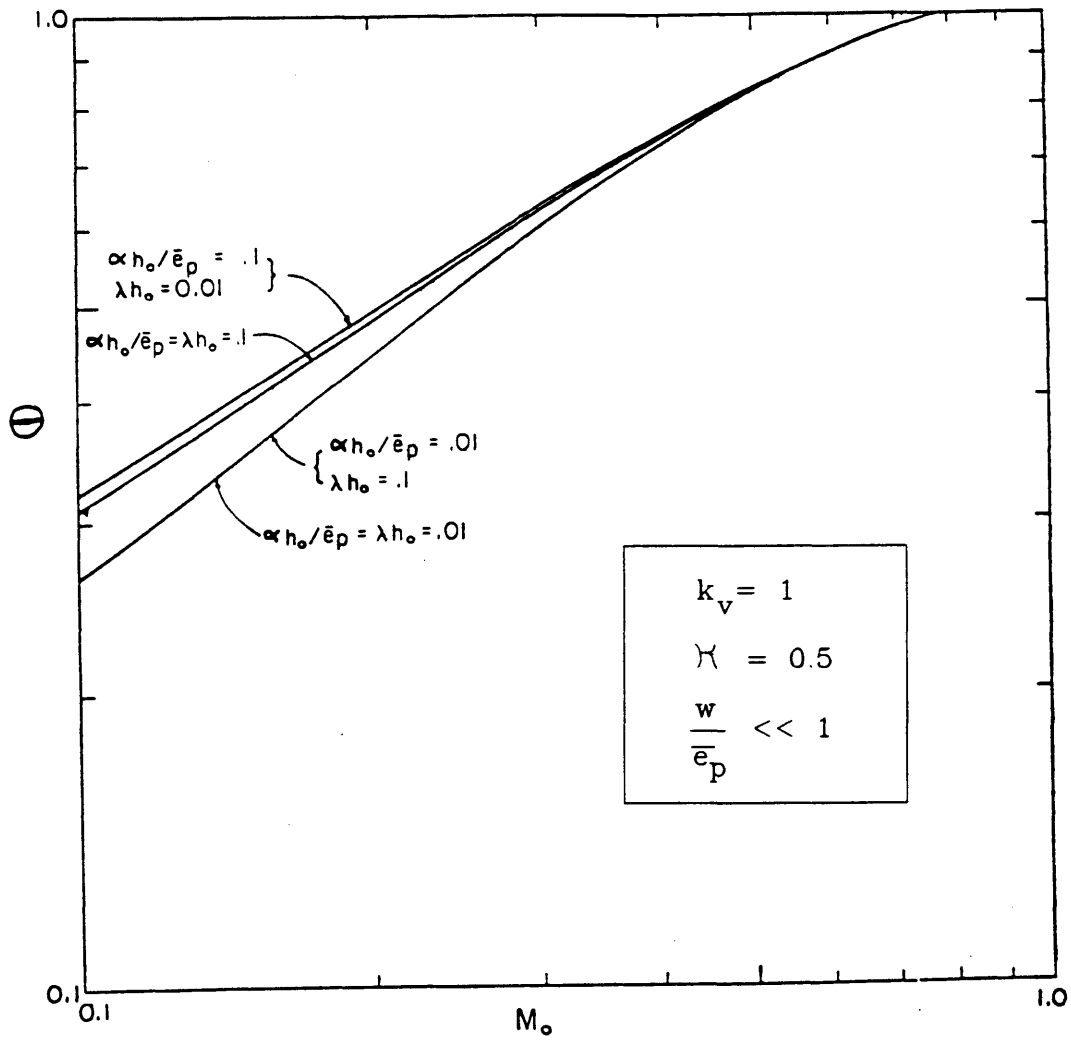$\quad \alpha_S$ = inverse of mean testing season time between storms (sec^{-1})

96

FIGURE 4.6: SENSITIVITY OF
NORMALIZED EVAPOTRANSPIRATION
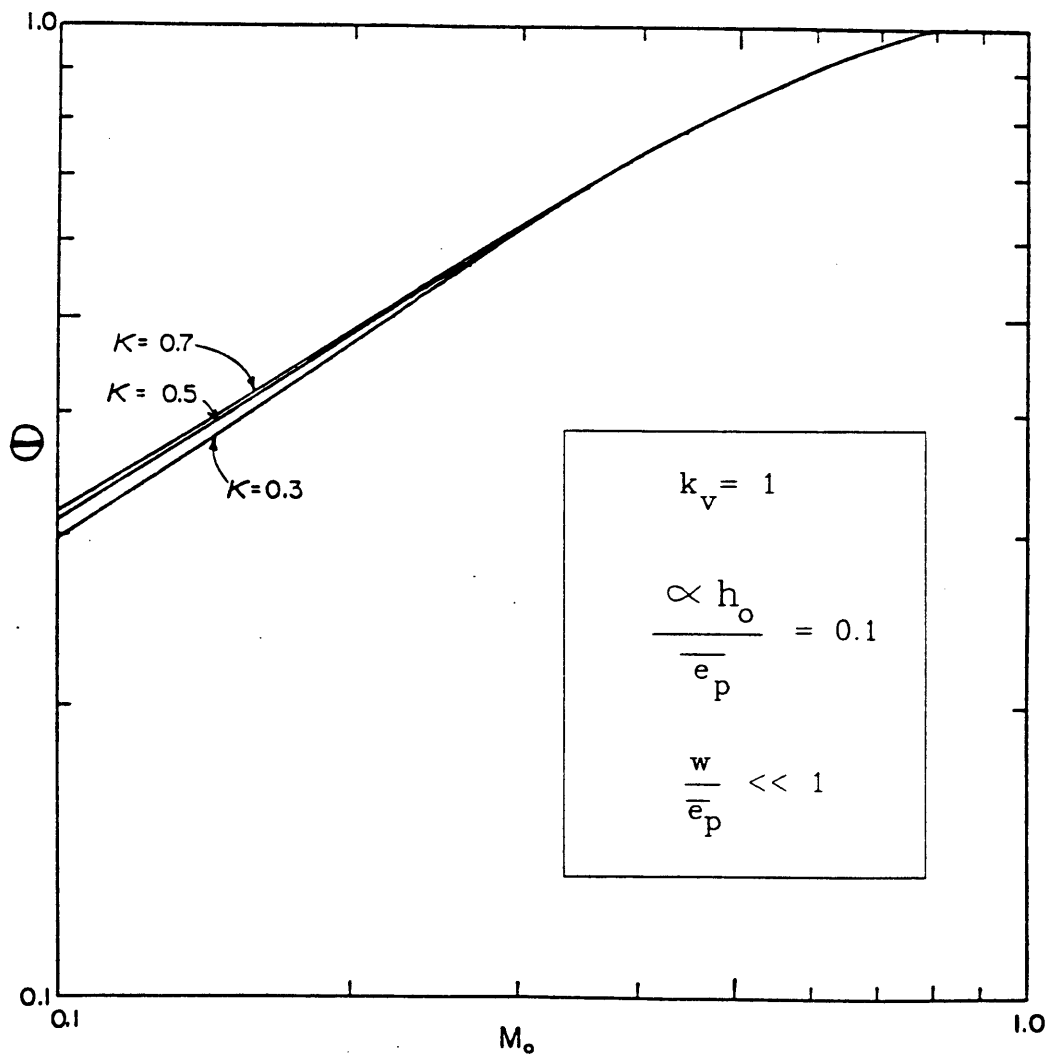TO THE DIMENSIONLESS PARAMETERS
$\propto h_o / e_p$ AND λh_o

FIGURE 4.7: SENSITIVITY OF
NORMALIZED EVAPOTRANSPIRATION
TO $\varkappa$

$\theta_{observed}$ is thus:

$$\theta_{observed} = \frac{ET_S}{E_{P_S}} = \frac{P_S - Y_S + R_W}{\overline{e}_{P_S} \, m_{v_S} \, \alpha_S^{-1}} \qquad (4.11)$$

As discussed in Section 4.2.2, to within about two percent, the product of the mean number of storms and the mean time between storms $(m_v \cdot \alpha^{-1})$ can be approximated by the mean season length (m_τ). With this approximation, 4.11 simplifies to

$$\theta_{observed} = \frac{P_S - Y_S + R_W}{\overline{e}_{P_S} \, m_{\tau_S}} \qquad (4.12)$$

The potential evaporation rates used in the above analysis are estimated in Appendix B.1.

Table 4.5 gives the resulting $\theta_{observed}$ for watersheds one through six (the woodland watersheds) and for the average of the data at watersheds seven through eighteen (remember we only have an average canopy density for these forested watersheds). Included in the table are: M_*, from Table 4.3; k_{v_*} from Appendix B.3; the average potential evaporation rates $\overline{e}_{P_S}$ and $\overline{e}_{P_W}$ from Appendix B.1; testing season average temperature $(\overline{T}_S)$; testing and off testing season precipitation P_S and P_W, and yield Y_S and Y_W; the years of data used (the untreated years); the estimated θ; the range of possible error in θ found by using $R_{W,min}$, $R_{W,max}$ in Eq. (4.12) instead of R_W; the testing season precipitation statistical parameters m_{t_b}, m_{t_r}

Table 4.5

Watershed Parameters and Water Balance Components

WS#	YEARS	M_*	k_v*	$\bar{e}_{p_S}$	$\bar{e}_{p_W}$	m_{τ_S}	m_{τ_W}	P_S	P_W	Y_S	Y_W	θ	θ_{max}	θ_{min}	R_W
				$(cm\ day^{-1})$	$(cm\ day^{-1})$	(day)	(day)	(cm)	(cm)	(cm)	(cm)				(cm)
1	58-62	.4 ±.02	0.6	0.35	0.15	205	160	23.7	22.0	0.17	.78	0.43	0.62	0.33	7.13
2	58-80	.42 ±.02	0.6	0.36	0.15	202	163	20.2	23.6	0.51	2.96	0.36	0.56	0.27	6.11
3	58-67	.4 ±.02	0.6	0.33	0.15	238	127	25.9	18.1	0.76	1.55	0.39	0.53	0.32	5.14
4	58-72	.52 ±.02	0.6	0.34	0.16	181	184	24.6	28.4	1.02	11.32	0.43	0.66	0.38	3.16
5	58-72	.53 ±.02	0.6	0.34	0.15	181	184	24.6	28.4	0.95	11.01	0.45	0.68	0.39	3.97
6	59-64	.52 ±.02	0.6	0.34	0.15	184	181	22.6	23.8	0.11	3.84	0.48	0.69	0.36	6.96
7-18	58-80	.85 ±.03	NA	0.32	0.18	169	196	22.3	39.1	0.67	12.80	0.79	0.88	0.40	20.99

m_{t_b}	m_{t_r}	λ	κ	h_o	$\bar{T}_S$
(day)	(day)	(cm^{-1})		(cm)	(oc)
5.33	0.12	0.96	0.61	0.1	18.5
6.20	0.12	0.72	0.45	0.1	19.3
6.06	0.14	0.80	0.53	0.1	17.7
5.69	0.12	0.62	0.49	0.1	16.4
5.69	0.12	0.62	0.49	0.1	15.8
5.85	0.12	1.0	0.73	0.1	15.5
5.32	0.12	0.56	0.41	0.1	14.2

λ and κ; and the surface retention parameter (h_o) which we set at the nominal value of 0.1 cm.

Fig. 4.8 shows the comparison of the hypothesized $\theta(M_o)$ relationship (for the estimated k_v value of 0.6) to the six woodland watershed (i.e., pinyon-juniper) observations listed in Table 4.3. The apparent goodness of fit is strong evidence of the validity of the short-term optimality hypothesis.

For comparison and sensitivity analysis, Fig. 4.9 shows the hypothesized $\theta(M_o)$ relationship for a range of k_v values (0.55 to 1) and the θ observations for both the woodland and forested watersheds.

The pinyon-juniper woodland watershed appears to be best fit with a k_{v_*} of 0.55, which is well within the accuracy of our k_{v_*} estimate of 0.6. The ponderosa pine watersheds appear best fit by a k_{v_*} of 0.8, but without an independent estimate of k_v the result is inconclusive.

As discussed in Section 2.3.2 (errata) the θ - M_0 pairs found in Eagleson and Tellers (1982) are represented here in correct form, in Fig. 4.10.

4.4 Test of Short Term Equilibrium Canopy Density with Observed Soil Hydraulic Properties

4.4.1 Original Formulation

A more rigorous test of the short term optimality hypothesis can be accomplished by simultaneous solution of
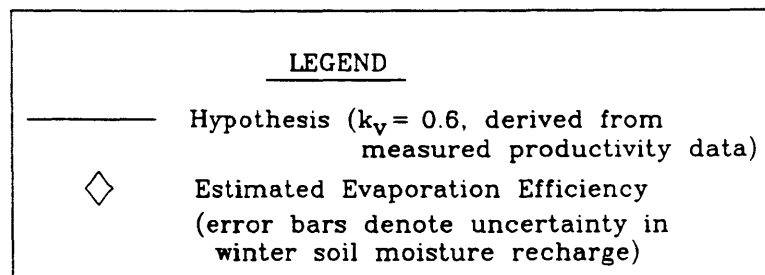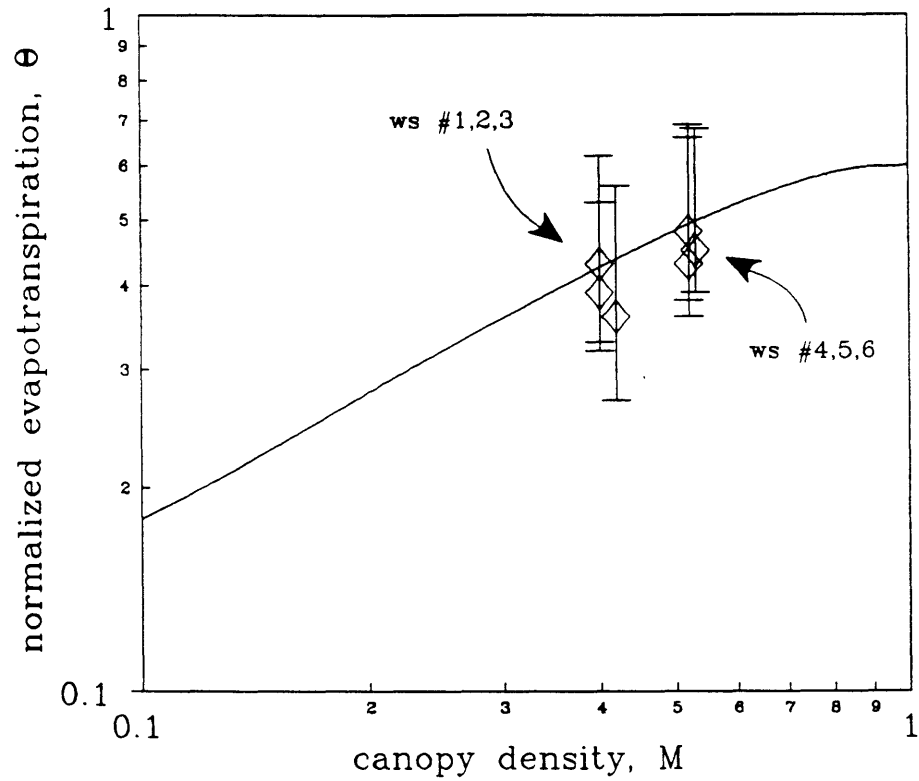
FIGURE 4.8: TEST OF SHORT TERM OPTIMALITY
HYPOTHESIS AT THE WOODLAND WATERSHEDS
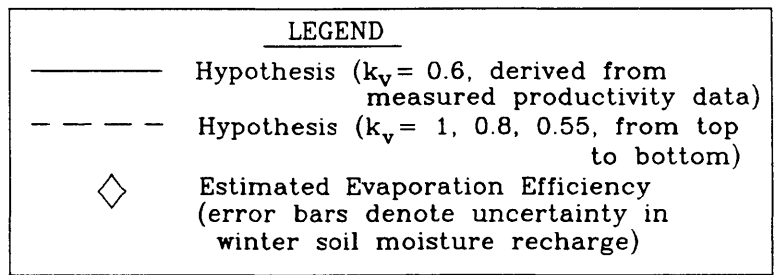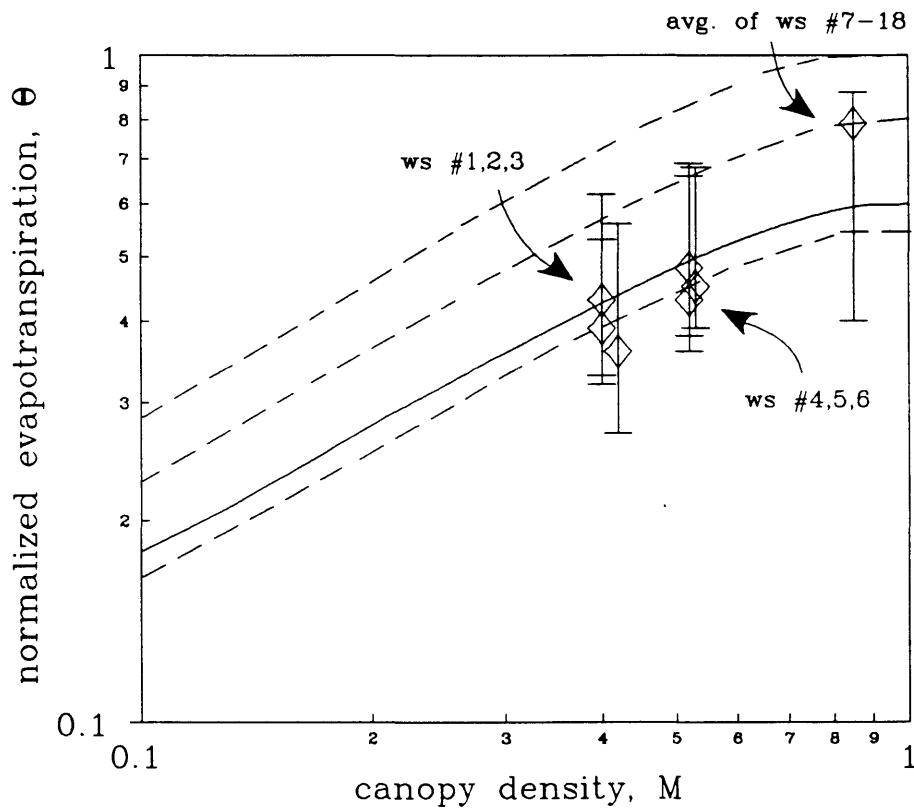
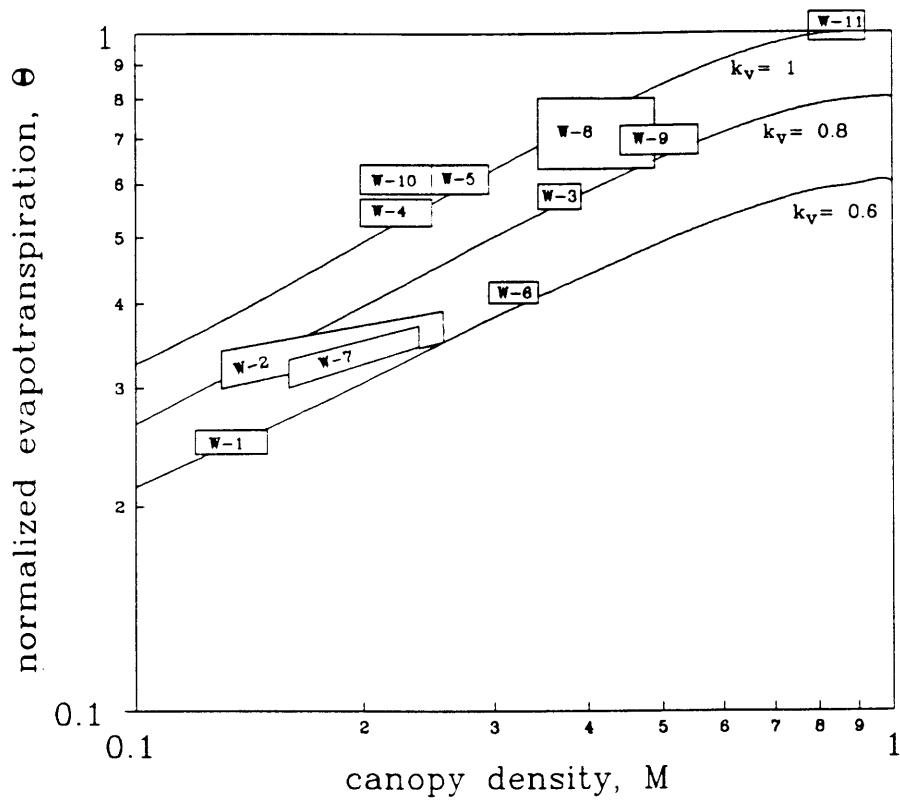FIGURE 4.9: SENSITIVITY OF SHORT TERM OPTIMALITY TEST TO CHANGES IN POTENTIAL TRANSPIRATION EFFICIENCY
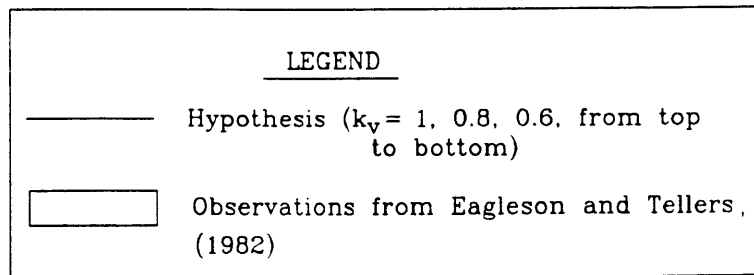
FIGURE 4.10: CORRECTED SHORT TERM
OPTIMALITY TEST FROM EXISTING
LITERATURE

the short-term hypothesis (Eq. 2.21) and the water balance
equation (Eq. 2.15). In the previous test the dimensionless
evaporation effectiveness, E, was "hidden" in the background
of each of the θ-M_o pairs which make up the theoretical curves
of Figs. 4.9 and 4.10. In specific cases, however, this
parameter (which contains not only soil and climate parameters
but also the system's state variable, s_o) will be fixed by the
water balance equation.

By solving the water balance equation with <u>observed</u> soil
properties (see Appendix B.2 for estimation), climate and
precipitation parameters (Table 4.5) and plant transpiration
coefficient at different canopy densities, one can cross-check
the optimality hypothesis with the water balance equation. To
the degree that the observed canopy density corresponds to the
maximum   equilibrium   soil   moisture   (or   minimum
evapotranspiration), and to the degree that this model
predicted evapotranspiration and yield match the observed
values, the hypothesis is further confirmed. Additionally,
this method of analysis provides a sensitivity analysis of the
hypothesis.

Figs. 4.11 through 4.13 demonstrate this analysis for
watersheds two, four and the average of watersheds seven
through respectively. In all cases, the observed canopy is
<u>two</u> to <u>three</u> times larger than the optimum canopy density.
Figs. 4.14 through 4.16 show the normalized water balance
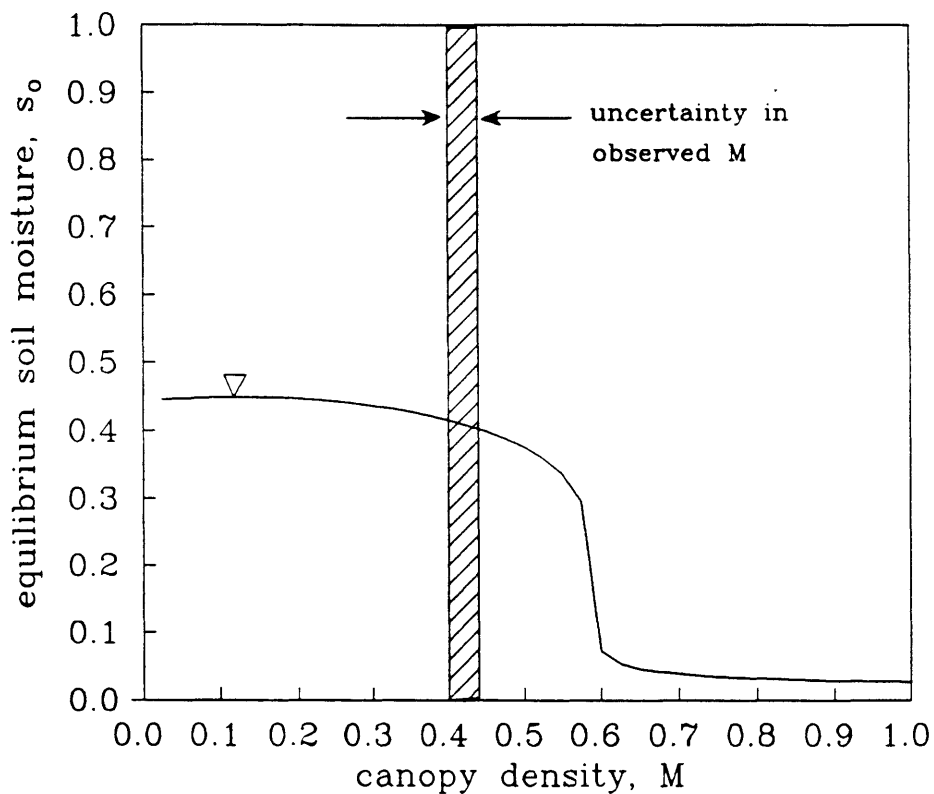component predictions and observation. At the optimum canopy
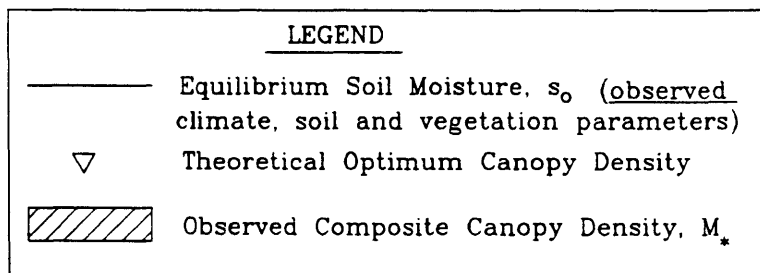
FIGURE 4.11: SENSITIVITY OF EQUILIBRIUM
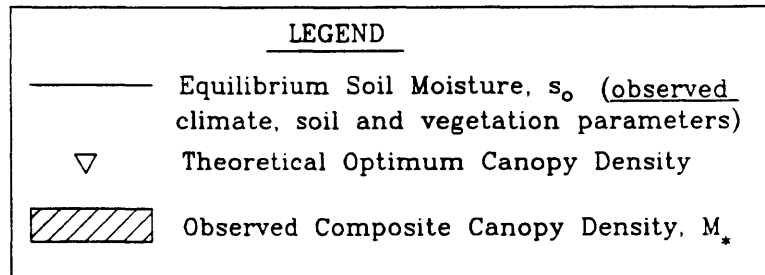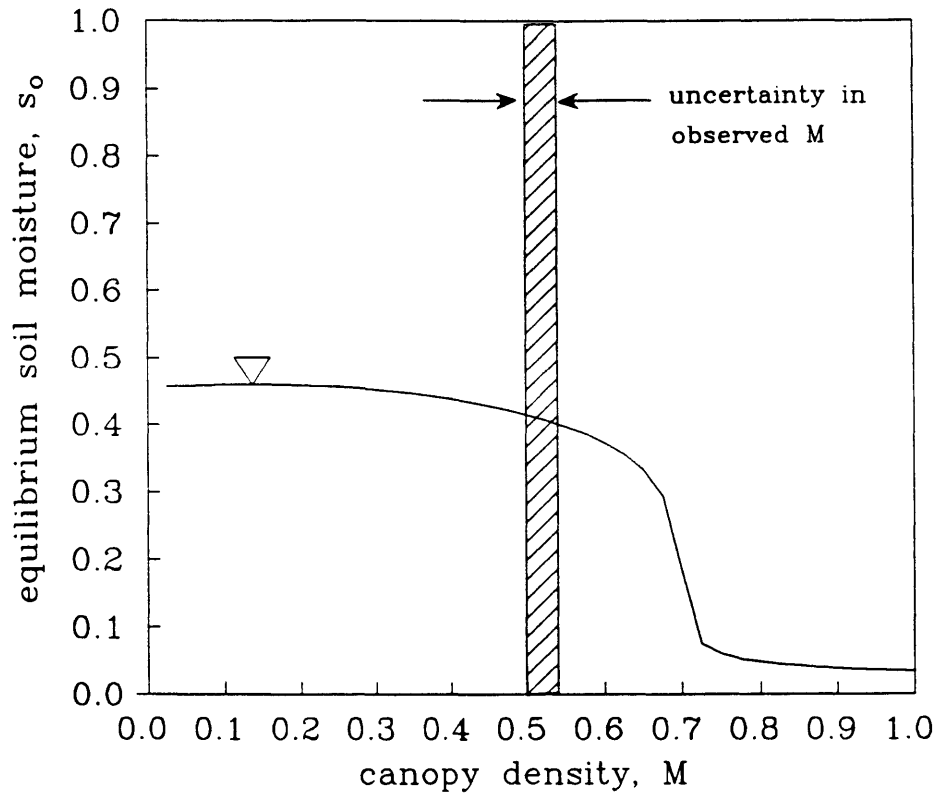SOIL MOISTURE TO CANOPY DENSITY,
WATERSHED #2, BEAVER CREEK ARIZONA

FIGURE 4.12: SENSITIVITY OF EQUILIBRIUM
SOIL MOISTURE TO CANOPY DENSITY,
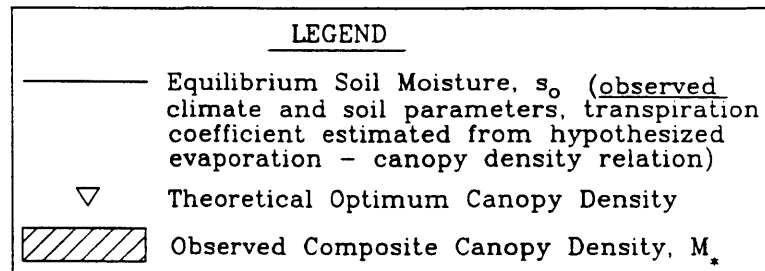WATERSHED #4, BEAVER CREEK ARIZONA
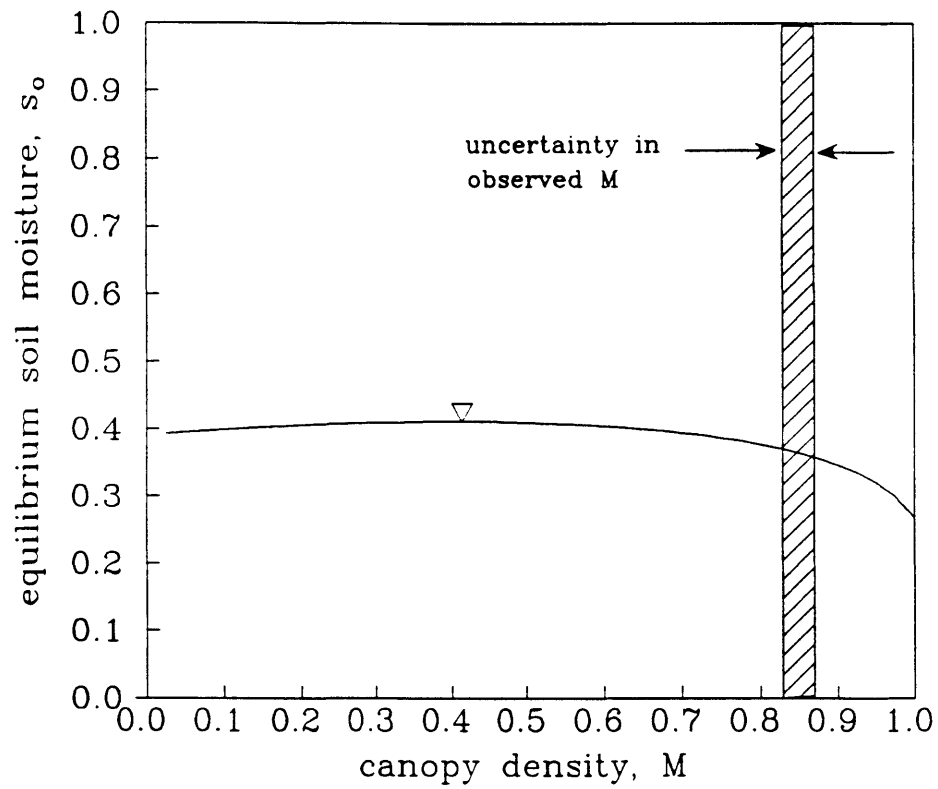
FIGURE 4.13: SENSITIVITY OF EQUILIBRIUM
SOIL MOISTURE TO CANOPY DENSITY,
FORESTED WATERSHEDS, BEAVER CREEK
ARIZONA

FIGURE 4.14: SENSITIVITY OF MEAN
WATER BALANCE TO CANOPY DENSITY,
WATERSHED #2, BEAVER CREEK ARIZONA
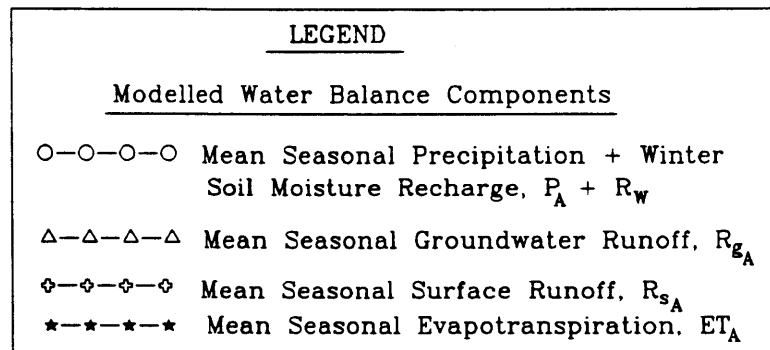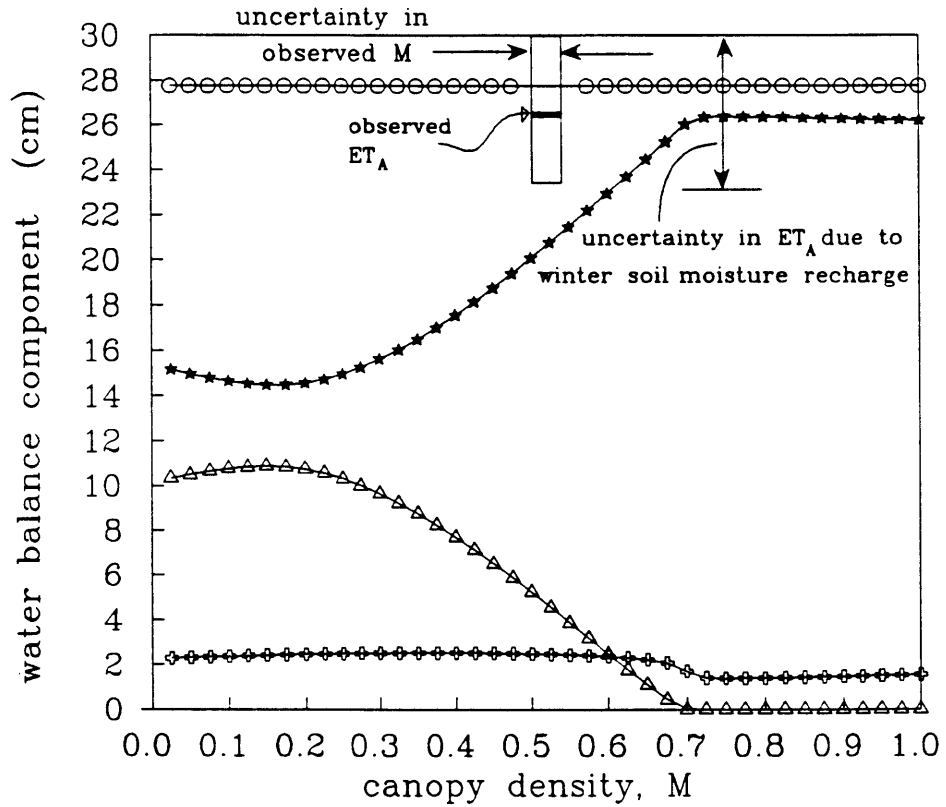
FIGURE 4.15: SENSITIVITY OF MEAN
WATER BALANCE TO CANOPY DENSITY,
WATERSHED #4, BEAVER CREEK ARIZONA

FIGURE 4.16: SENSITIVITY OF MEAN
WATER BALANCE TO CANOPY DENSITY,
FORESTED WATERSHEDS
BEAVER CREEK ARIZONA

density, the predictions are poor, especially for the groundwater component.

There are two possible interpretations of the preceding results. The first is that the previously promising results of Figs. 4.9 and 4.10 were fortuitous and the systems are not operating at the hypothetical optimum canopy densities. That the predicted evapotranspiration at the observed canopy densities matches the observed evapotranspiration reasonably well supports this interpretation. Under this interpretation, the canopy doesn't equilibrate at the canopy which produces the maximum soil moisture, but instead appears to maximize the evapotranspiration. An alternative interpretation is that the water balance equation is being misused. This possibility will be addressed in the following section.

4.4.2   Modification of Water Balance Model for Shallow
         Soils

4.4.2.1   Motivation

Careful inspection of Figs. 4.14 through 4.16 reveals that at the hypothetically optimum canopy density, a large groundwater component is predicted. However, the intermittent and "spiked" nature of the streamflow record in the Beaver Creek, especially in the summer, implies that the yield is mostly surface runoff. This nature can be seen in the hydrographs for the years 1962 - 1965 (Fig. 4.17). This observation raises the question of whether a groundwater component is sustainable under the hydrogeologic
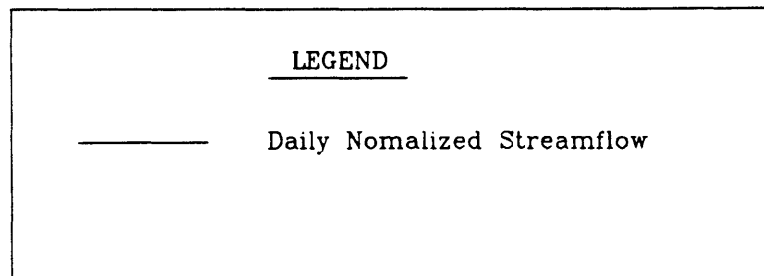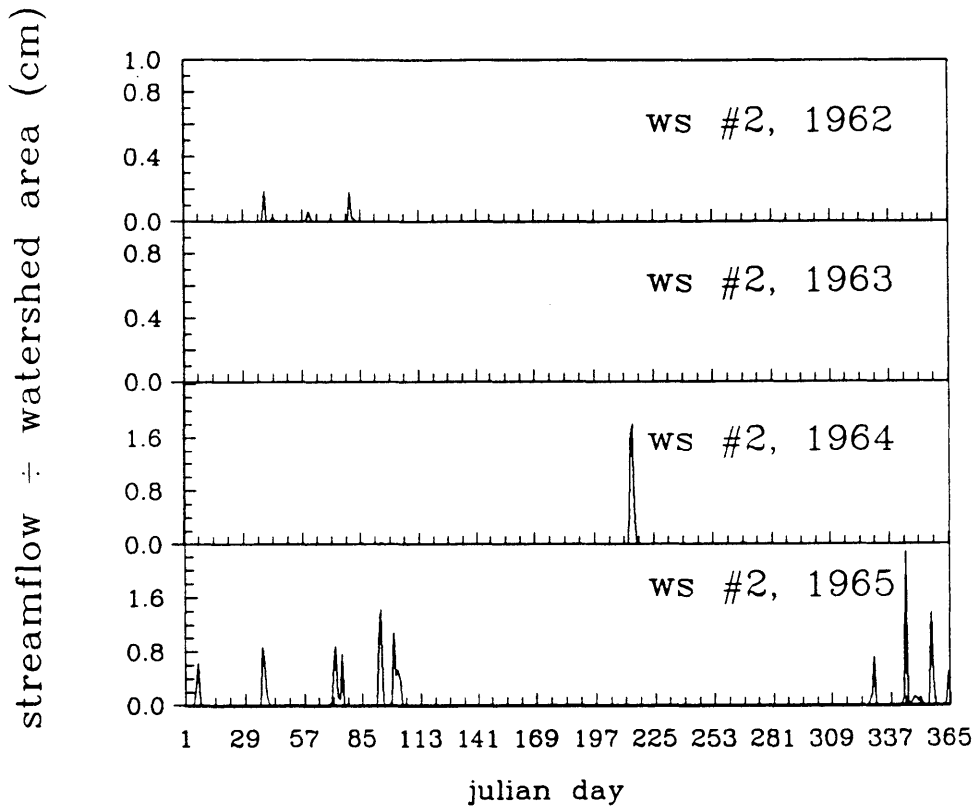
112

FIGURE 4.17: HYDROGRAPHS AT BEAVER
CREEK

conditions of the Beaver Creek. In the derivation of the water balance model, it is assumed that the aquifer's lateral transmissivity is sufficient to carry away the water accumulating in the aquaclude underlying soil column. It is also assumed in most applications (including this one up to this point) that the lateral transmissivity is sufficiently large that the net accretion rate may be approximated by the steady percolation term, i.e., that the apparent capillary rise is zero. This assumption eliminates the need to estimate the depth to the water table.

However, for the lateral transmissivity to be great enough to allow drainage of the accretion, the water table may need, under certain conditions, to rise to a height at which the apparent capillary rise cannot be neglected.

A first order analysis of the lateral flow system will now be carried out to investigate the applicability of this "infinite soil" assumption to the Beaver Creek watersheds.

4.4.2.2   Approximate Analysis of Lateral Flow Conditions
           at Beaver Creek

To determine whether or not the lateral transmissivity conditions could affect the surface water balance in these watersheds, the maximum possible steady state accretion rate that could be drained by the lateral transmissivity has been estimated in Appendix C.

The result of this analysis is that the maximum rate of accretion is less than one cm over the entire growing season.
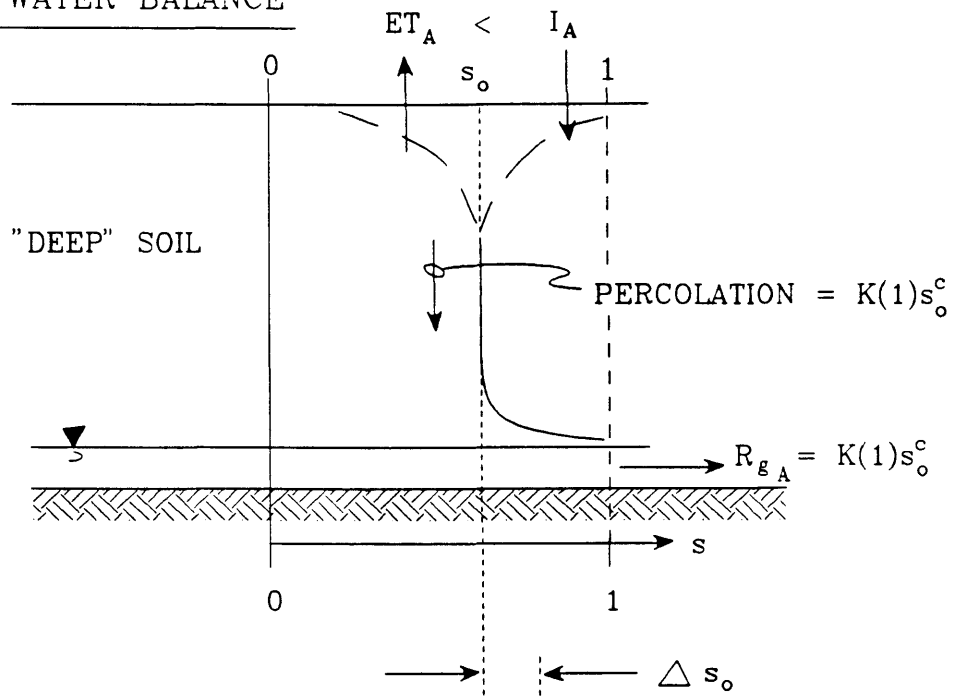
This maximum limiting value is much less than the seasonal groundwater flows predicted by the model in Figs. 4.14-4.16. The discrepancy arises, as noted in the previous discussion, from the condition that to laterally drain even one cm of accretion, the soil must be saturated almost to the ground surface over much of the watershed (see Appendix C). The existence of a saturated zone this near to the surface, however, is in contradiction with the zero capillary rise assumption made in Section 4.3.1.

We will thus modify the water balance model for this case of limiting lateral transmissivity by setting the sum of the percolation and capillary rise terms equal to zero, thereby forcing the surface fluxes to balance the seasonal water budget. This modification, and its effect on the average soil moisture, are qualitatively expressed in the cartoon of Fig. 4.18.

In this limiting case, the water balance can be thought of as occurring in a barrel of soil with impermeable sides and bottom. A saturated zone will grow to some equilibrium depth at which the moisture profile near the surface will cause the mean infiltration and exfiltration to balance.

Initially, if the soil in the barrel is dry, mean infiltration through the surface will exceed the exfiltration, and a net "accretion" will develop. Because this water will not be able to flow laterally through the sides of the "barrel", a saturated zone will develop. As this zone grows toward the surface, the whole mean equilibrium moisture

ORIGINAL WATER BALANCE

ET$_A$ < I$_A$

0   s$_o$ 1

"DEEP" SOIL

PERCOLATION = $K(1)s_o^c$

$R_{g_A} = K(1)s_o^c$

0   1

s

$\triangle$ s$_o$

MODIFIED WATER BALANCE

ET$_A$= I$_A$

0   s$_o$ 1

"SHALLOW"
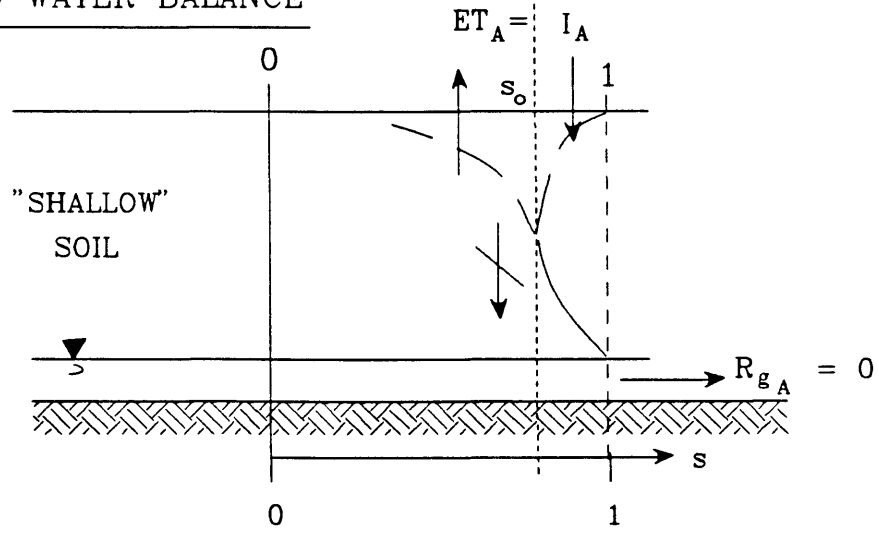SOIL

R_{g_A} = 0

s

0   1

FIGURE 4.18: MOISTURE PROFILE
UNDER DEEP AND SHALLOW SOIL
CONDITIONS

profile will get wetter until a state is reached where the mean infiltration and exfiltration balance.

4.4.2.3 Test Results with Water Balance Modification

With the aforementioned modification to the water balance equation, the optimum canopy density matches the observations much better (see Figs. 4.19A, 4.20A and 4.21). Additionally, the water balance component predictions are in excellent agreement with observation (Figs. 4.22, 4.23 and 4.24). Especially noteworthy is the surface runoff component.

Sensitivity of the short-term optimality condition to k_v can be seen in Figs. 4.19B and 4.20B. Here the equilibrium soil moisture is plotted as contours in M-k_v space. The dashed line, which connects points where $\frac{\partial s_o}{\partial M}\big|_{k_v} = 0$, represents the locus of optimum canopy M_o-k_v pairs.

Figure 4.19C and 4.20C show where our estimated effective transpiration efficiency ($k_{v_e} = \beta_v k_v$) and canopy density lie with respect to local maxima of soil moisture. In both cases (watersheds #2 and #4), the observation lies between the locus of M_o-k_{v_e} and the "cliff" (where the soil dries out and the vegetation spends a considerable amount of time in stress, see Section 3.3.1). This position may reflect a compromise between maximization of biomass potential (proportional to the product $M \cdot k_v$) and minimization of time spent in stress.

Note also, in Figures 4.22-4.24, that while the estimated annual evapotranspirations do match the model values, their sensitivity to M is almost nonexistent. Comparing the

observed $E[ET_A]$ to the minimum of the model $E[ET_A]$ is therefore not a statistically significant test of the hypothesis.

The reason for this insensitivity of $E[ET_A]$ to M is that in the Beaver Creek Watersheds the summer (i.e., growing season) climate is so dry that maximum equilibrium soil moistures do not produce significant runoff (both in reality and in this model. The evapotranspiration must therefore balance nearly the whole precipitation under any canopy density and therefore is insensitive to it.

Even though the evapotranspiration is nearly constant at different canopy densities, the equilibrium soil moisture which produces it depends strongly on how the evapotranspiration is generated. At low canopy densities, where most of the evapotranspiration is bare soil evaporation (which is a sensitive function of soil moisture), the equilibrium soil moisture is relatively low. At intermediate densities it reaches a maximum, and at high canopy densities, where most of the evapotranspiration is transpiration, it "bottoms out" near zero.

Because the soil moisture has not been measured, this analysis cannot provide a quantitative statistical hypothesis test. The location of the observed canopy densities very near to the tops of the soil moisture curves does, however, give strong support to the theory.

4.5   Test of Applicability of Soil Genesis Hypothesis

The soil hypothesis (see Section 2.2) is found not to apply under the conditions pertaining at Beaver Creek.
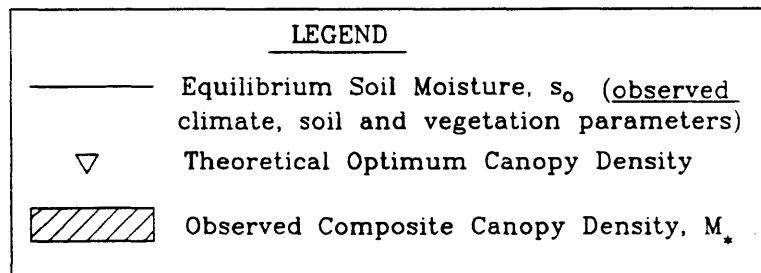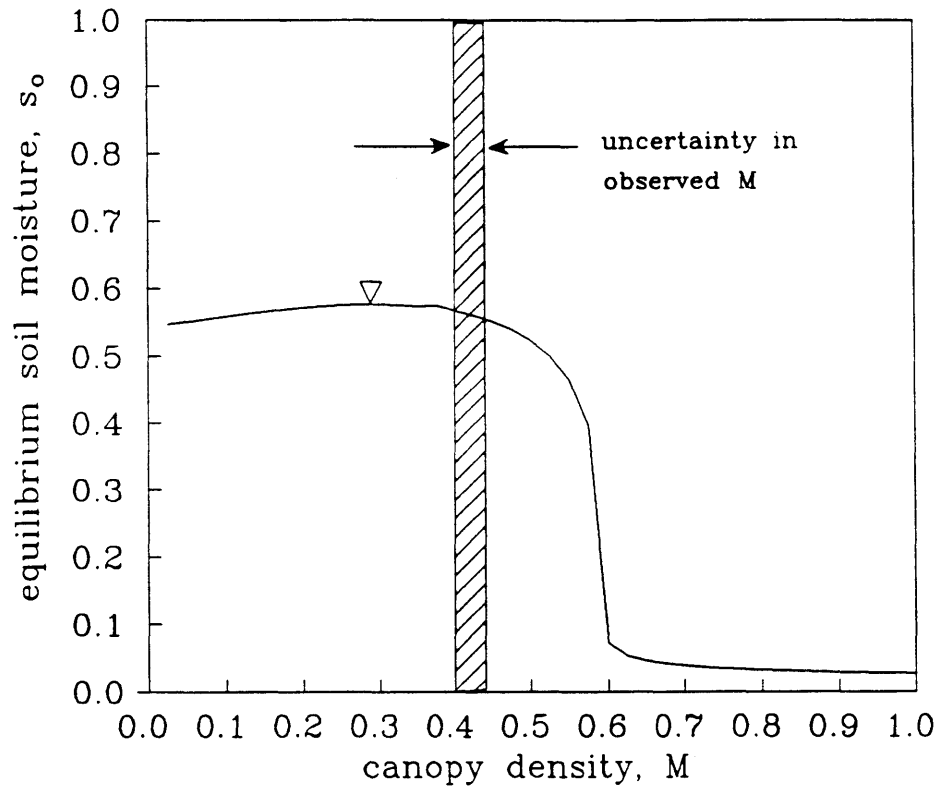
FIGURE 4.19A: SENSITIVITY OF EQUILIBRIUM
SOIL MOISTURE TO CANOPY DENSITY,
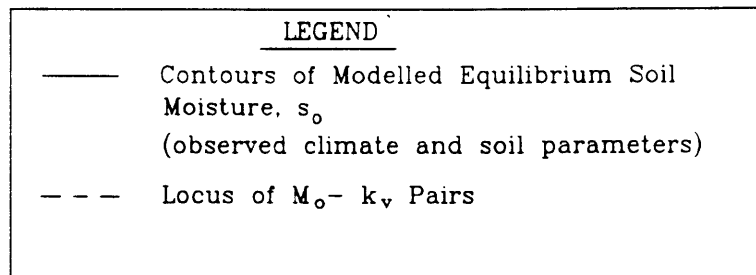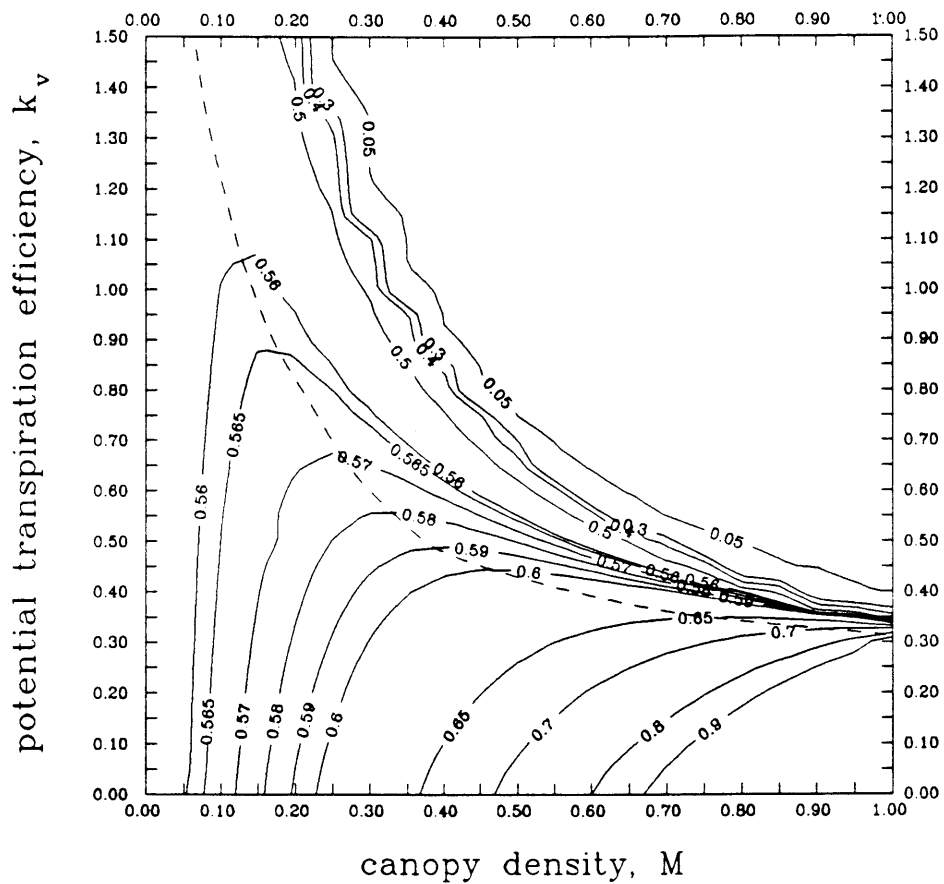MODIFIED WATER BALANCE MODEL,
WATERSHED #2, BEAVER CREEK ARIZONA

FIGURE 4.19B: CONTOURS OF EQUILIBRIUM
SOIL MOISTURE IN CANOPY DENSITY —
POTENTIAL TRANSPIRATION EFFICIENCY
SPACE, MODIFIED WATER BALANCE MODEL
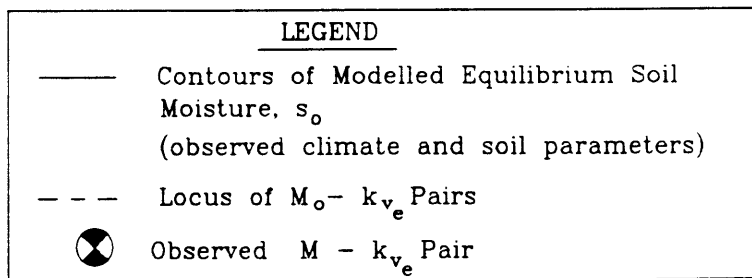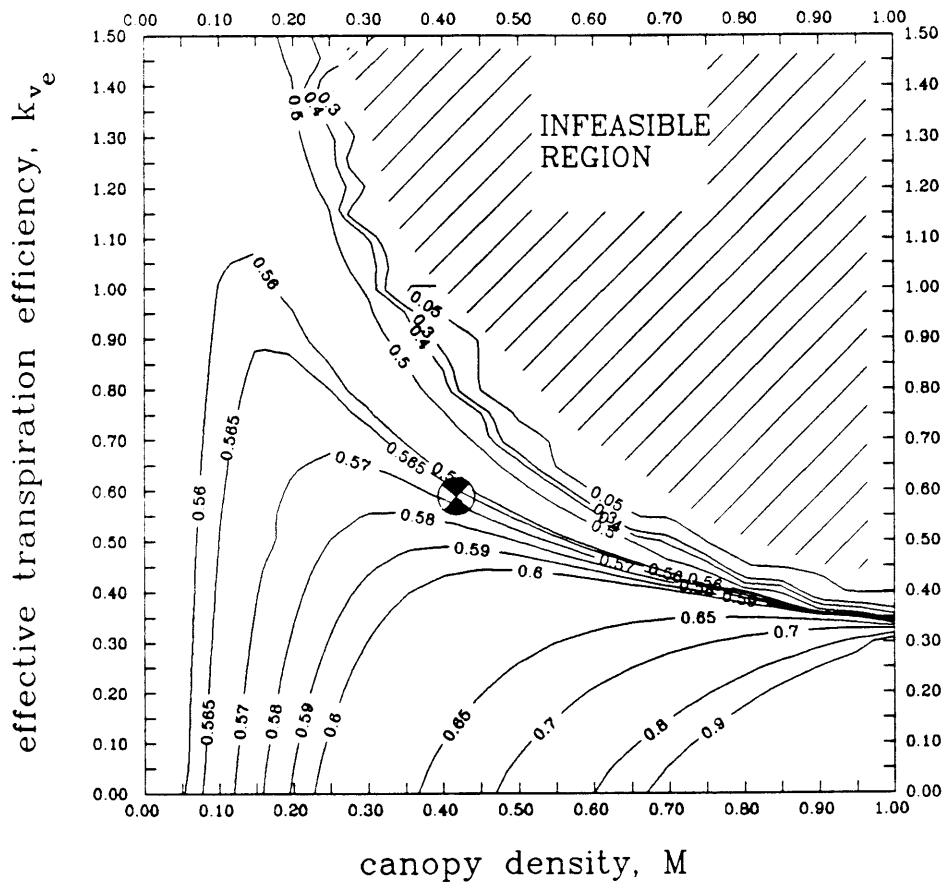WATERSHED #2, BEAVER CREEK ARIZONA

FIGURE 4.19C: CONTOURS OF EQUILIBRIUM
SOIL MOISTURE IN CANOPY DENSITY —
EFFECTIVE TRANSPIRATION EFFICIENCY
SPACE, MODIFIED WATER BALANCE MODEL
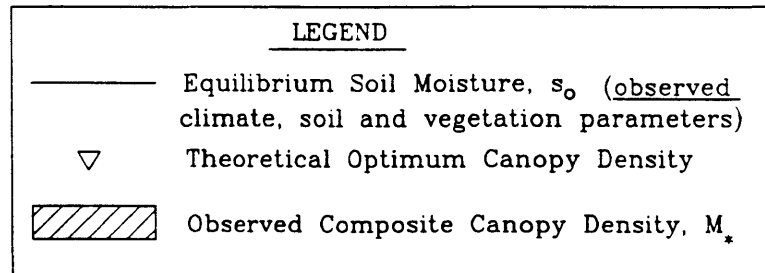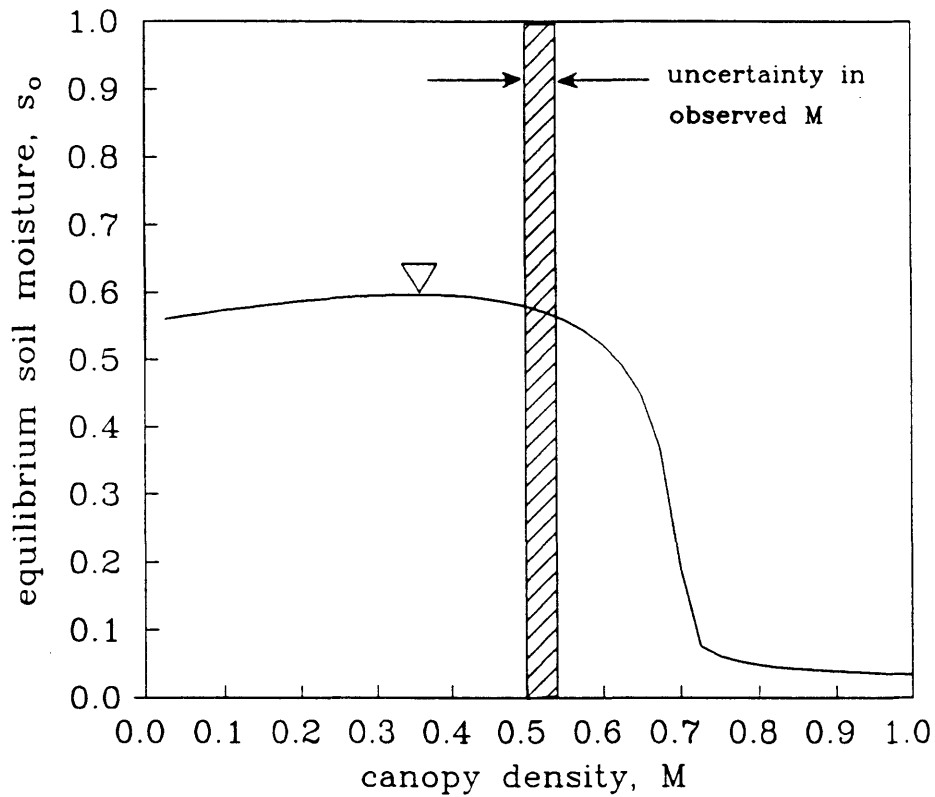WATERSHED #2, BEAVER CREEK ARIZONA

121

FIGURE 4.20A: SENSITIVITY OF EQUILIBRIUM
SOIL MOISTURE TO CANOPY DENSITY,
MODIFIED WATER BALANCE MODEL,
WATERSHED #4, BEAVER CREEK ARIZONA

FIGURE 4.20B: CONTOURS OF EQUILIBRIUM
SOIL MOISTURE IN CANOPY DENSITY –
POTENTIAL TRANSPIRATION EFFICIENCY
SPACE, MODIFIED WATER BALANCE MODEL
WATERSHED #4, BEAVER CREEK ARIZONA
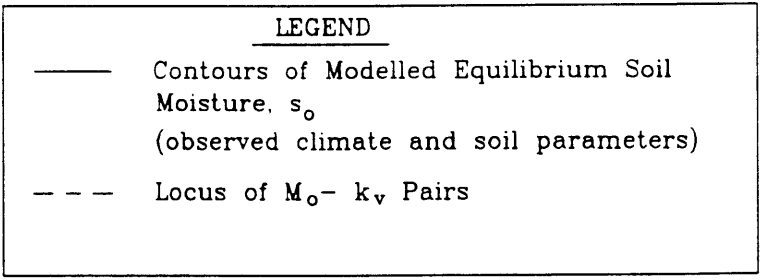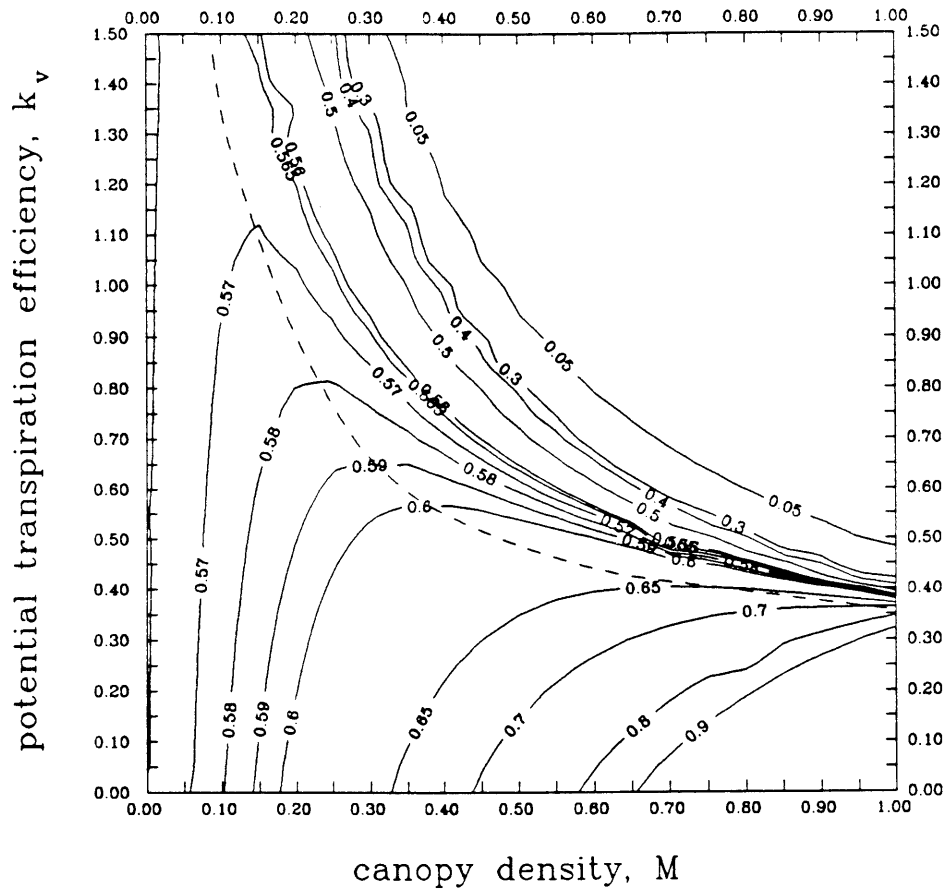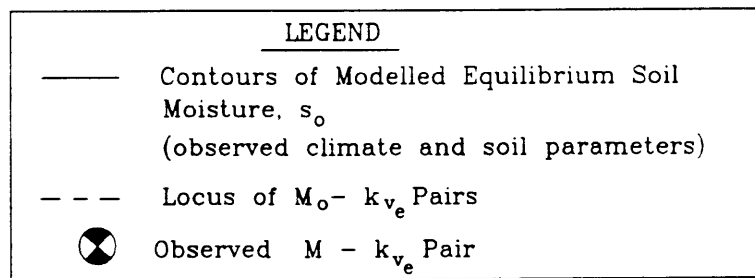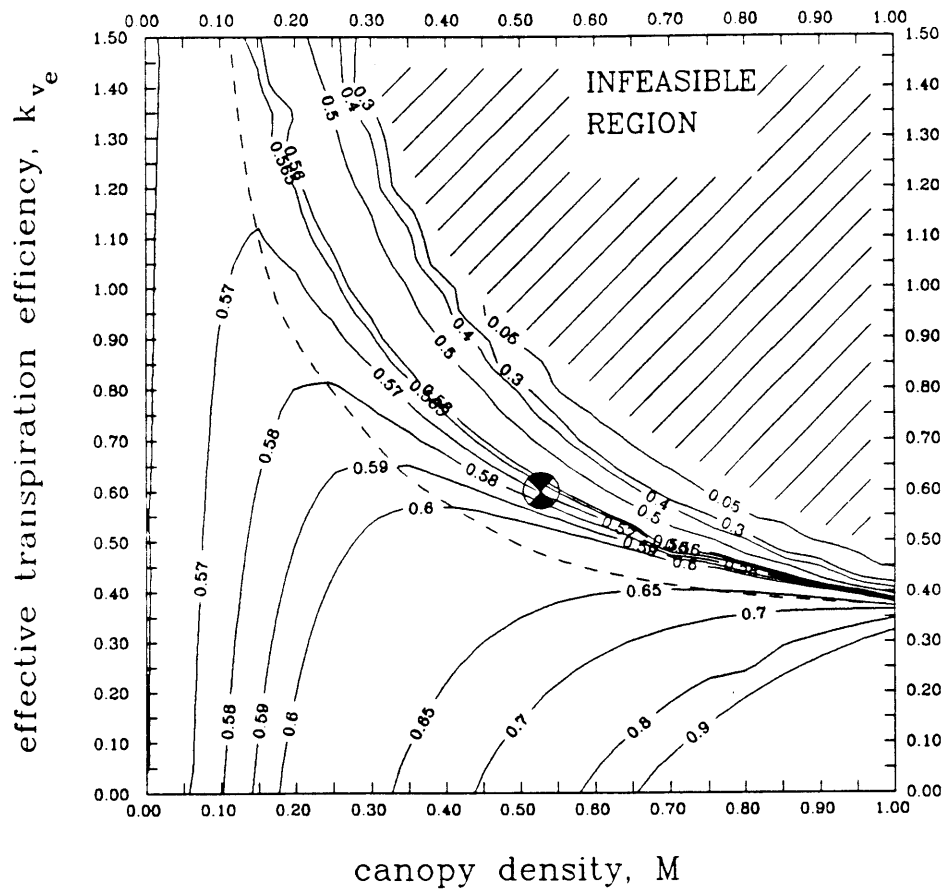
FIGURE 4.20C: CONTOURS OF EQUILIBRIUM
SOIL MOISTURE IN CANOPY DENSITY –
POTENTIAL TRANSPIRATION EFFICIENCY
SPACE, MODIFIED WATER BALANCE MODEL
WATERSHED #4, BEAVER CREEK ARIZONA
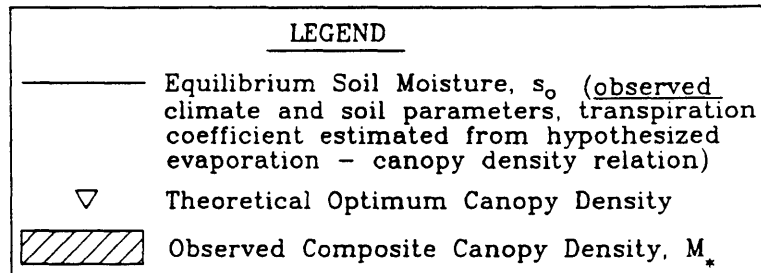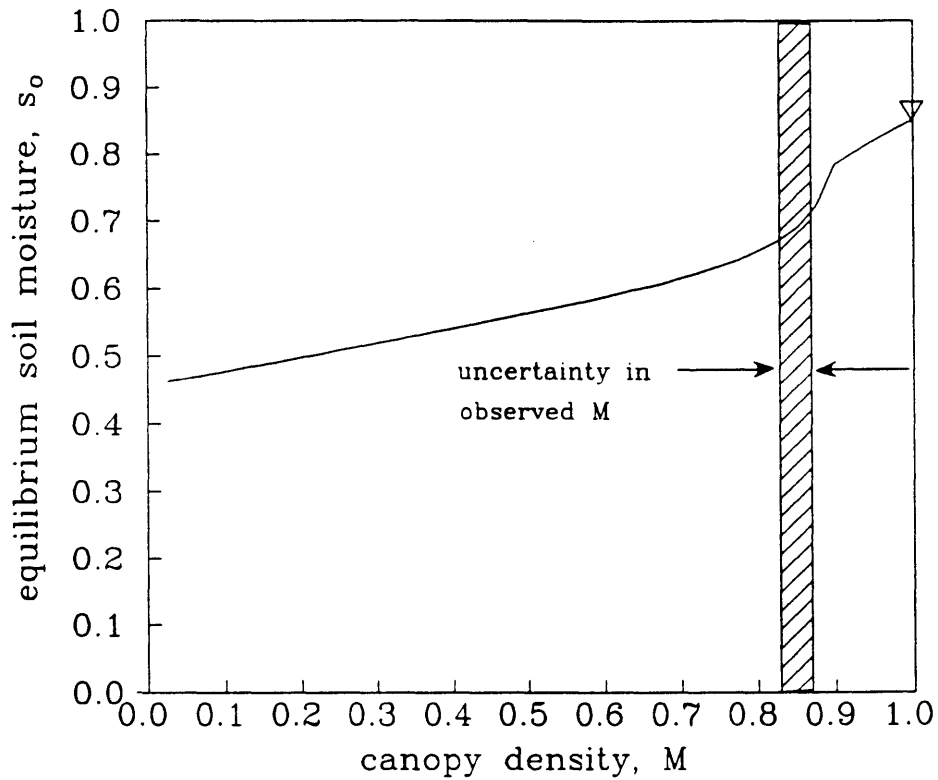
FIGURE 4.21: SENSITIVITY OF EQUILIBRIUM
SOIL MOISTURE TO CANOPY DENSITY,
MODIFIED WATER BALANCE MODEL,
FORESTED WATERSHEDS, BEAVER CREEK
ARIZONA

FIGURE 4.22: SENSITIVITY OF MEAN
WATER BALANCE TO CANOPY DENSITY,
MODIFIED WATER BALANCE MODEL,
WATERSHED #2, BEAVER CREEK ARIZONA

FIGURE 4.23: SENSITIVITY OF MEAN
WATER BALANCE TO CANOPY DENSITY,
MODIFIED WATER BALANCE MODEL,
WATERSHED #4, BEAVER CREEK ARIZONA

127

FIGURE 4.24:SENSITIVITY OF MEAN
WATER BALANCE TO CANOPY DENSITY,
MODIFIED WATER BALANCE MODEL
FORESTED WATERSHEDS
BEAVER CREEK ARIZONA

Specifically, the lack of gravitational percolation from the soil column (as discussed in the previous section) causes there to be only one se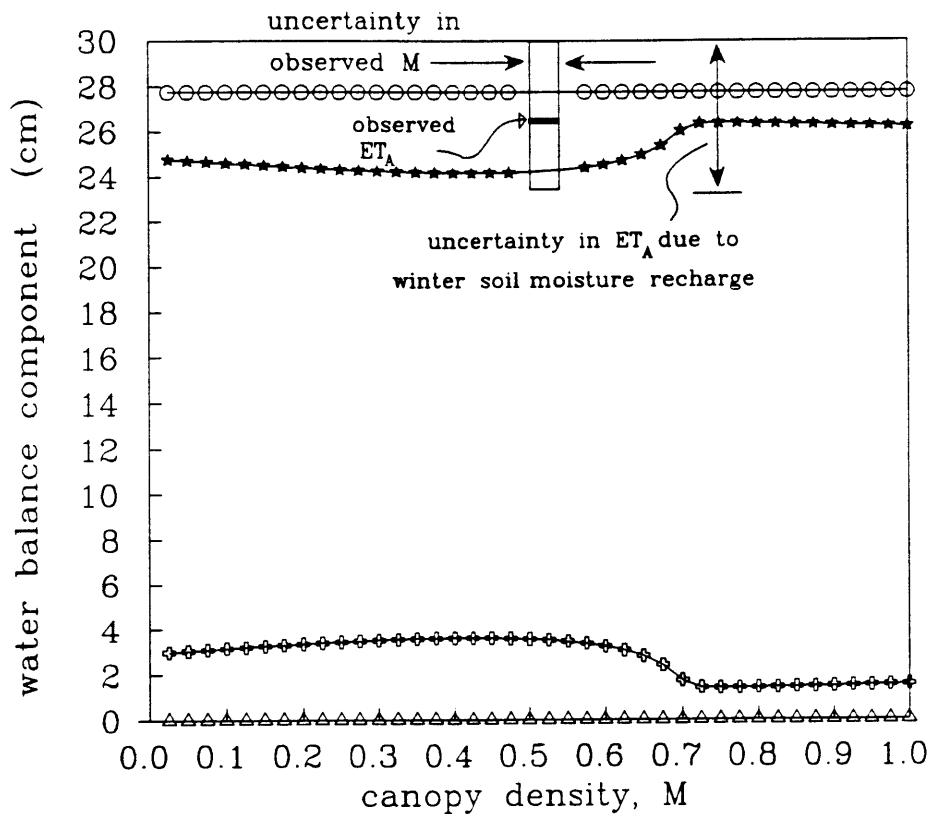t of permeability-pore disconnectedness index $(k(1)-c)$ pairs, for each M_o, which simultaneously satisfies the short term ecological optimality hypothesis (Eq. 2.21) and the Water Balance Equation (Eq. 2.15). Where the percolation term is non-negligible, as in the tests of Eagleson and Tellers (1982), there are two pairs of $k(1)-c$ values. This double root leads to the formation of a "hill" of M_o in $k(1)-c$ space, the top of which has a maximum M_o and thus satisfies the soil genesis hypothesis $\left(\frac{\partial M_o}{\partial k(1)} = 0, \frac{\partial M_o}{\partial c} = 0 \right)$.

The values of $k(1)$ and c which produce this maximum M_o are considered the climax soil properties.

The reason that the second solution is lost is as follows. When the percolation term is not included in the water balance, the surface runoff alone must balance the difference between precipitation and evapotranspiration. Along a contour of M_o, the evapotranspiration is "fixed" by the short term hypothesis (see sec. 4.3.2). Thus, to have the same value of M_o at two different values of $k(1)$ for a given c (i.e., for the contours to close and form the "hill"), not only the evapotranspiration but also the surface runoff would need to have the same value at both locations. This, however, is impossible because to have the same value of runoff at a higher (lower) permeability, the equilibrium soil moisture would need to be higher (lower), while to have the same value

of evapotranspiration at a higher (lower) permeability, the soil moisture would need to be lower (higher).

In addition, when the soil genesis hypothesis is tested, the soil porosity (n_e) remains constant, but the value of the saturated matric potential $(\psi(1))$, is allowed to vary in accordance with the following regression (Eagleson, 1978c):

$$\left[\frac{\sigma_w}{\gamma_w}\right]^2 \frac{n_e}{k(1)\,\psi^2(1)} = 10^{.66 + \frac{.55}{m} + \frac{.14}{m^2}} \qquad (4.13)$$

where

σ_w = surface tension of liquid water (dynes cm$^{-1)}$

and

γ_w = specific weight of liquid water (dynes cm$^{-3)}$

The value of $\psi(1)$ thus varies inversely as the square root of $k(1)$. The functional dependence of the surface runoff and evapotranspiration on $k(1)$ and $\psi(1)$ occurs as the product of $k(1)$ and $\psi(1)$ (e.g., see Eq. 2.5 and 2.10), which with Eq. 4.13, reduces to $\psi(1)$ varying directly as the square root of $k(1)$. Thus, the degree of freedom introduced by this regression alters the rate of change of the runoff and evaporation with changing permeability, but not the direction of change (i.e., runoff still monotonically decreases with increasing permeability, and evaporation still monotonically increases with increasing permeability). The soil moisture contradiction which removed the "hill" in $k(1)$-c space will thus remain even as $\psi(1)$ changes in the "background" of the $k(1)$-c space.

When the percolation term is allowed, on the other hand, both surface runoff and percolation balance the difference between precipitation and "fixed" evapotranspiration. Because the percolation and surface runoff are affected by permeability in opposite ways, there will always be the physical possibility of a high surface runoff, low percolation solution at a low permeability and a low surface runoff, high percolation solution at a high permeability.

The loss of the "hill" and the preceding arguments are illustrated in Fig. 4.22.

It is an interesting result that the soil depth (which, through its influence on lateral transmissivity, controls whether or not the water table will reside at a depth at which it "dampens" the percolation component) is a critical factor in the soil genesis hypothesis. In particular, it appears that the possibility of losing water to percolation is a necessary condition to allow the soil-vegetation system's evolutionary response to result in intermediate values of $k(1)$ and c. Without this "penalty", the system would evolve under conditions where an increase in the permeability of the soil always leads to an increase in M_o. Under these conditions we could expect that the soil-vegetation system would indeed evolve toward a maximum permeability.
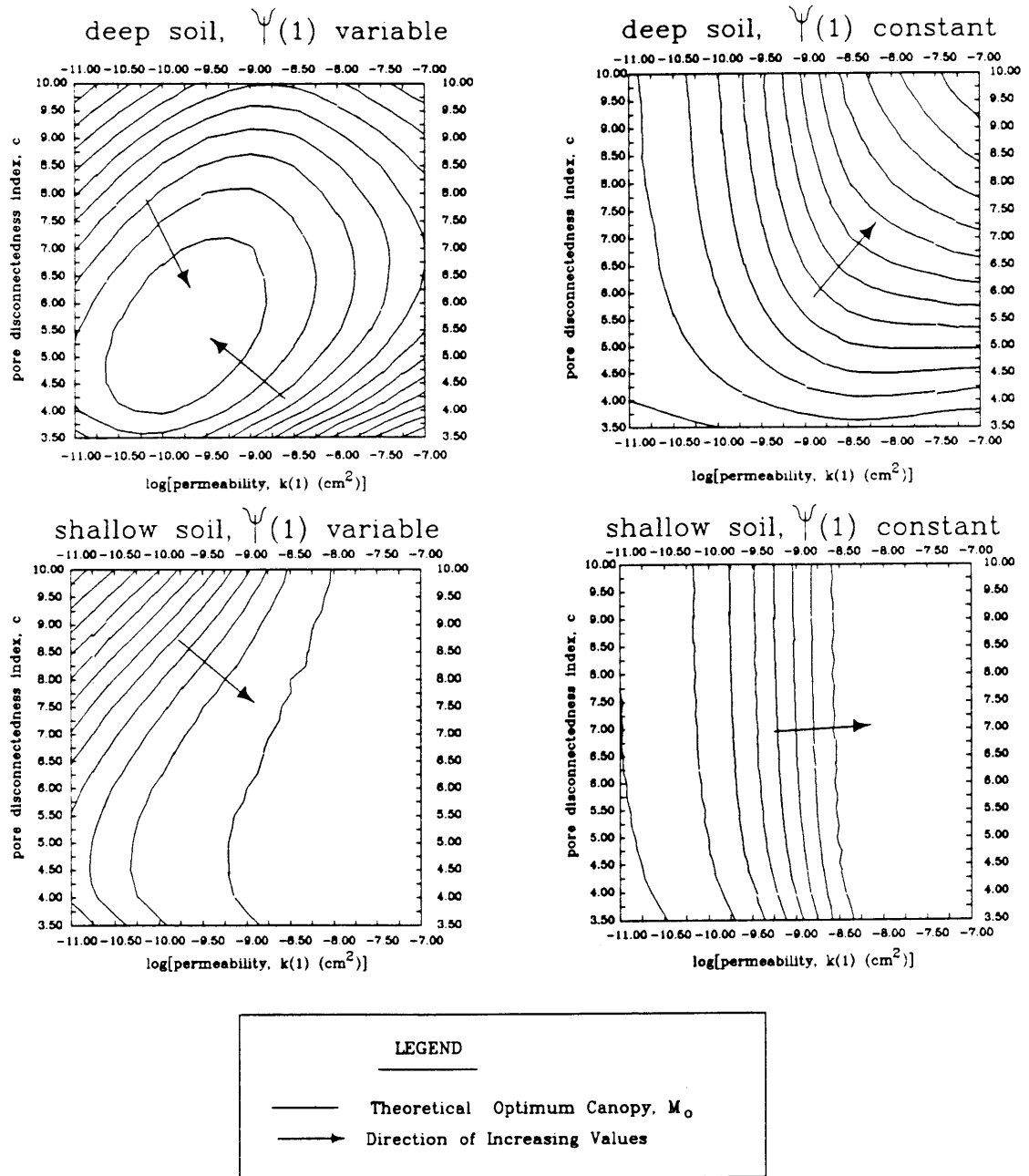
FIGURE 4.25: EFFECT OF VARIABLE SATURATED MATRIX POTENTIAL AND ELIMINATION OF PERCOLATION ON OPTIMUM CANOPY CONTOURS WATERSHED #2, BEAVER CREEK ARIZONA

4.6 Estimation of Soil Hydraulic Properties through the Short

Term Optimality Hypothesis

A test of the sensitivity of the short term hypothesis to soil properties and a demonstration of its use in parameter estimation, is realized by again viewing the equilibrium canopy density (M_o) in k(1)-c space and comparing the observed soil parameter values with those that produce the observed canopy density.

The four independent soil parameters listed in the water balance review (Section 2.1) have been estimated in Appendix B.2 for the Beaver Creek watersheds.. Holding the effective porosity (n_e) and the saturated matrix potential ($\psi(1)$) constant at their observed values, setting k_v equal to 0.55 for the woodland watersheds and equal to 0.8 for the forested watersheds (these values best fit the short term hypothesis (see Fig. 4.9)), and using the climate and precipitation parameters from Table 4.5, we again solve the short term hypothesis and water balance equations simultaneously in log (k(1)-c) space and plot contours of M_o. For consistency, the modified water balance is used for permeabilities less than $10^{-8.25}$ cm^2 and the original is used for permeabilities greater than 10^{-8} cm^2. The water balance modification and its range of application relative to permeability are discussed in section 4.4.2.2 and Appendix C.

The results of these tests are illustrated in Figs. 4.26, 4.27 and 4.28. In the woodland watersheds (e.g., WS #2, Fig. 4.26 and WS #4, Fig. 4.27), the observed soil properties

133

correspond to moderately lower canopy density than was observed. In the forested watersheds, Fig. 4.28, the corresponding optimum canopy is close to the observation, but is inside an "infeasible" region. This region, cross-hatched in Fig. 4.28, is a region where the modified water balance cannot be satisfied for high canopy densities, even at soil saturations approaching one. This causes a discontinuity in the soil moisture-canopy density relation and the optimality derivative $\frac{\partial s_0}{\partial M}\big|_{k_v}$ becomes non-existent.

The inability to satisfy the water balance for these values of M, c and k(1) stems from a contradiction in the modified water balance model. In this modification, the percolation was set equal to zero, but the surface runoff function, which is based on Philip's infiltration equation and has as its bottom boundary condition a steady flux rate of $K(1)s^c$, was left as is. If the percolation is indeed zero, the infiltration rate should be modified. Roughly, the effect of modification would be to remove the gravity term, A_0, from the infiltration rate (e.g., 2.7). This term is so large for saturations approaching unity that effectively no runoff is produced (i.e., A_0, is larger than most of the distribution of rainfall intensities, thus causing all the rainfall to be infiltrated). Removing this term would remedy this inconsistency and promote surface runoff generation. Improving this "patching" of the near surface unsteady

FIGURE 4.26: CONTOURS OF OPTIMUM CANOPY IN
LOG PERMEABILITY – PORE DISCONNECTEDNESS
INDEX SPACE MODIFIED WATER BALANCE,
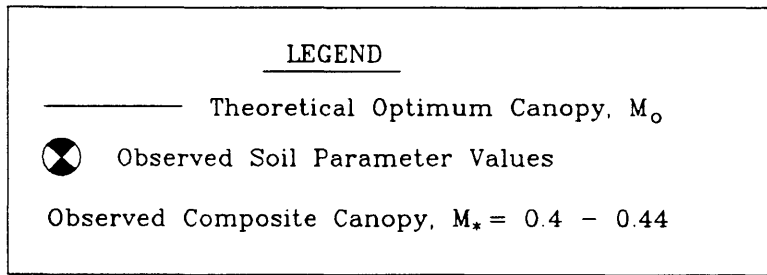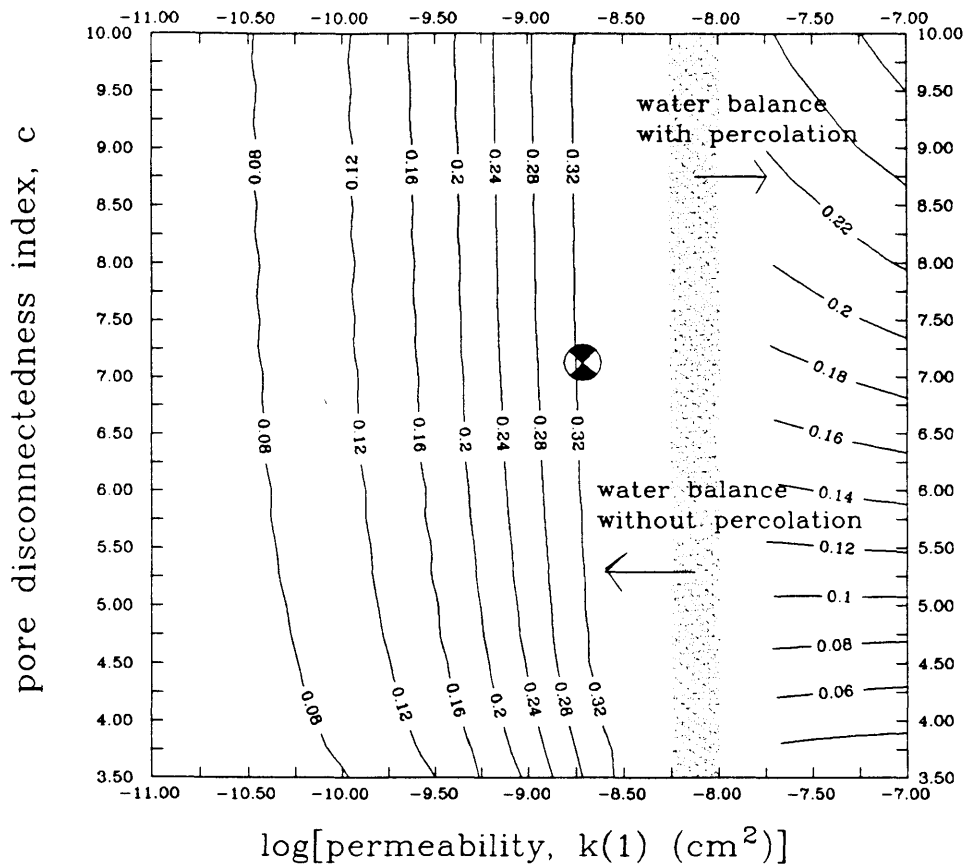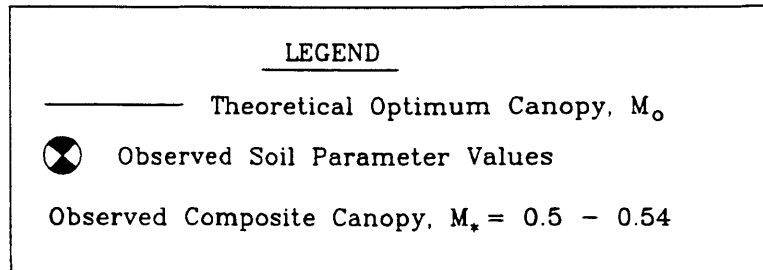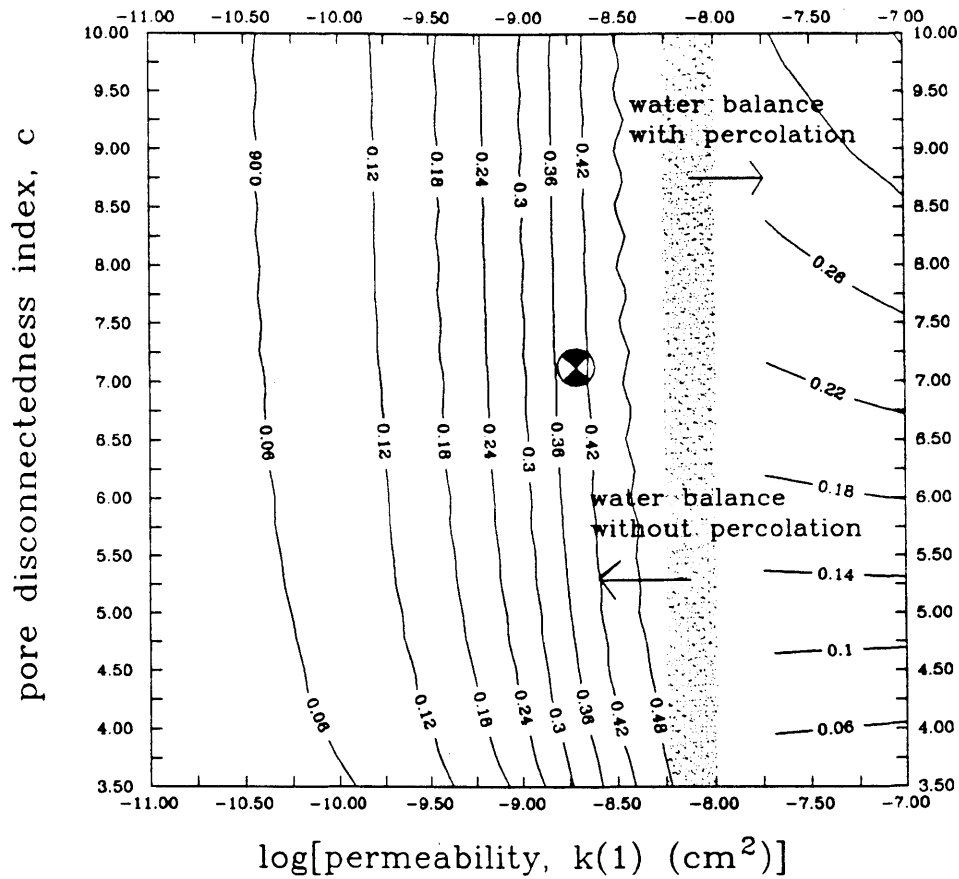WATERSHED #2, BEAVER CREEK ARIZONA

FIGURE 4.27: CONTOURS OF OPTIMUM CANOPY IN LOG PERMEABILITY – PORE DISCONNECTEDNESS INDEX SPACE : MODIFIED WATER BALANCE, WATERSHED #4, BEAVER CREEK ARIZONA
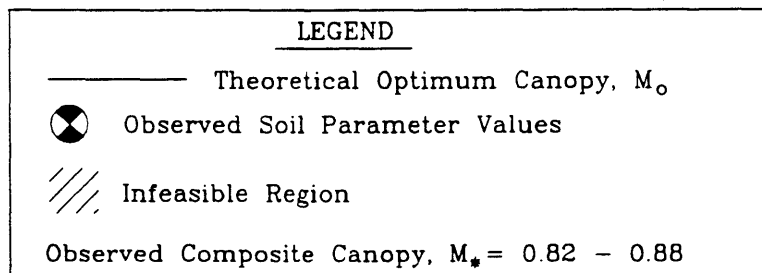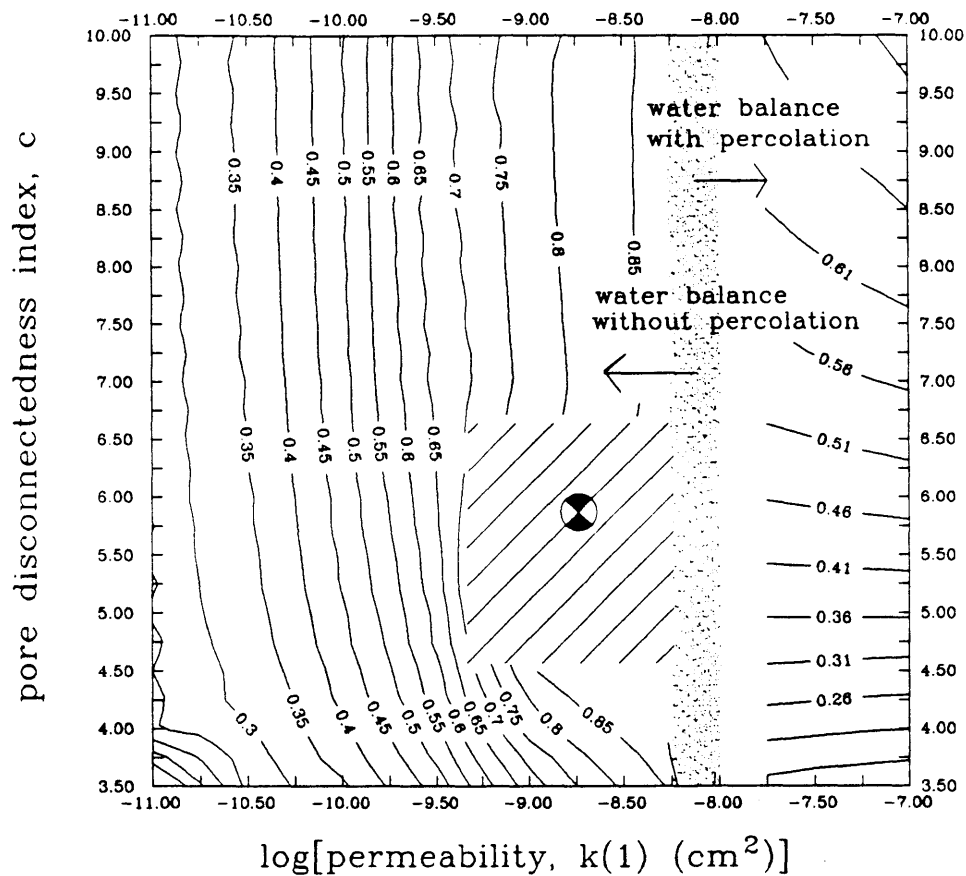
FIGURE 4.28: CONTOURS OF OPTIMUM CANOPY IN LOG PERMEABILITY — PORE DISCONNECTEDNESS INDEX SPACE : MODIFIED WATER BALANCE, FORESTED WATERSHEDS, BEAVER CREEK ARIZONA

diffusion rate and the steady state flux below it will be addressed in future research.

Also note that in general, the optimum canopy is very sensitive to k(1), which makes the canopy a robust estimator of k(1), but insensitive to c and thus inefficient for its estimation. The opposite holds true to the right of the shaded band, i.e., in the original model formulation.

4.7 Multi-Component Canopy Studies

In all of the preceding tests, the canopy density and potential transpiration ratio were treated as a lumped average of the component (e.g., overstory, T, and understory, u,) values (see Section 4.3.1). In what follows, an attempt is made to apply the short term optimality condition ($\partial s_o/\partial M = 0$) to each component separately. In this way the relative amounts of each component of the canopy could be tested (or "predicted"). Mathematically, the optimality conditions become:

$$\frac{\partial s_o}{\partial M_u} = 0, \qquad M_u = M_{u_o}$$

and   (4.14)

$$\frac{\partial s_o}{\partial M_T} = 0, \qquad M_T = M_{T_o}$$

For the observed climate and soil properties of watershed 2, contour plots were made of the equilibrium soil moisture in M_u - M_T space using Eq. 2.15 (the water balance equation). The plots were made for the following cases:

$$k_{v_T} > k_{v_U}; \quad k_{v_T} < k_{v_U}; \quad k_{v_T} = k_{v_U} \qquad 4.15$$

(see Figs. 4.29, 4.30 and 4.31. If a simultaneous solution existed to equations 4.14 and 4.15, it would appear as a closed contour in Figs. 4.29-4.31. The contour plots, however, show that the maximum soil moisture does not result from a mixture of canopies, but from a system comprised solely of the lower k_v canopy with the smaller k_v. When the k_v's are equal (which happens to be our estimation of the situation at Beaver Creek), the curves are simply symmetrical around the $M_U = M_T$ line.

One might conclude from this that if the trees and understory had different potential transpiration ratios, the component with the lower k_v might become dominant. It is important to remember, however, that lower k_v's lead to higher soil moisture and less potential for stress, but higher k_v's lead to larger biomass growth potential.
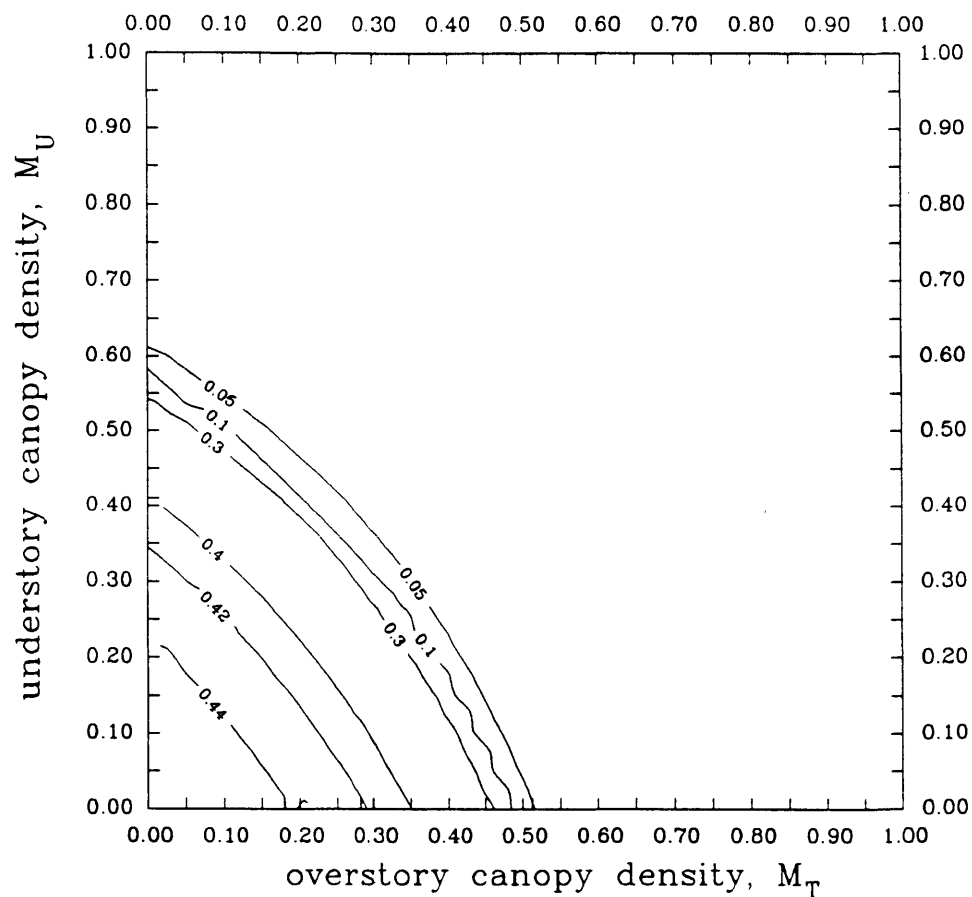
FIGURE 4.29: EQUILIBRIUM SOIL MOISTURE IN OVERSTORY CANOPY DENSITY – UNDERSTORY CANOPY DENSITY SPACE: CASE OF OVERSTORY POTENTIAL TRANSPIRATION EFFICIENCY EQUAL TO UNDERSTORY POTENTIAL TRANSPIRATION EFFICIENCY
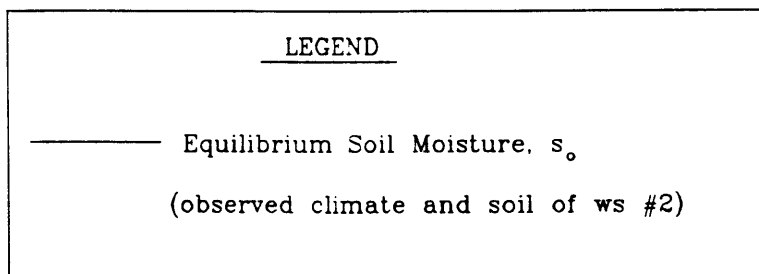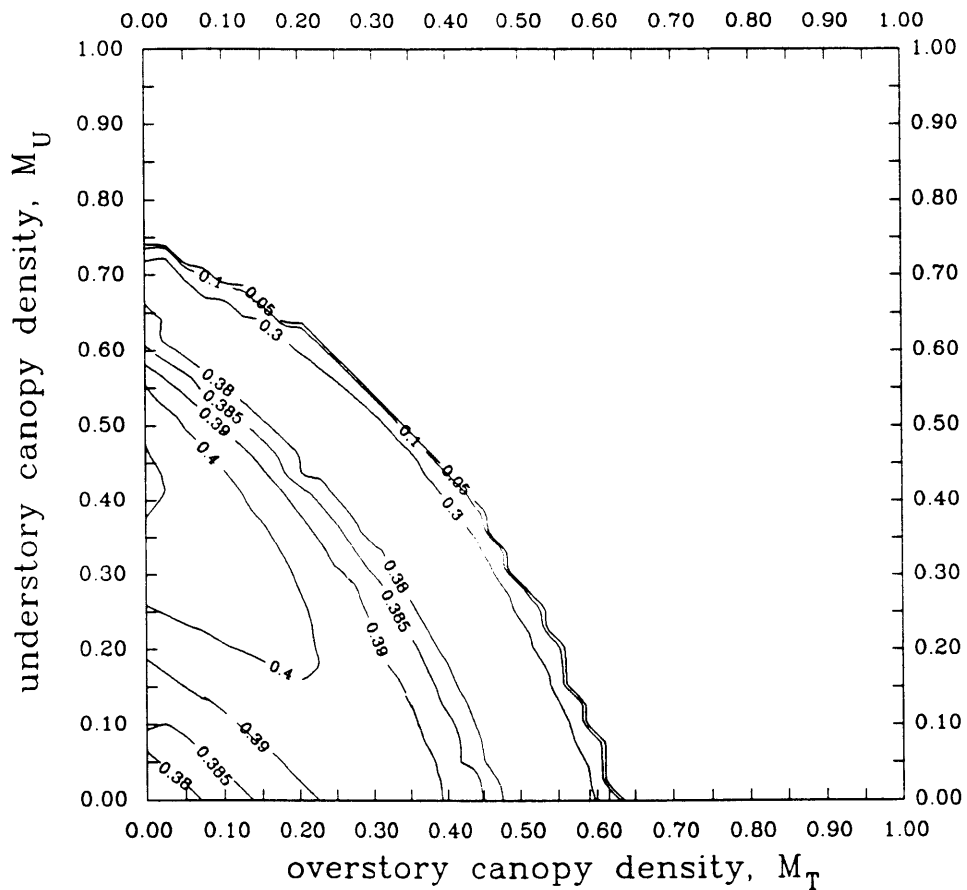
FIGURE 4.30: EQUILIBRIUM SOIL MOISTURE IN OVERSTORY CANOPY DENSITY — UNDERSTORY CANOPY DENSITY SPACE: CASE OF OVERSTORY POTENTIAL TRANSPIRATION EFFICIENCY GREATER THAN UNDERSTORY POTENTIAL TRANSPIRATION EFFICIENCY
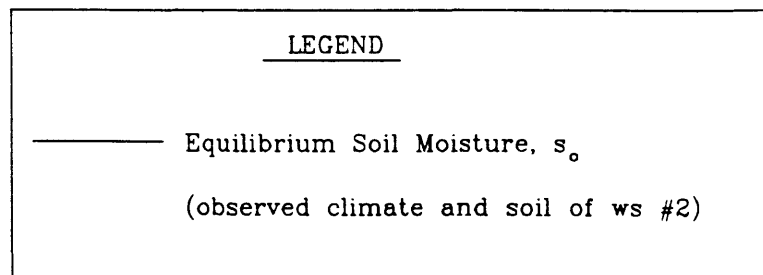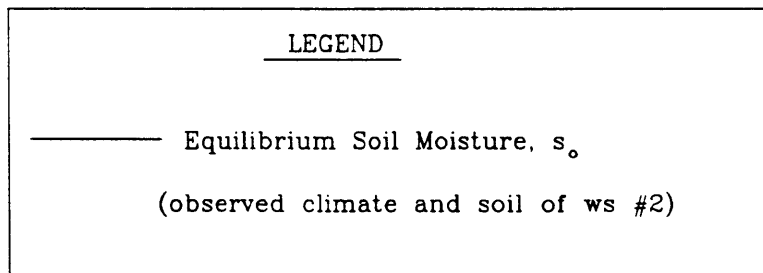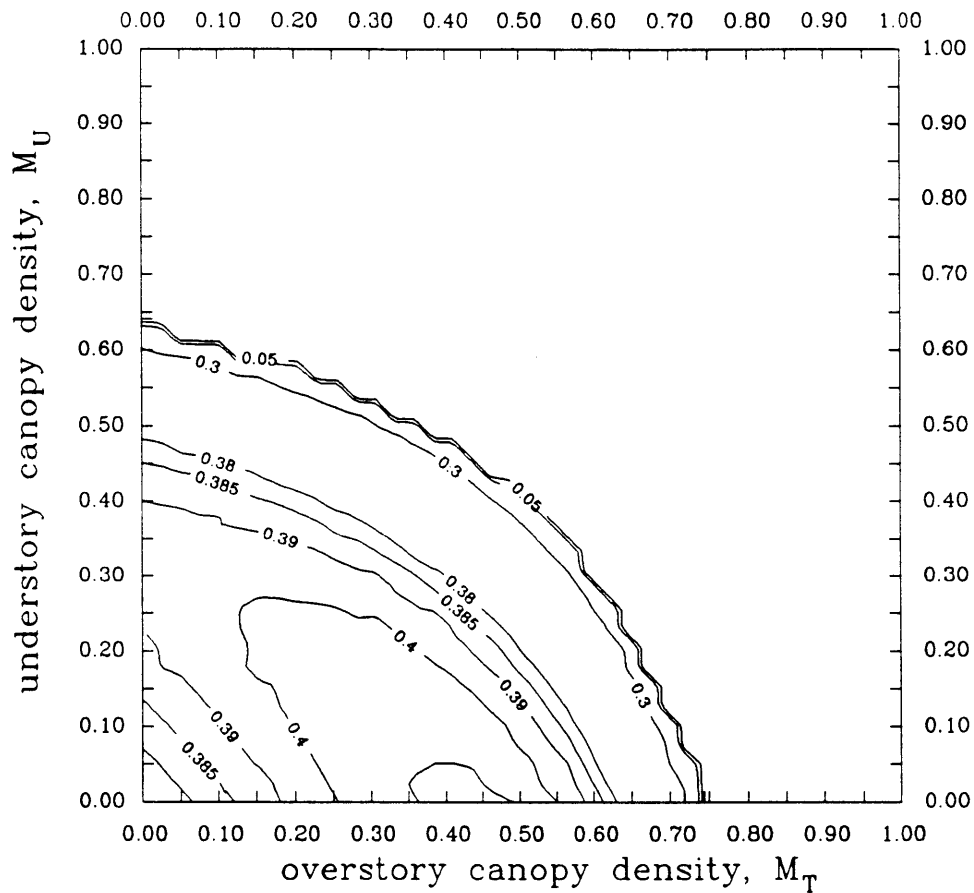
FIGURE 4.31: EQUILIBRIUM SOIL MOISTURE IN OVERSTORY CANOPY DENSITY − UNDERSTORY CANOPY DENSITY SPACE: CASE OF OVERSTORY POTENTIAL TRANSPIRATION EFFICIENCY LESS THAN UNDERSTORY POTENTIAL TRANSPIRATION EFFICIENCY

CHAPTER 5

Summary and Conclusions

5.1 Summary

In this report the "ecological optimality" hypotheses of Eagleson (1978-f, 1982) are revisited for the purpose of testing their validity against a uniquely comprehensive set of field observations from a set of small semi-arid watersheds near Flagstaff, Arizona.

The testing included rederivation of the entire statistical-dynamic water balance model (Eagleson, 1978), correcting errors, and removing expedient but poor assumptions where possible.

5.2 Conclusions

First Hypothesis:

At the Beaver Creek Watersheds, comparisons of observed canopy densities with the modified soil moisture-canopy density relationship (Figs. 4.19, 4.20) support the hypothesis that the canopy density which results in a maximum equilibrium soil moisture will be the optimal and thus the "equilibrium" condition. Testing of the direct hypothesis $\left(\frac{\partial s_o}{\partial M} \big|_{k_v} = 0 \right)$

by standard statistical methods is not possible because the soil moisture state has not been measured. A statistical test

143

of the indirect statement of the hypothesis, $\left(\dfrac{\partial E[ET_A]}{\partial M}\Big|_{k_v} = 0\right)$

is analytically possible, but lacks confidence due to the small sample size and to the large uncertainty in our estimate of $E[ET_A]$.

That the observed canopy densities of watersheds two and four lie in between the peak and "cliff" of soil moisture (Figs. 4.19A, 4.20A) may be the result of the many approximations inherent in the water balance model but it could also be an indication that the optimization hypothesis is too simple. By increasing its density beyond the value M_0 at which soil moisture is maximized, the canopy gains increased reproductive potential at the expense of sustaining a higher state of average stress. Perhaps what we are seeing is a natural tradeoff between these two environmental pressures.

Second Hypothesis:

The second hypothesis $\left(\dfrac{\partial s_0}{\partial k_v}\Big|_M = 0\right)$ is found to be

physically unrealistic because for constant M, there is no maximum of soil moisture with respect to k_v in a given climate (see Figs. 4.19B and 4.20B). Published reports of this

144

maximum (Eagleson, 1982; Eagleson and Tellers, 1982) were found to result from a computer programming error.

Alternative hypotheses to explain the dominance of certain vegetation types in given locations are currently under consideration.

Third Hypothesis:

The soil genesis hypothesis $\left(\frac{\partial M_o}{\partial c} \bigg|_{k(1)} = 0 \; ; \; \frac{\partial M_o}{\partial k(1)} \bigg|_c = 0 \right)$ is

found to be dependent upon the existence of a percolation component in the water balance. The lateral flow conditions in the Beaver Creek are found (by indirect observation and by theoretical reasoning) to prohibit the development of a percolation component. Therefore, hypothesis three is un-testable at Beaver.

State of Stress

The water balance model assumes (Eagleson, 1978) that the "equilibrium" vegetation parameters M and k_v are such that the canopy operates in the unstressed state as far as soil moisture is concerned. The observations at Beaver Creek, Arizona (Figs. 4.19B and 4.20B) and the calculations (Table 3.2) support this assumption. These results demonstrate that even in the semi-arid climate of Beaver Creek, the canopy density and water use coefficient are such that the system is "well watered" in the sense used by Arris

145

(1989), and Arris and Eagleson (1989) in their estimation of k_v from biomass production; the same estimation technique was used here.

Soil Parameter Estimation:

The equilibrium canopy density resulting from the first hypothesis is found to lack sensitivity to the pore disconnectedness index (c) in the absence of a percolation component in the water balance (Figs. 4.25--4.28). However, sensitivity to permeability is strong, making the canopy density a robust estimator of soil permeability under these circumstances.

CHAPTER 6

Recommendations for Future Research

Our first recommendation for future research focuses on the need to replace the species selection hypothesis (hypothesis 2). There are two main routes which we feel are worth consideration. The first involves further investigation of the possibility (discussed in Section 3.4) that the plant type whose value of k_v best balances the benefits of increased growth potential with the risks of increased time spent in stress will be dominant. The second possibility, not discussed in this report, involves the possibility that while the canopy density responds to and is determined by mean annual conditions, the transpiration coefficient responds to a different time scale. This time scale could be the interstorm scale or an aggregate of the annual time scale.

A second recommendation, focusing more on the underlying water balance model, is to improve the analytic coupling of the water table and surface zones and to incorporate coupling between the water table and drainage network. The importance of the effects of such changes on the vegetal hypotheses are illustrated in this work by the effects of the water balance modifications (e.g., the loss of applicability of the soil genesis hypothesis and the large shift in optimal canopy density).

References

1. Arris, L. L., A physiological explanation for vegetation ecotones in eastern North America, <u>SM Thesis</u>, Dept. of Civil Engineering, Massachusetts Institute of Technology, Cambridge, MA, 1989.

2. Arris, L. L. and P. S. Eagleson, A physiological explanation for vegetation ecotones in eastern North America, <u>Ralph M. Parsons Laboratory Rept. No. 323</u>, Massachusetts Institute of Technology, Cambridge, MA, 1989.

3. Baker, M. B., Jr. Hydrologic regions of forested areas in the Beaver Creek Watershed, <u>U.S.D.A. Forest Service General Technical Report RM-90</u>, 1982.

4. Baker, M. B., Jr., Effects of Ponderosa Pine treatment on water yield in Arizona, <u>Water Res. Res.</u>, 22(1), 67-73, 1986.

5. Barbour, M. G. and W. D. Billings, eds. <u>North American Terrestrial Vegetation</u>, Cambridge University Press, Cambridge, 1988.

6. Brix, H., The effect of water stress on the rates of photosynthesis and respiration in tomato plants and loblolly pine seedlings, <u>Physiol. Plant., 15</u>, 10-20, 1962.

7. Bras, R. L., <u>Hydrology: an Introduction to Hydrologic Science</u>, p. 352, Addison-Wesley Publishing Co., Inc., Reading, MA, 1990.

8. Brooks, R. H. and A. T. Corey, Properties of porous media affecting fluid flow, <u>J. Irrig. Drain. Div. Am. Soc. Civ. Eng., 92(IR2)</u>, 61-88, 1966.

9. Brown, H. E., M. B. Baker, Jr., J. J. Rogers, W. P Clary, J. L. Kovner, F. R. Larson, C. C. Avery and R. E. Campbell, Opportunities for increasing water yields and other multiple use values on Ponderosa Pine forest lands, <u>U.S.D.A. Forest Service Research Paper Rm-129</u>, 1974.

10. Budyko, M. I., <u>The Heat Balance of the Earth's Surface</u> (in Russian), Leningrad, 1956 (translated by N. A. Stepanova, Office of Technical Services, U. S. Dept. of Commerce, Washington, D.C., 1958).

11. Bunce, J. A., L. N. Miller and B. F. Chabot, Competitive exploitation of soil water by five eastern North American tree species, <u>Botanical Gazette, 138</u>, 168-173, 1977.

12. Clary, W. P., M. B. Baker, Jr., P. F. O'Conner, T. N. Johnsen, Jr. and R. E. Campbell, Effects of Pinyon-Juniper removal on natural resource products and uses in Arizona, <u>U.S.D.A. Forest Service Research Paper RM-128</u>, 1974.

13. Cooley, K. R., Evaporation from open water structures in Arizona, <u>Agricultural Experiment Station and Cooperative Extension Service, The University of Arizona</u>, Folder 159, 1970.

14. Das, B. M., _Principles of Geotechnical Engineering_, P.W.S.
    Publishers, Boston, MA 1985.

15. Doorenbos, J. and W. O. Pruitt, Guidelines for predicting
    Crop water requirements, _FAO Irrigation and Drainage_
    Paper 24. Food and Agriculture Organization of the
    United Nations, Rome, 1977.

16. Eagleson, P. S., Climate, soil, and the water balance: A
    framework for their analytical coupling, _Lecture notes_
    for the Tenth Annual John. R. Freeman Memorial Lecture,
    Massachusetts Institute of Technology, Cambridge, MA,
    1977.

17. Eagleson, P. S., Climate, soil and vegetation, parts 1-7,
    Water Resour. Res., 14(5), 705-776, 1978.

18. Eagleson, P. S., Ecological Optimality in water-limited
    natural soil-vegetation systems, 1. Theory and
    hypothesis, _Water Resour. Res._, 18(2), 325-340, 1982.

19. Eagleson, P. S. and T. E. Tellers, Ecological optimality
    in water-limited natural soil-vegetation systems, 2.
    Tests and Applications. _Water Resour. Res._, 18(2), 341-
    354, 1982.

20. Eagleson, P. S. and R. I. Segarra, Water-limited
    equilibrium of savanna vegetation systems, _Water Resour._
    Res., 21(10), 1483-1493, 1985.

21. El-Hemry, I. I., Water balance estimates of the Machar
    Marshes, _Masters Thesis_, Department of Civil
    Engineering, Massachusetts Institute of Technology,
    Cambridge, MA, 1980.

22. El-Hemry, I. I. and P. S. Eagleson, Water balance estimates of the Machar Marshes, <u>Ralph M. Parsons Laboratory Rept. No. 260</u>, Massachusetts Institute of Technology, Cambridge, MA, 1980.

23. Farnsworth, R. K., E. S. Thompson and E. L. Peck, Evaporation atlas for the contiguous United States, <u>N.O.A.A. Technical Report NWS 33</u>, National Weather Service, Washington, D.C., 1982.

24. Ffolliot, P. F. and W. T. Swank, eds., Potentials of noncommercial forest biomass for energy, <u>University of Arizona, College of Agriculture, School of Renewable Natural Resources</u>, Technical Bulletin No. 256, 1986.

25. Hamon, W. R., Estimating potential evapotranspiration, <u>Proc. ASCE, J. Hydraulics Division</u>, 87, No. HY3, 107-120, 1961.

26. Havranek, W. M. and U. Benecke, Influence of soil moisture on water potential, transpiration and photosynthesis of conifer seedlings, <u>Plant and Soil, 49</u>, 91-103, 1978.

27. Hinckley, T. M., R. G. Aslin, R. R. Aubuchon, C. L. Metcalf and J. E. Roberts, Leaf conductance and photosynthesis in four species of the oak hickory forest type, <u>For. Sci., 24</u>, 73-84, 1978.

28. Hinckley, T. M., M. O. Schroeder, J. E. Roberts, and D. N. Bruckeshoff, Effect of several environmental variables and xylem pressure potential on leaf surface resistance in white oak, <u>For. Sci., 21</u>, 201-211, 1975.

29. Jasinski, M. F. and P. S. Eagleson, Estimation of subpixel vegetation cover using red-infrared scattergrams, <u>IEEE Transactions on Geoscience and Remote Sensing</u>, 28(2), 1990.

30. Jensen, M. E. and H. R. Haise, Estimating evapotranspiration from solar radiation, <u>J. Irrig. Drain., Div. Am. Soc. Civ. Eng.</u>, 89 (IR4), 15-41, 1963.

31. Larcher, W., <u>Physiological Plant Ecology</u>, 2nd Ed., 303 pp., Springer-Verlag, Berlin, 1983.

32. Loposhinsky, W., Stomatal closure in conifer seedlings in response to leaf moisture stress, <u>Bot. Gaz., 130</u>, 258-263, 1969.

33. Lowe, C. H., <u>Arizona's Natural Environment</u>, The University of Arizona Press, Tucson, 1985.

34. Metzger, B. H., The effect of annual storage and random potential evapotranspiration on the one-dimensional annual water balance, <u>SM Thesis</u>, Department of Civil Engineering, Massachusetts Institute of Technology, Cambridge, MA, 1980.

35. Metzger, B. H. and P. S. Eagleson, The effects of annual storage and random potential evapotranspiration on the one-dimensional annual water balance, <u>Ralph M. Parsons Laboratory Rept. No. 251</u>, Massachusetts Institute of Technology, Cambridge, MA, 1980.

36. Priestley, C. H. B. and R. J. Taylor, On the assessment of surface heat flux and evaporation using large-scale parameters, <u>Mon. Wea. Rev.</u>, 100, 81-92, 1972.

37. Tellers, T. E., Estimation of Effective hydrologic properties of soils from observations of vegetation density, <u>SM Thesis</u>, Department of Civil Engineering, Massachusetts Institute of Technology, Cambridge, MA, 1980.

38. Tellers, T. E. and P. S. Eagleson, Estimation of effective hydrologic properties of soils from observing of vegetation density, <u>Ralph M. Parsons Laboratory Rept. No. 254</u>, Massachusetts Institute of Technology, Cambridge, MA, 1980.

39. Williams, J. A., and T. C. Anderson, Jr., <u>Soil Survey of Beaver Creek Area, Arizona</u>, U.S.D.A. Forest Service and Soil Conservation Service and Agricultural Experiment Station, 75 pages, 1967.

Appendix A

Comparability of Observed Precipitation with Assumed Model

In the following three sets of graphs (Figs. A.1, A.2 and A.3) the cumulative distributions of the important storm properties (depth, duration, intensity, and time between) and of the seasonal total precipitation are compared with the model distributions at three elevations in the Beaver Creek watershed during the summer. The model assumes exponentially distributed intensity, duration and time between storms and gamma distributed storm depths. The solid lines in these graphs are these assumed distributions, fit by the method of moments to the observed storm properties. The lower graph in each figure compares the derived distribution of total seasonal precipitation with the actual values ranked by the Thomas method. The derived distribution is based on the assumed Poisson arrival of gamma distributed storm depths and is given by Eagleson (1978b) as

$$P\left(\frac{P_A}{m_{P_A}} < z\right) = e^{-m_v} \cdot \left\{1 + \sum_{v=1}^{\infty} \frac{(m_v)^v}{v!} \cdot P[v\kappa, m_v\kappa z]\right\} \qquad (A.1)$$

where

$\quad m_v \quad$ = mean number of independent storms per year (season)

$\quad \kappa \quad$ = kappa of gamma distribution of storm depth

$\quad P[\ ] \quad$ = Pearson's Incomplete Gamma Function

154

The Thomas plotting positions are found by ranking the seasonal totals by amount and then setting the exceedance probability equal to:

$$\text{Prob}\left[\frac{P_A}{m_{P_A}} < z\right] = \frac{m_z}{N+1} \qquad (A.2)$$

where

m_z = Rank order of observation of magnitude z

N = Number of years (seasons of record)

The apparent goodness of fit at all three elevations assures us of the applicability of this storm model.
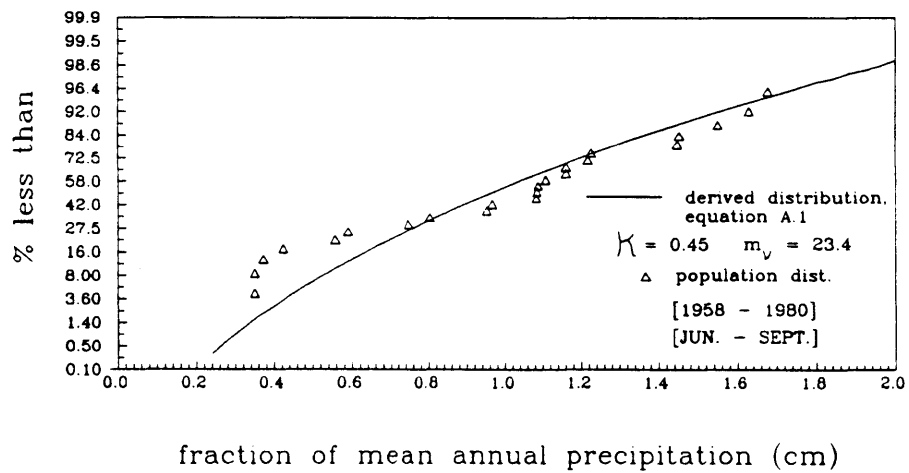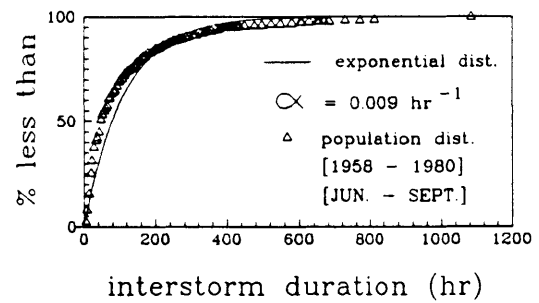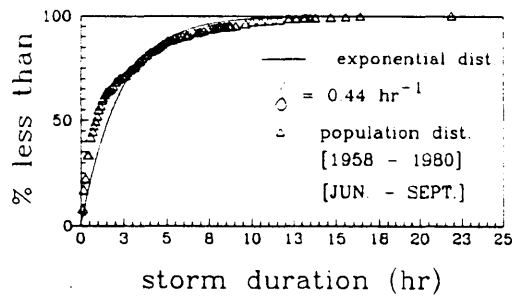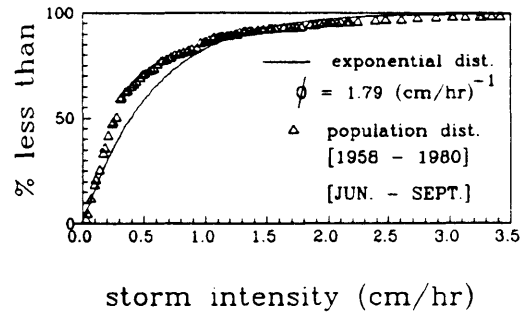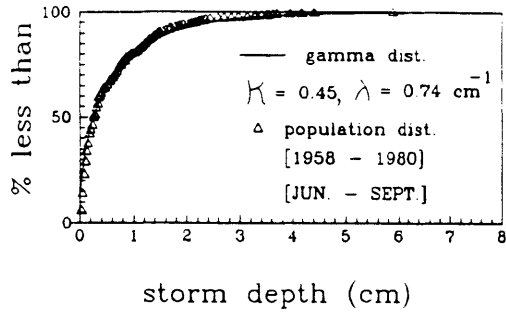
FIGURE A.1: SUMMER PRECIPITATION
DISTRIBUTIONS AT WATERSHED #2,
BEAVER CREEK ARIZONA
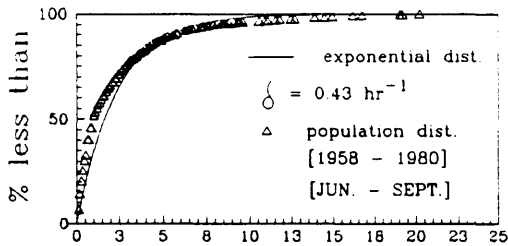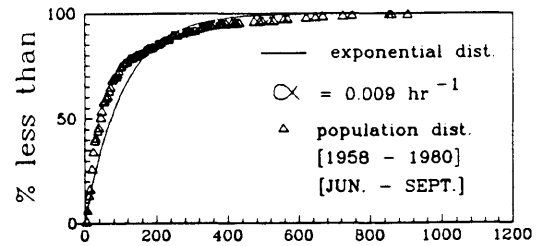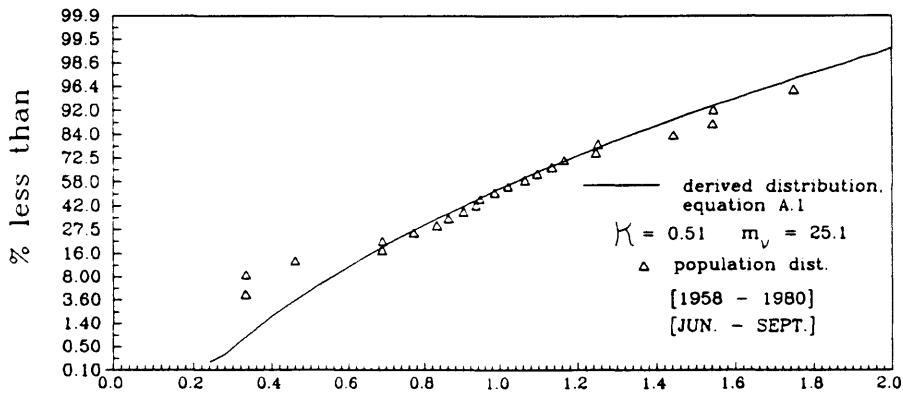
FIGURE A.2: SUMMER PRECIPITATION
DISTRIBUTIONS AT WATERSHED #4,
BEAVER CREEK ARIZONA
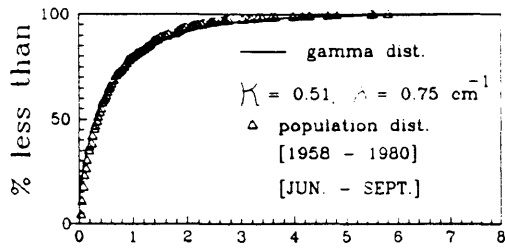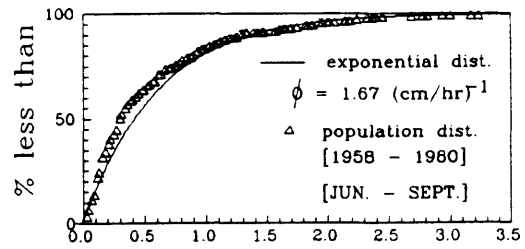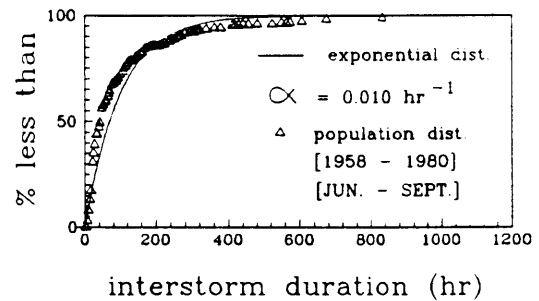
157
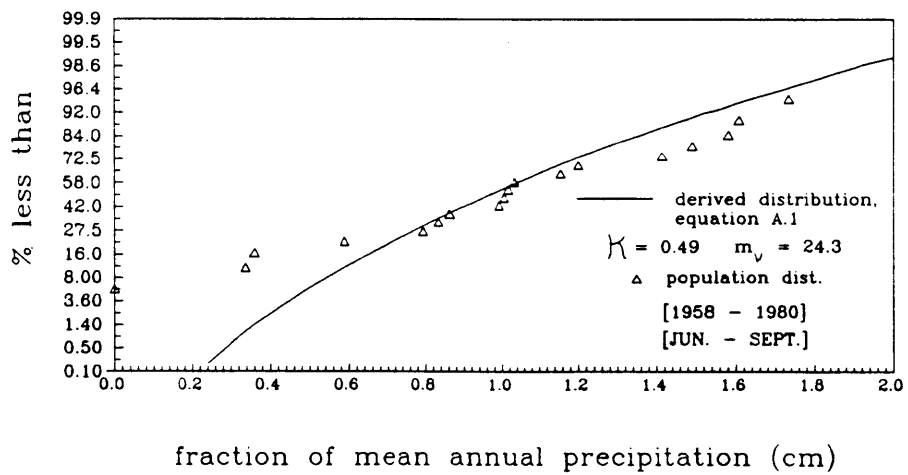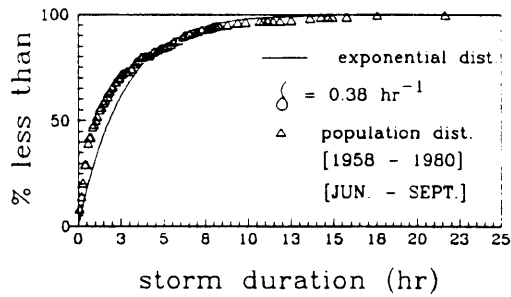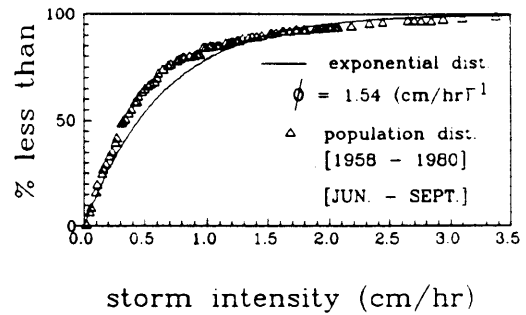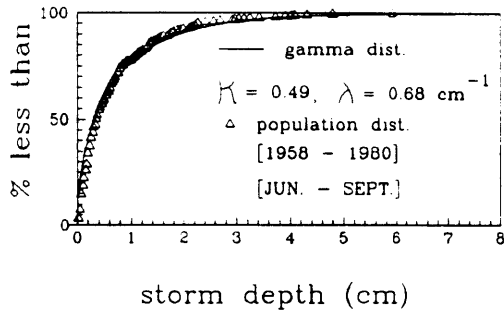
FIGURE A.3:   SUMMER PRECIPITATION

DISTRIBUTIONS AT WATERSHED #18,

BEAVER CREEK ARIZONA

Appendix B

Parameter Estimation

B.1 Potential Evaporation

One of the most important parameters of the ecological optimality expressions is the average potential evaporation rate $\bar{e}_p$. A lack of on-site measurement of pan evaporation at Beaver Creek necessitated the estimation of this parameter. Multiple estimation methods exist in the literature, and those whose data requirements could be met were used. These included: the Hamon method (Hamon, 1961); the Blaney-Criddle method (Doorenboos and Pruitt, 1977), the Radiation method (Doorenboos and Pruitt, 1977), the Priestly-Taylor method (Priestly and Taylor, 1972), and the Van Bavel equation as modified by Eagleson (Eagleson, 1977; see Eagleson and Tellers, 1982). The range of values obtained by these methods in estimating the annual potential evaporation at Flagstaff is presented in Table B.1. The method of Eagleson and the Priestly-Taylor method best reproduced the observed annual lake evaporation (Fig. B.1, reprinted from Farnsworth et al., 1982). The method of Eagleson was chosen between the two because it explicitly uses temperature and humidity data, which are available at five elevations in the Beaver Creek Basin, thereby allowing $\bar{e}_p$ estimation at each watershed.

The set of equations use to estimate the annual potential evaporation by Eagleson's method are:

Table B.1

Estimates of Annual Lake Evaporation at Flagstaff, AZ

Method	Surface*	E_p annual (cm)
Hamon	Land[1]	51.3
Blaney-Criddle	Land[1]	101.8
Priestly Taylor[2]	Land	48.8
Priestly Taylor[3]	Lake	113.0
	Land	79.6
Radiation Method	NA	157.9
Eagleson[3]	Lake	106.6
	Land	80.3

Notes:

[1] It is not possible to estimate lake evaporation by these methods.

[2] Net annual radiation from Hamon Regression (1961)

[3] Incoming net shortwave radiation from regression with latitude by Jensen and Haise (1963).

* in all cases, land surface implies that Albedo used = 0.25

    lake surface implies that Albedo used = 0.07
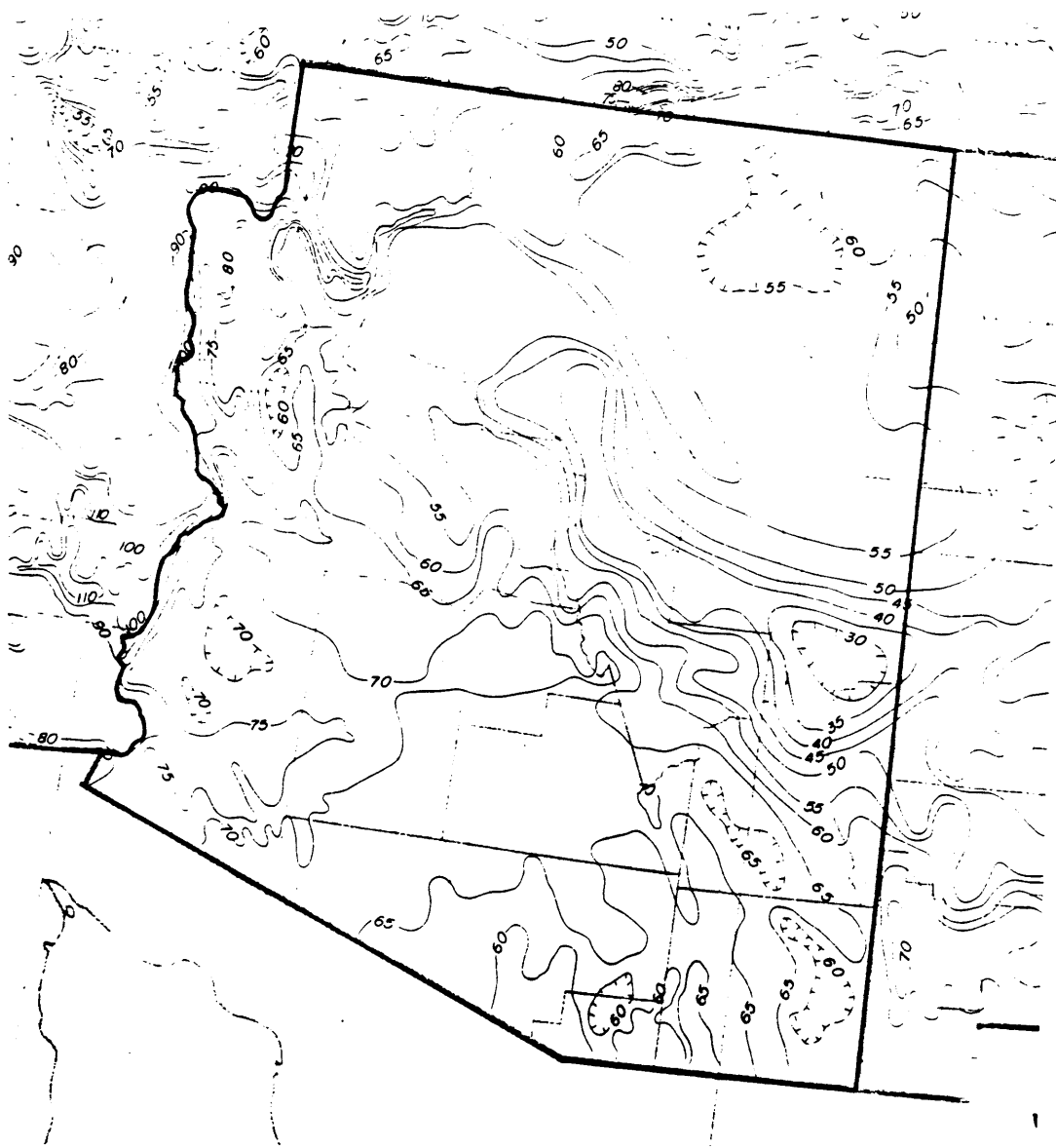
FIGURE B.1: ANNUAL LAKE EVAPORATION
IN ARIZONA   (INCHES)

$$\bar{e}_p = \frac{\bar{q}_i(1-A_s) - \bar{q}_b + H}{\rho L_e (1 + \frac{\gamma}{\Delta})} \tag{B.1}$$

$$\bar{q}_b = (1 - .8N)(.245 - .145 \times 10^{-10} \, \bar{T}_A^4) \tag{B.2}$$

$$H = \frac{\bar{q}_b}{.25 + \frac{1}{1 - RH_A}} \tag{B.3}$$

where

$\bar{q}_i$ = average seasonal rate of insolation at surface (cal cm^{-2} sec^{-1})

A_s = shortwave albedo of moist surface (dimensionless)

$\bar{q}_b$ = average net rate of outgoing longwave radiation (cal cm^{-2} sec^{-1})

ρ = mass density of liquid water (gm cm^{-3})

L = latent heat of vaporization (cal gm^{-1})

γ/Δ = atmospheric parameter, function of temperature (Eagleson, 1970, p. 228) (dimensionless)

N = average fractional cloud cover

$\bar{T}_A$ = average atmospheric temperature (°C)

RH_A = annual average relative humidity (dimensionless)

Equation B.3 is an empirical regression from Eagleson (1977, see Eagleson and Tellers, 1982). It is reproduced here in Fig. B.2.

162

$$\frac{\overline{q}_b}{H} = 0.25 + \frac{1}{1 - \overline{RH}_A}$$

$\overline{q}_b / H$

$\overline{RH}_A$ - SATURATION RATIO

FIGURE B.2: RATIO OF NET LONGWAVE
BACK RADIATION TO DRYING POWER
OF AIR (EAGLESON, 1977)

163

That this equation reproduced the annual lake evaporation at Flagstaff is partly affirmation of the equation itself, and partly affirmation of the incoming shortwave radiation vs. latitude regression of Jensen and Haise (1963). This regression is reproduced here as Fig. B.3.

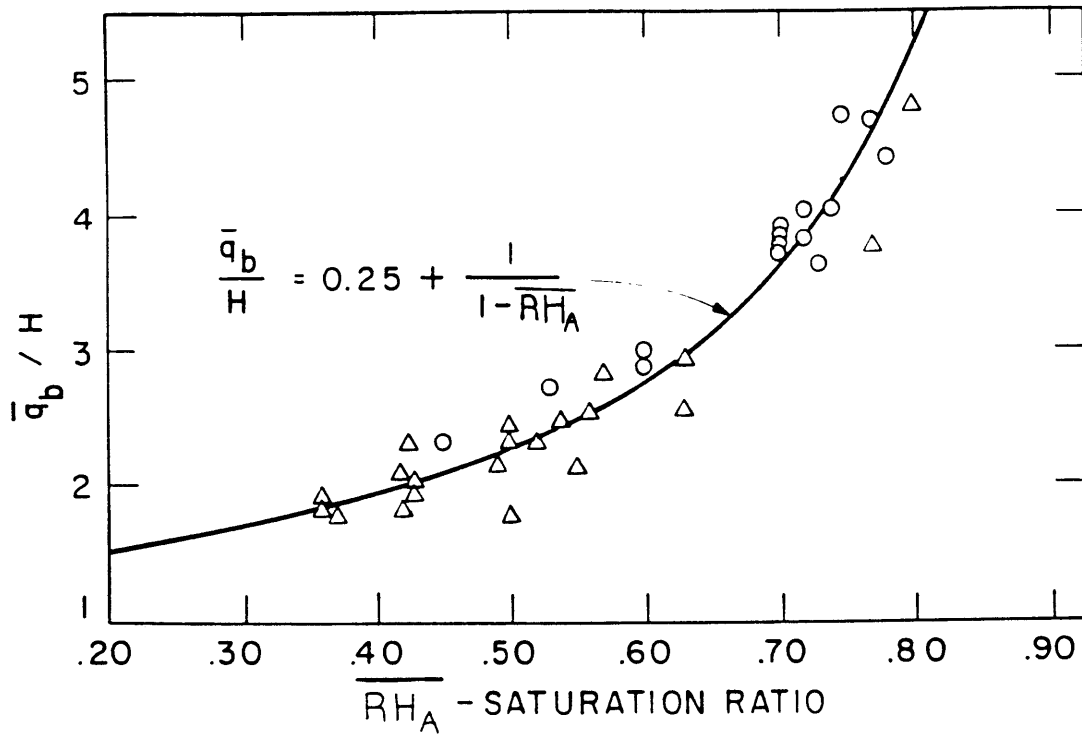For use in the watersheds of Beaver Creek, which is approximately 50 miles southeast of Flagstaff, the same insolation rate will be used. The albedo will be approximated at 0.25 (for vegetated land surface). The annual average temperature ($\overline{T}_A$) and humidity ($\overline{RH}_A$) are obtained from a regression made from twenty-five years of data at five elevations (Figs. B.4 and B.5). The fractional cloud cover (N) has been estimated from data for Flagstaff from NOAA (Table B.2). In this way, the annual land surface potential evaporation rate becomes a function of elevation on the Beaver Creek. This function is graphed in Fig. B.5.

To be used in the ecological hypothesis tests of Chapter 4, this annual potential evaporation rate must be distributed throughout the year in such a way that the fraction of it occurring in the "testing" season can be separated from the fraction in the "non-testing" or winter season. A monthly distribution of potential evaporation for the state of Arizona (Cooley, 1970) was used to create a cumulative distribution of the percentage of the total annual potential evaporation as a function of Julian day. This regression is presented in Fig. B.7.
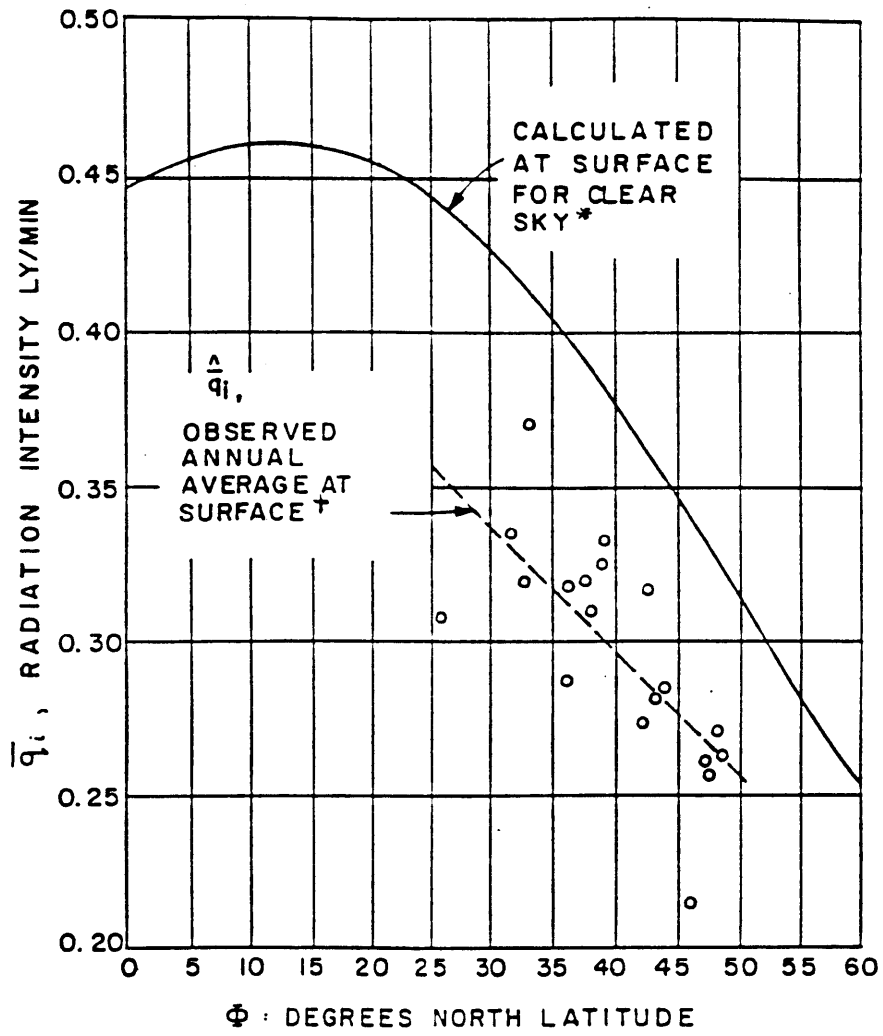
FIGURE B.3: INSOLATION AT EARTH'S
SURFACE (EAGLESON, 1977)
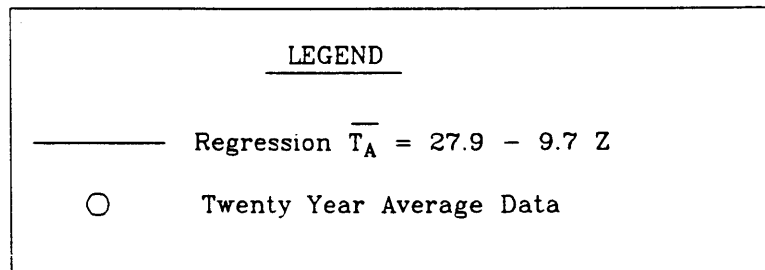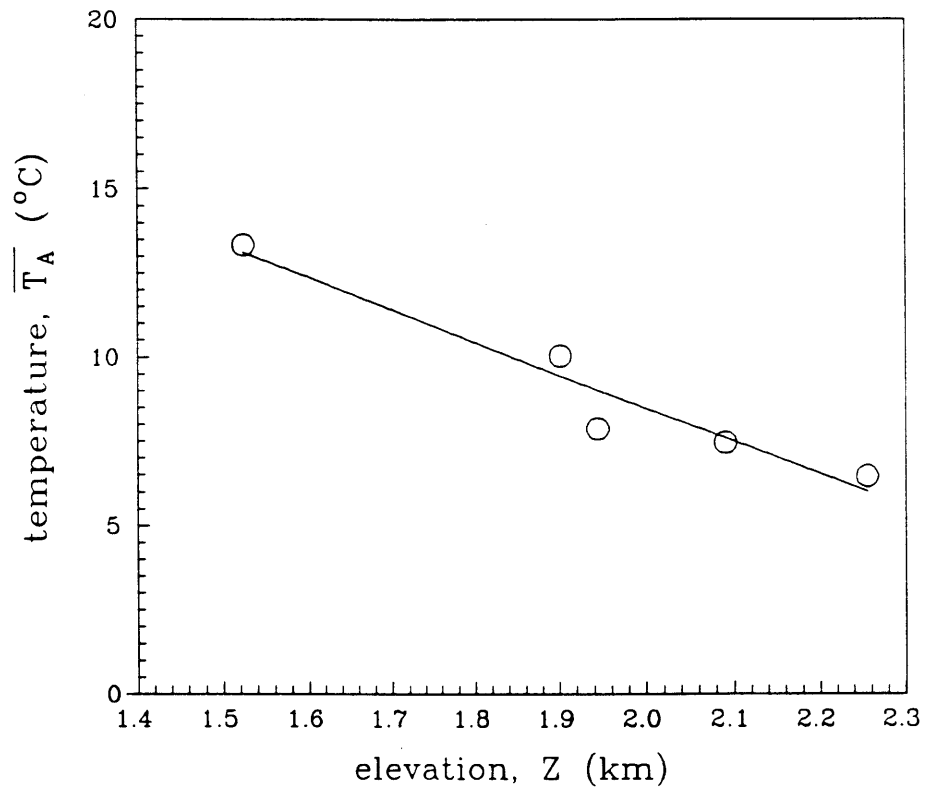
FIGURE B.4: AVERAGE ANNUAL TEMPERATURE

LAPSE RATE AT BEAVER CREEK
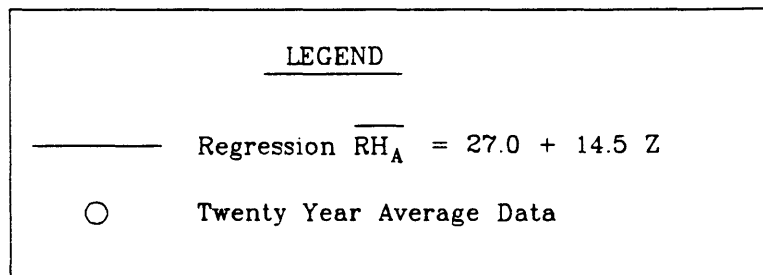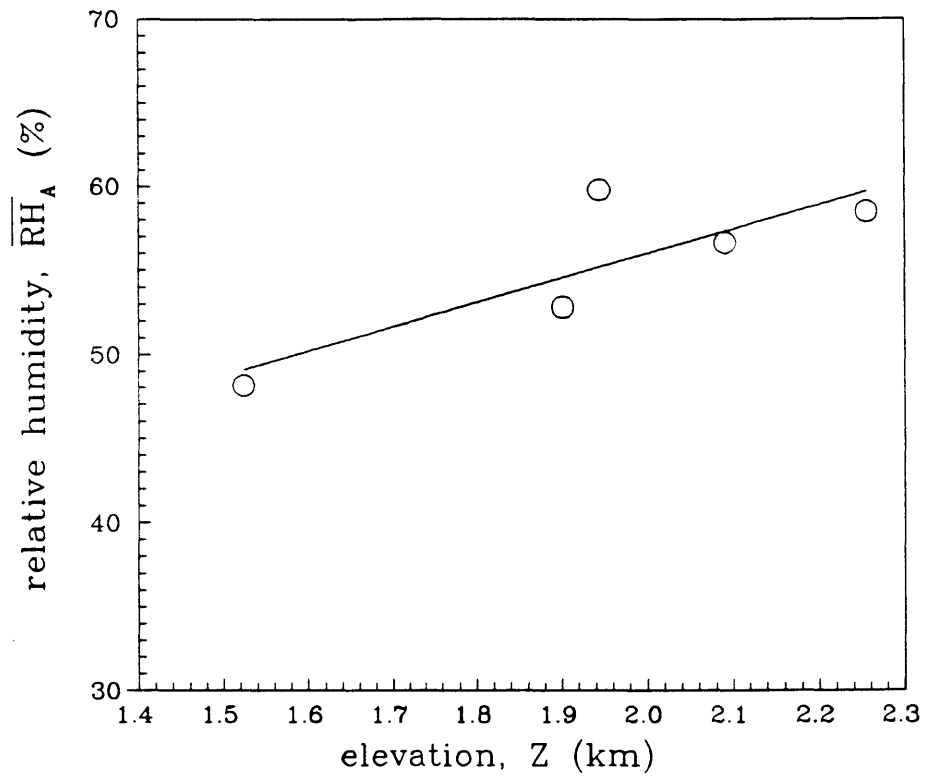
FIGURE B.5: AVERAGE ANNUAL RELATIVE
HUMIDITY LAPSE RATE AT BEAVER CREEK
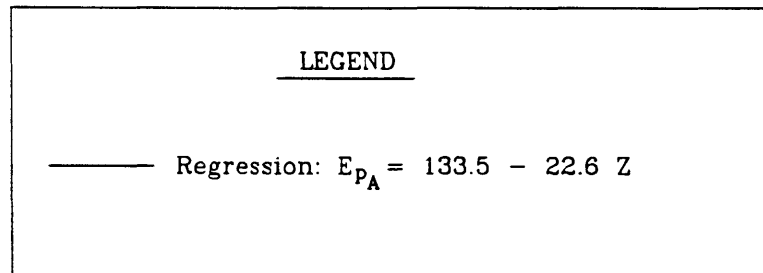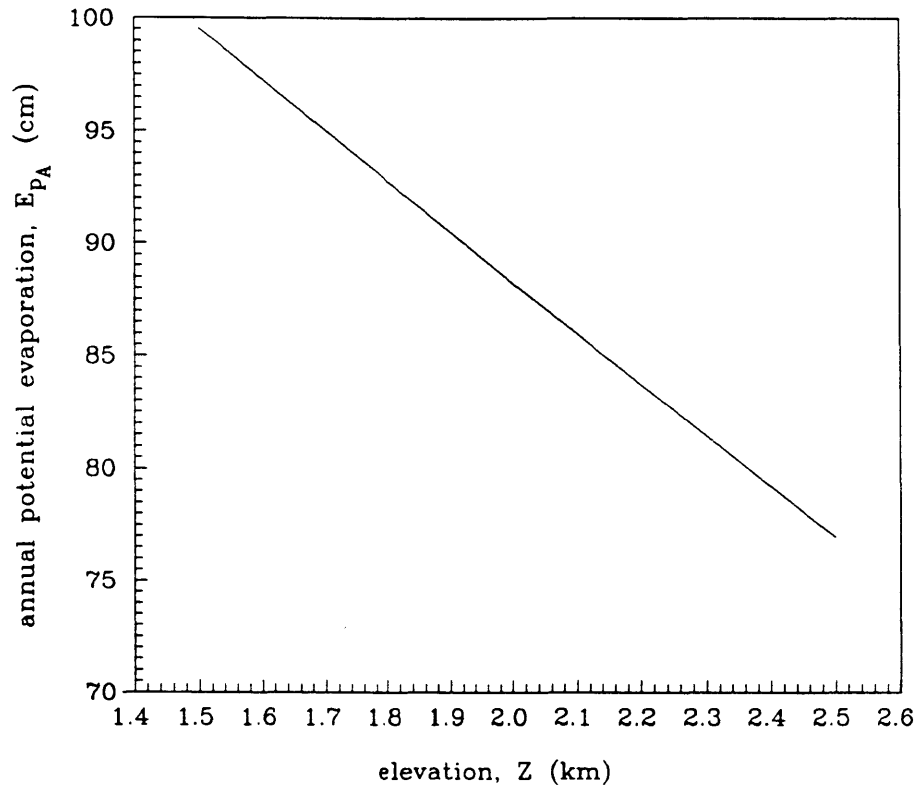
FIGURE B.6: ANNUAL POTENTIAL EVAPORATION
LAPSE RATE AT BEAVER CREEK
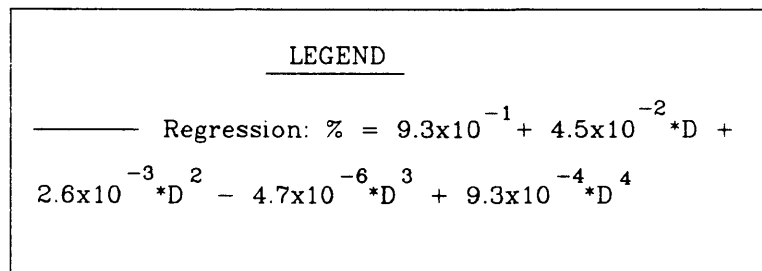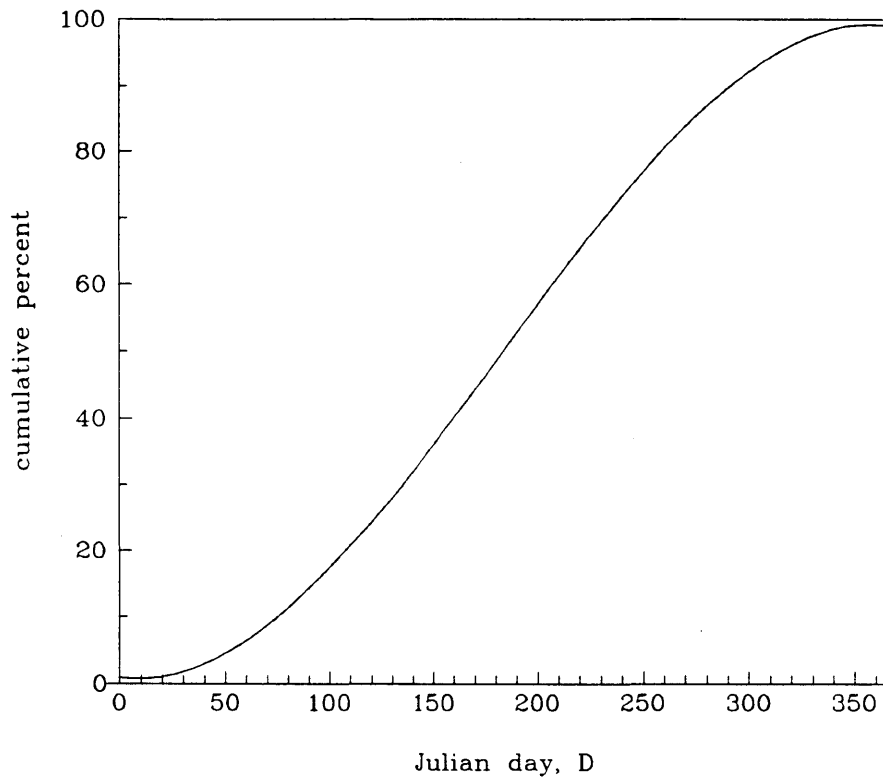
FIGURE B.7: CUMULATIVE DISTRIBUTION OF POTENTIAL EVAPORATION BY JULIAN DAY AT BEAVER CREEK

Table B.2

Cloudiness at Flagstaff, AZ

MONTH	CLEAR DAYS	PTLY CLOUDY DAYS	CLOUDY DAYS	FRACTIONAL CLOUD COVER (DAY WEIGHTED)%
JUN	19	7	4	32
JUL	9	13	9	49
AUG	10	13	8	46
SEP	16	10	4	35
OCT	17	7	7	38
NOV	16	6	8	39
DEC	14	6	11	45
JAN	12	6	13	49
FEB	11	6	11	48
MAR	12	8	11	47
APR	13	9	8	43
MAY	16	9	6	38
YEAR	163	101	101	43

NOTE: CLEAR = 0 to 30% COVER

PTLY CLOUDY = 30 to 70% COVER

CLOUDY = 70 to 100% COVER

In summary, to estimate the average potential evaporation rate in a given watershed in a given season, one needs to: find the average annual humidity and temperature from the elevation regressions (Figs. B.4 and B.5); apply equations B.1 through B.3 with the parameter values listed in this discussion (e.g., A_s = .25) and multiply $\bar{e}_p$ by 365 to obtain $\bar{E}_{P_A}$; find the cumulative percent of the annual evaporation between the two Julian days marking the beginning and end of the season of interest; and then multiply $\bar{E}_{P_A}$ by this percentage and divide this by the number of days in the season.

The potential evaporation values listed in Table 4.5 were found in this way.

B.2 Potential Transpiration Coefficient

Arris (1989) presents a method of determining the potential transpiration efficiency (k_v) from annual biomass productivity data. The method is based on the observed correlation between water use (i.e., transpiration) and biomass production. Physically, this correlation arises because water is part of the pathway of carbon dioxide assimilation during photosynthesis (the CO_2 must be in solution to diffuse through the cell membrane). While the water at the site of assimilation is exposed to the atmosphere, some evaporates, necessitating root soil moisture extraction to maintain the plant's water balance.

The ratio (χ), between carbon assimilation and water use has been measured for various plant types by Larcher (1983, p.

231). Following the method of Arris, these ratios have been corrected by a factor ranging from 13 to 35% to account for (unmeasured) below ground biomass accumulation, and then averaged by type. In this way, one average coefficient for herbaceous plants (the understory), and one for coniferous woody plants (the overstory) have been estimated. They are 0.003 gm C/gm H_2O and .0016 gm C/gm H_2O, respectively.

If we now assume that the vegetation is amply supplied with water such that it transpires throughout the whole season, the x ratio may be written for the growing season totals of carbon assimilation and water use. Arris (1989) makes this assumption (page 61, par. 2), and arrives at a useful equation for estimating k_v. Following her approach:

$$ET_S = \chi^{-1} \cdot NPP \qquad (B.4)$$

$$Mk_v\bar{e}_{P_S} \, m_{v_S}\alpha_S^{-1} = \chi^{-1} \cdot NPP \qquad (B.5)$$

or, rearranging:

$$k_v = \frac{\chi^{-1} \cdot NPP}{M \cdot E_{P_S}} \qquad (B.6)$$

In the above, NPP is the above-ground biomass production in weight of carbon per unit area of land.

Application of (B.6) with the value of the herbage yield (when $M_u = 1$, see Section 4.3.1) presented by Clary et al. (1974, pg. 18), and the average growing season potential

172

evaporation for the six watersheds (1-6) for which the yield value applies, yields an understory potential transpiration coefficient (k_{v_u}) of 0.6 (see Table B.3 for details.

Estimating k_v for the woodland component involved using regional pinyon-juniper production data instead of Beaver Creek specific data. Ffolliot (1986), gives the average standing yearly accumulation of woodland stems (i.e., NPP minus below ground production minus foliage) for the "Four Corner states" and Nevada. Larcher (1983, p. 132) estimates the foliage component of evergreen conifers in this region to be four to five percent. Correcting Ffolliot's values by this factor, and applying the same methodology as above, one obtains an overstory potential transpiration coefficient of 0.6 (see Table B.3). In this calculation the average canopy density [(used in (B.6)]) of the six Beaver Creek woodland watersheds was used. This implicitly assumes that the Beaver Creek pinyon juniper woodland densities are typical of the densities of the "Four Corner States" and Nevada. Barbour and Billings (1988, p. 224) give the "higher plant cover" of these woodlands as 40-80 percent. If by higher plant cover they mean canopy density, then this represents a contradiction to our assumption. We feel, however, that a canopy density of 40-80 percent sounds too high, and that the "higher plant cover" is a different measure of vegetation.

The potential transpiration coefficient of the ponderosa pine forest type could not be determined due to a lack of production data.

Table B.3

Estimation of Potential Transpiration Efficiency Coefficients

Vegetation Type	Herbaceous Understory	Coniferous Woody Overstory
$\chi^{-1}\left(\dfrac{gm\,H_2O}{gm\,C}\right)$	400 - 670	200 - 300
$\chi\left(\dfrac{gm\,C}{gm\,H_2O}\right)$	2.5×15^{-3} - 1.5×15^{-3}	5.0×15^{-3} - 3.3×15^{-3}
χ corrected for underground growth	2.2×10^{-3} - 9.7×10^{-4}	4.4×10^{-3} - 2.2×10^{-3}
$\overline{\chi}$	1.6×10^{-3}	3.3×10^{-3}
$NPP\left(\dfrac{gm\,C}{cm^2}\right)$	6.3×15^{-2}	2.7×10^{-2}
E_{P_S} cm	66.5	66.5
M	1	0.21
k_v	0.6	0.6

The continuous transpiration assumption that was made in the above estimation (which is necessitated by the restriction that we only have measurements of seasonal totals of production and not a daily accounting) is equivalent to assuming that the transpiration reduction coefficient, β_v, is unity (see Chapter 3). Whereas the above estimates place our "observed" M-k_v pair to the left of the soil moisture "cliff" in Figs. 4.19B and 4.20B, β_v will indeed be unity and our assumption is not self-contradicting.

B.3 Soil Properties

B.3.1 A review of the Brooks and Corey Model

The Brooks and Corey Model (Brooks and Corey, 1966) is a set of functions relating the unsaturated capillary pressure, ψ, and unsaturated conductivity, K, to the effective soil moisture (s) and to each other. The form of the equations area:

$$\psi(s) = \psi(1) s^{-1/m} \qquad (B.7)$$

$$K(s) = K(1) s^c \qquad (B.8)$$

and

$$s = \frac{s_T - s_r}{1 - s_r} \qquad (B.9)$$

where s_r is the residual saturation and s_T is the total saturation, or the percentage of total pore space (n_T) filled with water. Brooks and Corey (1966) show that for a wide range of soil types the two exponents of (B.7) and B.8) can be related by:

$$c = \frac{2 + 3m}{m} \qquad (B.10)$$

This reduces the number of parameters to be estimated to five: $K(1)$, $\psi(1)$, m, n_T and s_r.

The validity of Eq. B.10 depends on the correct estimation of s_r. In the original work (Brooks and Corey, 1966), s_r was estimated directly from unsaturated conductivity-saturation data (i.e., at $s = s_r$, the moisture in

176

the soil becomes discontinuous and the conductivity becomes zero). In practice, however (and in the application), one often only has capillary pressure-saturation data. Thus S_r must be estimated indirectly, leaving the validity of B.10 questionable. The model is known to be inaccurate near the extremes of soil moisture concentration, particularly at the wet end.

B.3.2   Estimation of Soil Parameter Values

B.3.2.1   Sources of Data

Data on soil properties came from two sources: an SCS survey (Anderson, 1967) and an unpublished report by the University of Arizona at Tucson, Department of Watershed Management. In the latter, four of the Beaver Creek watersheds were sampled and laboratory-tested for moisture retention characteristics.

The soils in Beaver Creek, which contain high amounts of clay, demonstrate strong shrink-swell characteristics, and thus make analysis difficult. The water balance (Eagleson, 1978) and ecological optimality modeling (Eagleson and Tellers, 1982) used in this study incorporate the Brooks and Corey parameterization of soil hydraulic properties. This model does not strictly apply to soils whose porosity changes with moisture content. Nevertheless, an approximate method of estimating the parameters was developed. This required using the available data on the shrink-swell characteristics of the soil. Unfortunately the Arizona report contained only two

177

moisture content versus volume curves, and those were distin-
guished only by their SCS soil name. The final results of the
soil analysis are thus two sets of Brooks and Corey parame-
ters, one each for the soil types "Springerville" and
"Brolliar".

While the SCS classification is unsatisfactory in many
ways, it can serve to distinguish between the predominantly
Brolliar and predominantly Springerville watersheds. It has
been well documented (Williams and Anderson, 1967) and can be
seen by comparing SCS maps with vegetation maps, that the
higher altitude watersheds which support Ponderosa Pine trees
contain the Brolliar soil series, while the lower altitude
watersheds, which support mostly pinyon-juniper vegetation,
contain the Springerville soil series.

B.3.2.2. Hydraulic Conductivity

The SCS report describes the Springerville soil series as
a stoney clay loam. It lists the hydraulic conductivity of
these soils (found on watersheds 1 through 6) as 5.6 to
17×10^{-4} cm/sec for the top three inches of soil and "less
than" 3.5×10^{-5} cm/sec for the bottom 41 inches. For the
Brolliar Series, also a stoney clay loam, the top five inches
has a conductivity of 1.4 to 5.6×10^{-5} cm/sec and the bottom
30 inches, a conductivity of 3.5 to 14×10^{-5} cm/sec.

To estimate the effective conductivity of the soils, the
average of the topsoil range and bottomsoil range have been
geometrically averaged, i.e.,

$$\log(K(1)) = \frac{\log\left(\overline{K}(1),_{top}\right) + \log\left(\overline{K}(1),_{bot}\right)}{2} \qquad (B.11)$$

The results of this averaging are presented in Table B.4.

B.3.2.3   Moisture Retention Parameters

B.3.2.3.1   Method

Arriving at the (unsaturated) Brooks and Corey parameters is more complicated. The moisture retained (ω) by weight, (i.e., weight of water/weight of solids) by the soil samples at six pressures ranging from 0.33 to 15 bars were listed in the University of Arizona report. The higher pressure data (3-15 bars) were considered problematic by the authors of that report due to laboratory testing problems. The soil samples used for these pressures were prepared differently: they were undisturbed for the 0.33 and 0.66 bar tests, but pulverized and "re-packed" for the higher pressure runs. Nevertheless, the full data set will be used.

The depth and sample average of these data are presented in Table B.5.

In order to arrive at the Brooks and Corey moisture retention parameters we first estimate the total porosity and residual water content. Next we convert the moisture retained by weight (ω) to effective saturation ratios (s), and then

Table B.4

Hydraulic Conductivity Estimation

	Springerville	Brolliar
Topsoil	1.13×10^{-3} cm/sec	3.5×10^{-4} cm/sec
Bottom soil	3.5×10^{-5} cm/sec	8.75×10^{-5} cm/sec
Log average	1.99×10^{-4} cm/sec	1.75×10^{-4} cm/sec

Table B.5

Depth and Sample-Averaged Moisture Retention

ψ(bars)	Springerville $\omega\left(\dfrac{gmH_2O}{gmSolids}\right)$	Brolliar $\omega\left(\dfrac{gmH_2O}{gmSolids}\right)$
0.33	0.361	0.335
0.66	0.329	0.305
3	0.323	0.272
5	0.309	0.263
10	0.304	0.240
15	0.291	0.231

estimate m and $\psi(1)$ by fitting Eq. B.7 to the six data points (i.e., s at ψ = 0.33, 0.66, 3, 5 and 15 bars.

B.3.2.3.2   <u>Total Porosity</u>

The total porosity (n_T) is estimated by the following relationship (Das, 1985)

$$n_T = 1 - \frac{\rho_d}{G_s} \qquad (B.12)$$

where ρ_d is the air dry bulk density and G_s is the specific weight of the soil particles. Because these soils shrink when they dry, the measured bulk density must be corrected (before applying Eq. (B.12)) so that the estimated total porosity reflects the pore space at saturation. The University of Arizona report states that the Springerville and Brolliar soils dry to 48% and 65% of their saturated volume, respectively. The same report gives the air dry bulk density for each sample tested for moisture retention. The depth and sample average of these data are $\overline{\rho}_d$ = 1.72 for the Springerville and $\overline{\rho}_d$ = 1.62 for the Brolliar type. Correcting these average values by the shrink-swell factor (0.48 and 0.65) and applying Eq. B.12 with G_s = 2.71 (also listed in the University of Arizona report) yields total porosities of 0.695 and 0.611 for the Springerville and Brolliar soils.

B.3.2.3.3   <u>Residual Saturation</u>

To find the residual saturation s_r, one must first convert the moisture retained by weight (ω) to total saturation (s_T) and then plot these values vs. their respective

pressures and estimate where the resulting "moisture reten-
tion" curve becomes vertical. To convert the moisture content
by weight to saturation, we have (Das, 1985):

$$s_T = \omega \cdot G_s \left(\frac{1}{n_T} - 1 \right) \qquad \text{(B.13)}$$

Applying B.13 to the data of Table B.5 and the previously
calculated total porosity yields the saturations listed in
Table B.6 and plotted in Figs. B.7 and B.8. Because the slope
of ψ vs. s approaches infinity (i.e., vertical) as ψ approach-
es the maximum measured value of 15 bars, we will choose the
corresponding value of s (s at ψ = 15 bars), as s_r. This
yields values of 0.346 for the Springerville and 0.398 for the
Brolliar soil type. These residual saturations are in the
range reported by Brooks and Corey (1966) of 0.085 to 0.577.
Also, 15 bars is the approximate capillary pressure at which
trees cease transpiration. The moisture unavailable to
exfiltration will thus be equal to the moisture unavailable to
transpiration, lending consistency to the distributed root
sink-soil column model used in this report.

B.3.2.3.4.   Pore Soil Distribution Index

To estimate the pore size distribution index (m), one
must plot the log of the effective saturation vs. the log of
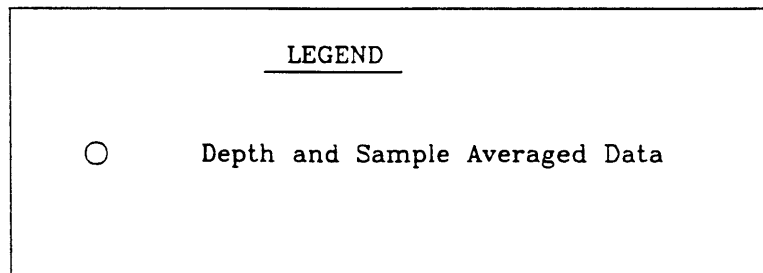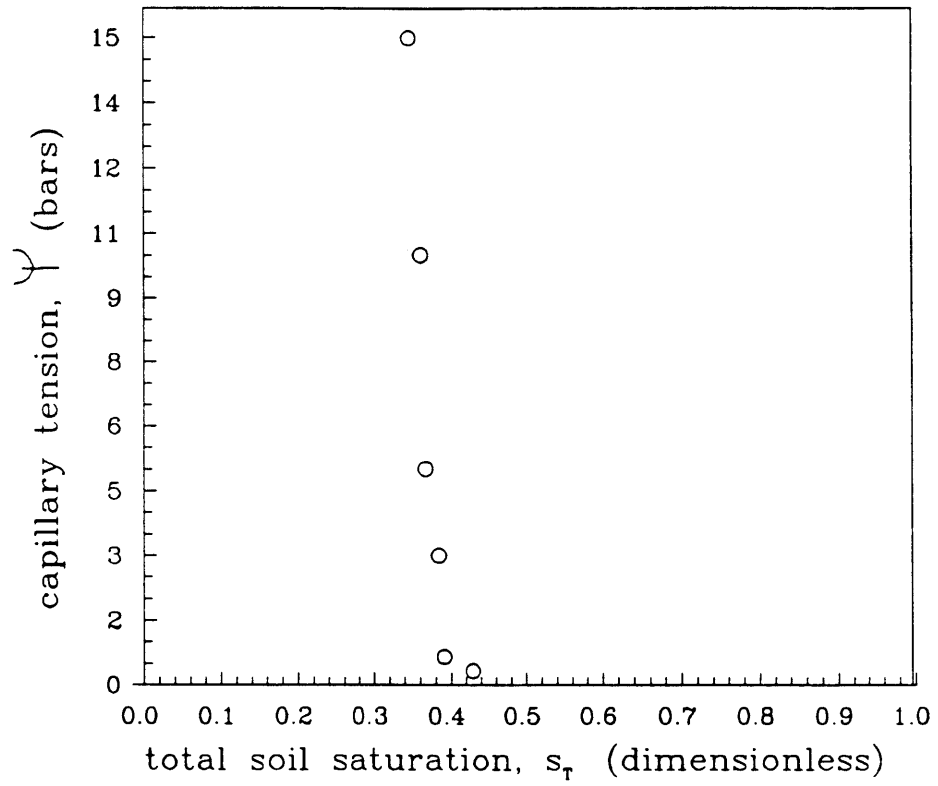the corresponding pressure intensity and perform a linear
regression.

FIGURE B.8: CAPILLARY PRESSURE HEAD VS.
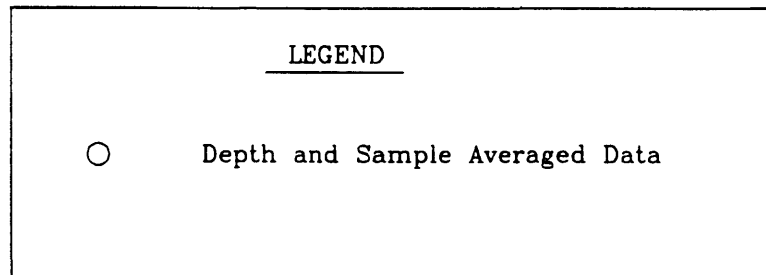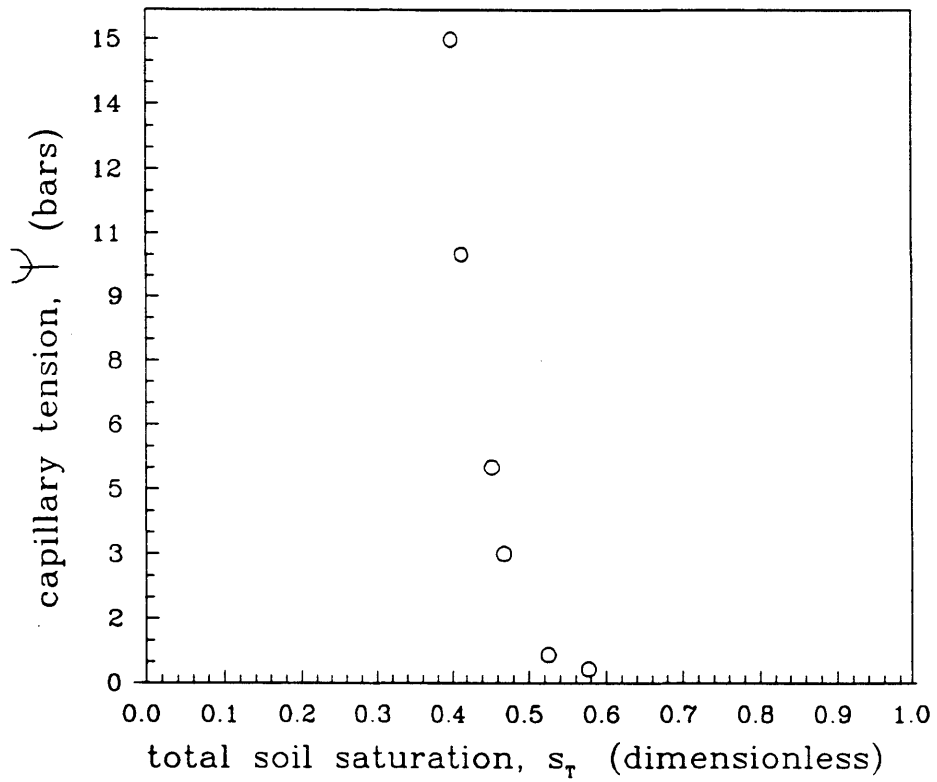
SATURATION, SPRINGERVILLE SOIL TYPE

FIGURE B.9: CAPILLARY PRESSURE HEAD VS.

SATURATION, BROLLIAR SOIL TYPE

Table B.6

Total Saturations Converted from Moisture Content

by Weight

ψ (bars)	Springerville s_T (dimensionless)	Brolliar s_T (dimensionless)
0.33	0.429	0.577
0.66	0.391	0.525
3	0.384	0.468
5	0.367	0.453
10	0.361	0.413
15	0.346	0.398

The resulting slope is m, and the zero intercept is the log of $\psi(1)$. The effective saturation, s, is found by application of Eq. B.9, i.e.,

$$s = \frac{s - s_r}{1 - s_r} \qquad (B.14)$$

with the previously estimated s_r. The resulting effective saturations are listed in Table B.7. Figures B.10 and B.11 illustrate the linear regression through the log(s)-log(ψ) data. The 15 bar data point could not be used in the regression, since its effective saturation is zero and the log of zero is undefined.

The pore disconnectedness index, c, can now be estimated by application of Eq. B.10. The Brooks and Corey parameters resulting from the preceding analysis are presented in Table B.8. Also included are the effective porosity (n_e), found by application of

$$n_e = n_T(1 - s_r) \qquad (B.15)$$

and the log of the saturated intrinsic permeability k(1). The permeability is related to the hydraulic conductivity by

$$k(1) = K(1) \frac{\mu_w}{\gamma_w} \qquad (B.16)$$

where μ_w is the dynamic viscosity and γ_w is the specific weight of water. The log permeability values in Table B.8 were converted by Eq. B.16 with μ_w and γ_w evaluated at room temperature, 20°C. These are the independent soil parameter estimations used in the various ecological optimality tests of Chapter 4.
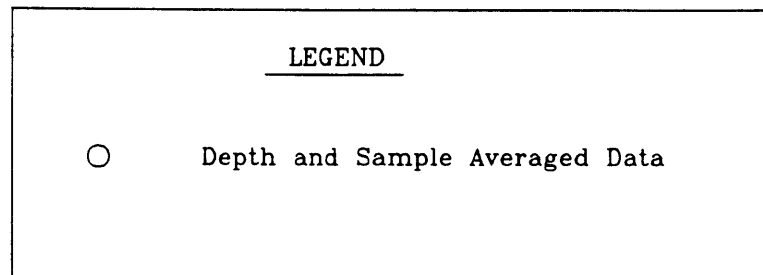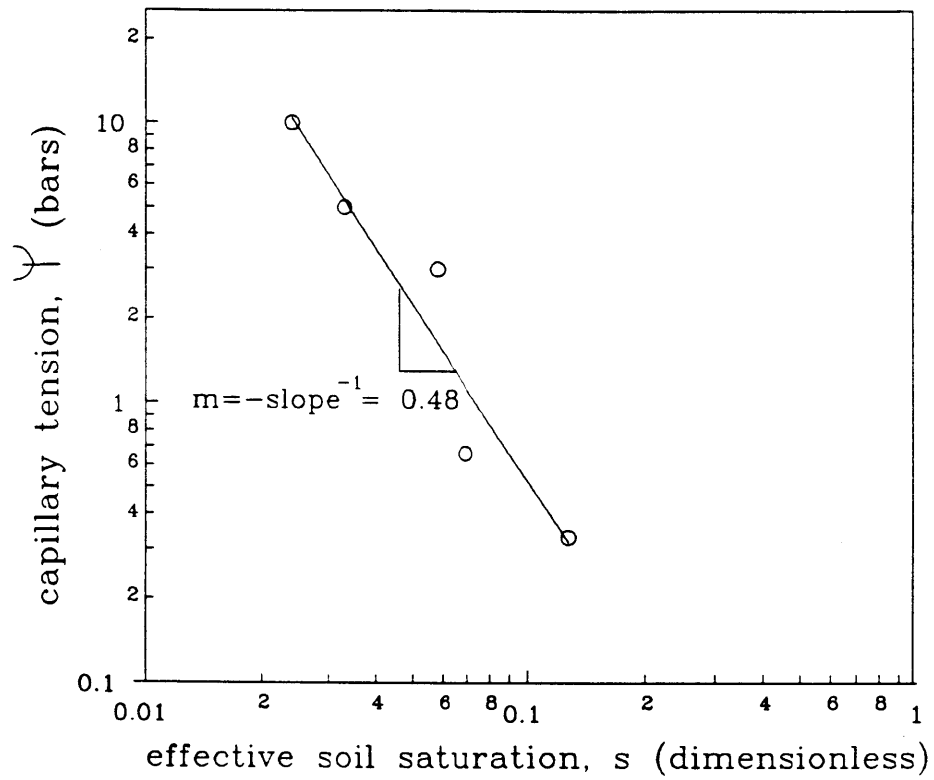
FIGURE B.10: LOG (Ψ) — LOG (s)
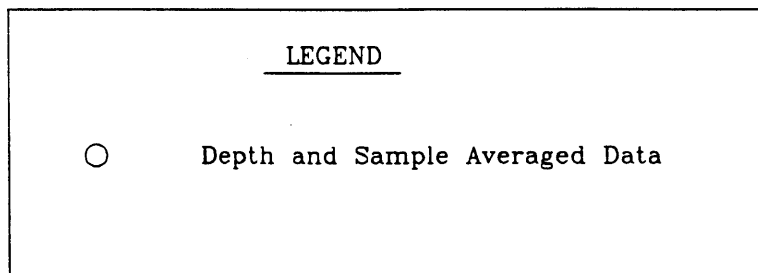
REGRESSION, SPRINGERVILLE SOIL TYPE
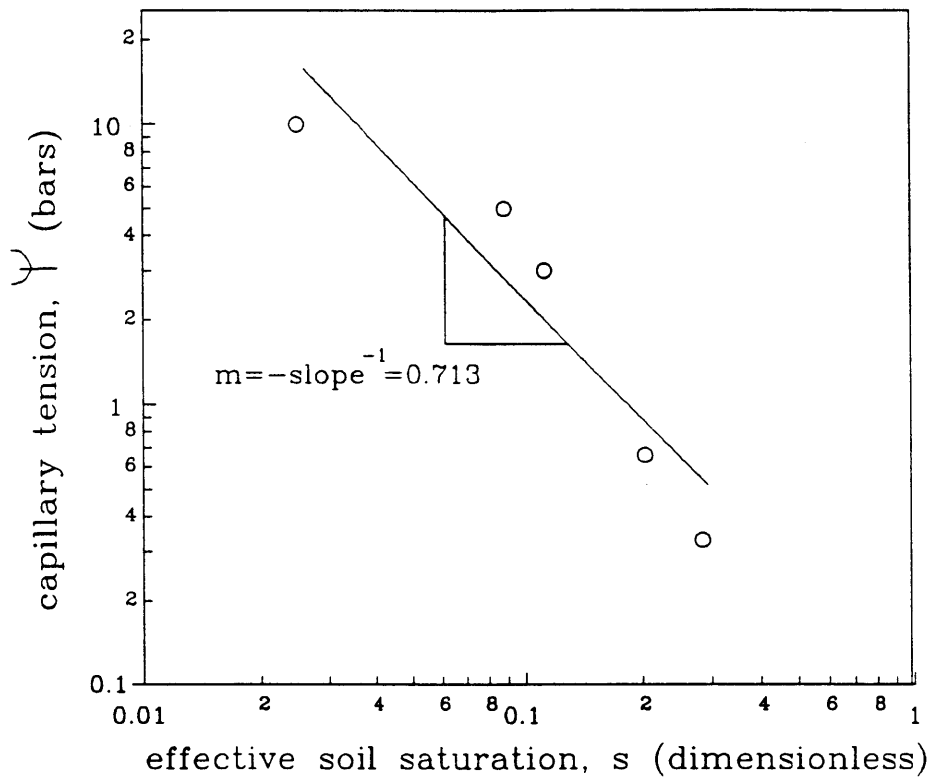
FIGURE B.11: LOG (Υ) — LOG (s)

REGRESSION, BROLLIAR SOIL TYPE

Table B.7

Effective Saturation, s

ψ (bars)	Springerville s (dimensionless)	Brolliar s (dimensionless)
0.33	0.127	0.297
0.66	0.069	0.212
3	0.058	0.117
5	0.033	0.092
10	0.024	0.026
15	0.000	0.000

Table B.8

Estimated Soil Parameter Values

	Springerville	Brolliar
m	0.48	0.713
c	7.13	5.8
$\psi(1)$	4.51 cm	92.8 cm
$n^{\intercal}$	0.695	0.611
S_r	0.346	0.398
n_e	0.455	0.368
log (k(11))	-8.70	-8.75

Appendix C

Analysis of Lateral Groundwater Flow

Anderson (1967) reports that the mean depth of soil on the Beaver Creek Watersheds is approximately one meter. Under this shallow soil layer is relatively impermeable bedrock (Baker, 1982). Also, inspection of topographic maps of the watersheds illustrates that the slopes perpendicular to the watersheds' drainage channels are approximately five percent. These maps also yield an approximate distance from the channels to the watersheds'divide of 300 meters.

With reference to the idealized hillslope-channel geometry of Fig. C.1, a simple mass conversion statement can be to determine the _maximum_ possible accretion rate:

$$\overline{N}_M \cdot L \leq K_1 \overline{h} \tan \theta \qquad \text{(C.1)}$$

where

$\overline{N}_M$ = maximum possible accretion rate averaged over hillslope, cm sec^{-1}

L = hillslope length

K_1 = saturated hydraulic conductivity, cm sec^{-1}

$\overline{h}$ = average depth at _saturated_ soil

θ = slope of hillslope (which is approximately equal to the slope of the bedrock and the slope of the saturated bare surface), (dimensionless)
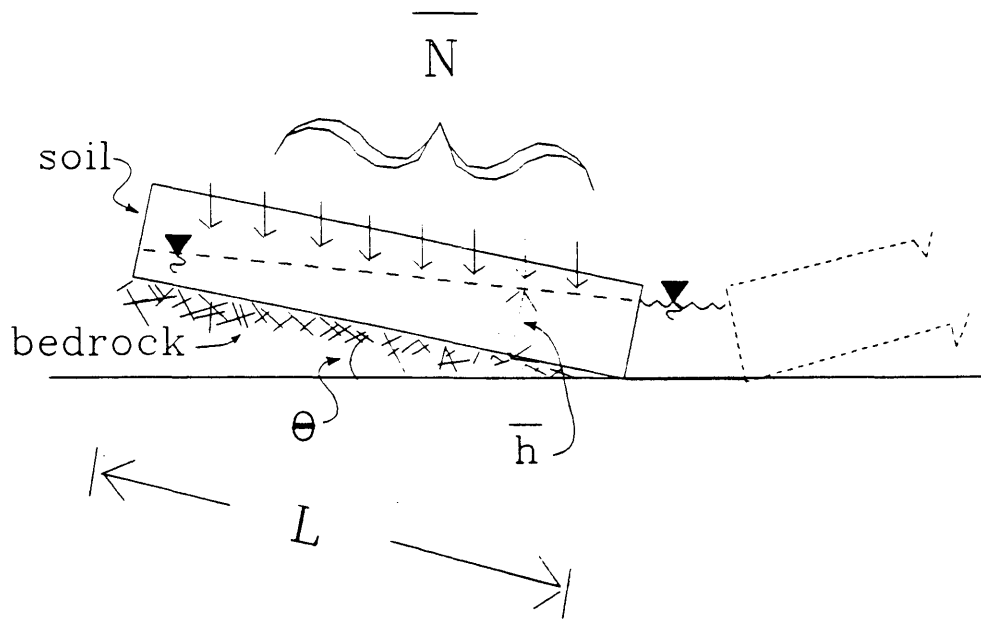
FIGURE C.1: SIMPLIFIED HILLSLOPE —
CHANNEL GEOMETRY

Recognizing and multiplying by season length, m_τ, Eq. C.1 yields:

$$\bar{N}_M = \frac{K_1 \bar{h} \tan\theta}{L} m_\tau \qquad (C.2)$$

For the typical Beaver Creek values instead of the above discussion and in the soils appendix, C.2 yields (for a two-hundred-day season), 0.6 cm of recharge.

Note that in the analysis carried out in Section 4.6, the water balance and optimality statements are solved for a range of values of permeability. For permeability values one order of magnitude greater than that used in the above analysis, the recharge could be as much as six cm, in which case the barrel analogy described in Section 4.4.2.2 might not hold. The analysis was thus carried out in two parts: as the modified water balance for permeabilities to the left of the band in Figs. 4.23-4.25; and as the original water balance to the right. Application of Eqs. C.2 and C.16 (to convert permeability to conductivity), reveals that this band represents a region of approximately two cm of recharge.